

Electronic Thesis and Dissertation Repository

11-17-2021 1:00 PM

Neuroanatomical characterization of fruitless P2 neurons and assessment of their role in female mate receptivity

William Yeung, *The University of Western Ontario*

Supervisor: Moehring, Amanda J., *The University of Western Ontario*

A thesis submitted in partial fulfillment of the requirements for the Master of Science degree in Neuroscience

© William Yeung 2021

Follow this and additional works at: <https://ir.lib.uwo.ca/etd>



Part of the [Behavioral Neurobiology Commons](#), and the [Molecular Genetics Commons](#)

Recommended Citation

Yeung, William, "Neuroanatomical characterization of fruitless P2 neurons and assessment of their role in female mate receptivity" (2021). *Electronic Thesis and Dissertation Repository*. 8350.
<https://ir.lib.uwo.ca/etd/8350>

This Dissertation/Thesis is brought to you for free and open access by Scholarship@Western. It has been accepted for inclusion in Electronic Thesis and Dissertation Repository by an authorized administrator of Scholarship@Western. For more information, please contact wlsadmin@uwo.ca.

Abstract

In behaviourally isolated species, preferential mate choice for conspecifics over heterospecifics is a primary isolating barrier for reducing interspecific gene flow. *Drosophila* males court heterospecific females more frequently than females are sexually receptive to courting heterospecific males, emphasizing the importance of female mate preference in reproductive isolation. The neurogenetic bases of female mate preference have been elusive historically, but recent research identified the *D. melanogaster fruitless (fru)* P2 exon to influence both conspecific and heterospecific female receptivity. I have expanded on these findings by creating a transgenic line that expresses Gal4 under *fru*^{P2} regulation. Driving a fluorescent reporter using this line revealed *fru*^{P2}-neurons in the optic tissues, brain, and ventral nerve cord. Hyperactivating or silencing these neurons significantly decreased female receptivity to conspecific male courtship. The diverse distribution of *fru*^{P2}-neurons and their strong modulating role in female receptivity implies that complex multimodal signalling is integrated to control female copulatory decision-making.

Keywords: sexual isolation, female rejection, CRISPR/Cas9-HDR, Trojan-GAL4-UAS, epi-fluorescent imaging, behavioural neurogenetics

Summary for Lay Audience

Speciation, the splitting of one species into two or more, underlies much of the biological diversity observed on Earth. For speciation to occur, barriers must prevent the exchange of genetic material between speciating groups. Decreased genetic exchange leads to increased differences between groups over time and eventually leads to their complete and irreversible divergence, such that they cannot reunite into a single group. Changes in mate preferences may be one of the first barriers to arise for preventing mating between speciating groups with geographical overlap. In fruitflies, males readily attempt to mate with females of other species, while females more likely reject males from other species, showing that females are the “choosier” sex. However, it is not clear how females decide if they should mate with a prospective male. Decision-making requires information processing in the brain, and development of the brain and central nervous system is dependent on instructions encoded by genes. Thus, investigating how female mating decisions arise requires consideration of both neural and genetic components.

In this project, I used gene editing to make a custom mutant fruitfly for studying neurons expressing a specific gene product, *fru*^{P2}. Disrupting a genomic location unique to *fru*^{P2} was previously found to affect how often females accept mating attempts from males. I predicted that the neurons expressing *fru*^{P2} influence female mating decisions. First, I manipulated these neurons to fluoresce, which allowed them to be mapped in the central nervous system. Second, I manipulated these neurons to increase or decrease in activation, which allowed assessment of their role in female mating decisions. Neurons expressing *fru*^{P2} were found in the eyes, brain, and ventral nerve cord (fruitfly equivalent of a spinal cord). In the ventral nerve cord, neurons expressing *fru*^{P2} were found in regions connecting to the legs, wings, and reproductive organs. Increasing or decreasing activation of these neurons caused females to reject males at significantly higher rates than usual. These findings suggest that neurons expressing *fru*^{P2} transmit sensory information from the eyes, legs, wings, and/or reproductive organs to the brain and influence a female’s decision to accept or reject a prospective male mate.

Acknowledgements

First, I would like to express my most sincere appreciation to my supervisor, Dr. Amanda Moehring. Thank you for all of your cumulative hundreds of hours spent discussing ideas and brainstorming experiments with me, for the incredible guidance and encouragement that has fuelled my growth and confidence as a scientist, and for always having my back. You inspire me to become a better researcher, scientific communicator, and human being altogether.

I am deeply indebted to my advisors Dr. Rob Cumming, Dr. Martin Duennwald, Dr. Ingrid Johnsrude, Dr. Jamie Kramer, and Dr. Anne Simon. Thank you all for your invaluable feedback and advice, and for pushing me to view things from outside of the box. I am extremely grateful to Dr. Martin Duennwald for acting as my interim supervisor and thesis reader. Thank you for your continued guidance and encouragement, and for checking in when things were tough. I also want to extend my gratitude to Dr. Greg Gloor for his microinjection needle puller, Dr. Ben Rubin for his statistical wisdom, and Dr. Jamie Kramer for his assay apparatus design.

Completion of this thesis would not have been possible without my colleagues in the Moehring laboratory. Thank you to Dr. Tabashir Chowdhury for your expertise, encouragement, friendship, and shared love for croissants. This project would literally not exist without you. Thank you to Joshua Zad Isaacson, from whom I learned the microinjection techniques that were indispensable for this project. I hope that you roll natural 20's for all eternity. Big shout out to 'Big O' El-Deeb for braving this storm with me, through thousands of hours of troubleshooting and more. Cheers to Brendad Charles and Amber Kulinski, two of the best friends I could have asked for. Thank you to Sebastian Heine for your time in guiding me through immunostaining, confocal imaging, and basic economics. Last, but absolutely not least, thank you to Ziemniak Jagiello, 'Cash Man Pran' Gandhi, Olivia Siemens, Alannah Mattice, Arshad Panchbhaya, Lucas Khodaei, Sofia Savona-Jofre, Mahsa Farmanbar, Asil El Galad, and all the other Moehring laboratory members of past and present. You all make this lab feel like a second home to me.

Special thanks to all of my friends for the love and support, including the Neuro crew and LNC. Thank you to Shay for your endless care and support throughout this thesis and beyond. Finally, I cannot begin to express my appreciation for my family. Thank you to my mother and father for being the most accepting and supportive of my wildest dreams, whether they were to become a truck driver, to become a starving artist, or to pipette liquids from tube to tube. Thank you to my brother for having to tolerate me for over 20 years, but still always being there for me.

Authorship Statement

Vectors obtained from the *Drosophila* Genomics Resource Center (NIH 2P40OD010949) and *Drosophila* stocks obtained from the Bloomington *Drosophila* Stock Center (NIH P40OD018537) were used in this project. All laboratory work described in this project was performed by me.

Table of Contents

Abstract.....	ii
Summary for Lay Audience.....	iii
Acknowledgements.....	iv
Authorship Statement.....	v
Table of Contents.....	vi
List of Tables.....	ix
List of Figures.....	x
List of Abbreviations, Symbols, and Nomenclature.....	xii
Graphical Overview.....	xvii
1 Introduction.....	1
1.1 Speciation.....	2
1.2 Pre-zygotic isolating barriers.....	3
1.3 Behavioural isolation.....	4
1.3.1 Genetic basis of behavioural isolation.....	5
1.4 <i>Drosophila</i> as a model organism for behavioural isolation.....	5
1.4.1 Male reproductive behaviour.....	6
1.4.2 Female reproductive behaviour.....	7
1.4.3 Female mate preferences and their neural bases in <i>Drosophila</i>	8
1.4.4 Genes underlying heterospecific mate preferences in <i>Drosophila</i>	10
1.4.5 Neurogenetic basis of conspecific mate preference in <i>Drosophila</i>	12
1.5 The <i>fruitless</i> gene.....	14
1.5.1 Sex-specific splice variants of <i>fru</i>	15
1.5.2 Non-sex-specific splice variants of <i>fru</i>	17
1.6 Genetic tools in <i>Drosophila melanogaster</i> for investigating <i>fru</i> ^{P2}	19
1.6.1 CRISPR/Cas9 targeted gene editing.....	19
1.6.2 Gal4-UAS binary expression system.....	21
1.6.3 Trojan-GAL4 for targeting alternatively spliced genes.....	23
1.7 Experimental objectives.....	24
1.7.1 Hypotheses and predictions.....	24
2 Materials and Methods.....	25

2.1 <i>Drosophila</i> husbandry and stocks.....	25
2.1.1 Genetic crosses.....	25
2.2 General molecular and microbiological methods.....	26
2.2.1 Genomic DNA extraction.....	26
2.2.2 Bacterial propagation	26
2.3 Transgenesis of T-GEM using CRISPR/Cas9-mediated HDR.....	26
2.3.1 Design of targeted insertion site.....	28
2.3.2 gRNA expression vector preparation	29
2.3.3 T-GEM donor vector preparation.....	30
2.3.4 Microinjection preparation and protocol.....	32
2.3.5 Screening for successful T-GEM transgenesis.....	34
2.4 Imaging techniques.....	36
2.4.1 Microdissection for extraction of whole central nervous systems.....	36
2.4.2 Epi-fluorescent compound microscopy	36
2.5 Behavioural assay methods	38
2.5.1 Mating assays.....	39
2.5.2 Assay scoring and statistical analysis	40
3 Results.....	41
3.1 Generation of a transgenic line expressing Gal4 in <i>fru</i> ^{P2} -expressing tissues	41
3.2 <i>fru</i> ^{P2} is expressed in female neural tissues	43
3.3 <i>fru</i> ^{P2} -expressing neurons modulate female receptivity.....	47
4 Discussion.....	52
4.1 Transgenic line caveats.....	53
4.1.1 <i>fru</i> ^{P2-T-GEM} captures both <i>fru</i> ^{P1} and <i>fru</i> ^{P2} expression in males	53
4.1.2 <i>fru</i> ^{P2-T-GEM} may feminize Fru ^M proteins in males.....	56
4.1.3 <i>fru</i> ^{P2-T-GEM} captures expression of an identified <i>fru</i> ^{P2} transcript in both sexes..	57
4.1.4 <i>fru</i> ^{P2-T-GEM} may disrupt regulation of downstream <i>fru</i> transcripts.....	58
4.1.5 CRISPR/Cas9 off-targeting.....	59
4.2 Female neuroanatomy of <i>fru</i> ^{P2} -expressing tissues	60
4.2.1 Female optic tissues express <i>fru</i> ^{P2}	60
4.2.2 Female central brain regions express <i>fru</i> ^{P2}	61

4.2.3 Female ventral nerve cord regions express <i>fru</i> ^{P2}	62
4.3 Female receptivity is modulated by <i>fru</i> ^{P2} -expressing neurons	64
4.3.1 Constitutive silencing of <i>fru</i> ^{P2} -expressing neurons reduces receptivity	64
4.3.2 Hyperactivation of <i>fru</i> ^{P2} -expressing neurons reduces receptivity.....	66
4.3.3 Ablation of <i>fru</i> ^{P2} -expressing tissues does not affect receptivity	67
4.4 Future directions	68
4.5 Final conclusions	69
References	71
Supplementary Tables	83
Supplementary Figures	85
Curriculum Vitae.....	95

List of Tables

Table S1. <i>Drosophila</i> stocks obtained from Bloomington <i>Drosophila</i> Stock Centre.....	83
Table S2. <i>Drosophila</i> lines produced in this project	83
Table S3. Primers used for PCR and related Sanger sequencing	84
Table S4. Cas9 target oligonucleotides	84
Table S5. Microinjection mix recipe	84
Table S6. Apple juice agar recipe.....	84
Table S7. Primers used for RT-PCR and related Sanger sequencing	84

List of Figures

Figure 1. Schematics of <i>fruitless</i> genomic locus and alternatively spliced transcripts.....	15
Figure 2. Schematic of the T-GEM construct	27
Figure 3. Method for producing a transgenic line expressing Gal4 under <i>fru</i> ^{P2} regulation.....	28
Figure 4. Schematic of <i>Drosophila</i> CNS anatomy.....	38
Figure 5. Schematic of mating assay apparatus	40
Figure 6. Agarose gel electrophoresis of digested (single cut) pT-GEM ^{phase2} plasmids for verification of homology arm insertions into T-GEM donor vector.....	41
Figure 7. Agarose gel electrophoresis of PCR amplicons generated for verifying successful T-GEM transgenesis into an RFP ⁺ G ₁ fly population.....	42
Figure 8. Agarose gel electrophoresis of RT-PCR amplicons generated from <i>fru</i> transcripts	43
Figure 9. Epi-fluorescent imaging of whole-mounted adult female and male CNSes expressing mCD8::GFP under <i>fru</i> ^{P2} and <i>fru</i> ^{P1} regulation.....	45
Figure 10. Epi-fluorescent imaging of whole-mounted adult male brain expressing mCD8::GFP under <i>fru</i> ^{P2} and <i>fru</i> ^{P1} regulation.....	46
Figure 11. Epi-fluorescent imaging of whole-mounted adult female brain expressing mCD8::GFP under <i>fru</i> ^{P2} regulation	47
Figure 12. Proportion of pairs mated when hyperactivating <i>fru</i> ^{P2} -expressing neurons using TrpA1.....	48
Figure 13. Proportion of pairs mated when silencing <i>fru</i> ^{P2} -expressing neurons using Shibire ^{ts} ..	49
Figure 14. Proportion of pairs mated when silencing <i>fru</i> ^{P2} -expressing neurons using K _{ir} 2.1	50
Figure 15. Proportion of pairs mated when silencing <i>fru</i> ^{P2} -expressing neurons using TeTxLC .	51
Figure 16. Proportion of pairs mated when ablating <i>fru</i> ^{P2} -expressing neurons using Reaper	52
Figure S1. Sexing flies in late-pupal stage by presence or absence of sex combs.....	85
Figure S2. Sanger sequencing chromatogram sample figure with annotations	86
Figure S3. Embryo collection basket apparatus components and assembly.....	86
Figure S4. Embryonic microinjection	87
Figure S5. Epi-fluorescent imaging of late-stage pupae for screening successful transgenesis ..	87
Figure S6. Epi-fluorescent imaging of whole-mounted adult female head for screening successful transgenesis of T-GEM and preliminary verification of Gal4 functionality	88
Figure S7. Dissection pad apparatus	88

Figure S8. Mounting slide apparatus and usage	89
Figure S9. Sanger sequencing chromatogram of PCR amplicon generated for verifying presence and fidelity of the Cas9 target sequence in the injection line genome	89
Figure S10. Sanger sequencing chromatogram of pU6-gRNA+target plasmid for verifying successful insertion of Cas9 target sequence into gRNA expression vector	90
Figure S11. Sanger sequencing chromatograms of pT-GEM ^{phase2} (with 5' and 3'-homology arms) plasmid for verifying successful insertion of 5'-homology arm and 3'-homology arm into T-GEM donor vector	90
Figure S12. Sanger sequencing chromatogram of PCR amplicons for verifying successful transgenesis of T-GEM ^{phase2} into the intron downstream of the P2 exon in an RFP ⁺ G ₁ population	90
Figure S13. Sanger sequencing chromatograms of RT-PCR amplicons from <i>fru</i> ^{P2-T-GEM/TM6B} , <i>Tb</i> ¹ females produced using P2 forward and GAL4 reverse primers	91
Figure S14. Sanger sequencing chromatograms of RT-PCR amplicons from <i>fru</i> ^{P2-T-GEM/TM6B} , <i>Tb</i> ¹ males produced using P2 forward and GAL4 reverse primers	91
Figure S15. Sanger sequencing chromatogram of RT-PCR amplicon from <i>fru</i> ^{P2-T-GEM/TM6B} , <i>Tb</i> ¹ males produced using S forward and GAL4 reverse primers.....	92
Figure S16. Sanger sequencing chromatograms and analysis of RT-PCR amplicon produced from extended <i>fru</i> ^{P2} transcript in <i>fru</i> ^{P2-T-GEM/TM6B} , <i>Tb</i> ¹ females	92
Figure S17. Epi-fluorescent imaging of whole-mounted adult CNSes for <i>fru</i> ^{P2-T-GEM} and UAS- <i>mCD8::GFP</i> genetic controls.....	93
Figure S18. Epi-fluorescent imaging of whole-mounted adult female CNSes expressing <i>mCD8::GFP</i> under <i>fru</i> ^{P2} regulation	94

List of Abbreviations, Symbols, and Nomenclature

List of abbreviations

3xP3	artificially multimerized paired box 6 homeodomain binding site P3/RSC1
7-T	7-tricosene
7,11-HD.....	7,11-heptacosadiene
A-D	<i>fruitless</i> zinc finger-encoding exons A to D
aLN(al).....	antennal mechanosensory and motor center GABAergic local interneuron
AmNp.....	accessory metathoracic neuropils
aPN1.....	antennal mechanosensory and motor center projection neuron 1
BDSC	Bloomington Drosophila Stock Center
BSC	Biological Species Concept
BTB.....	Broad-Complex, Tramtrack, and Bric a brac
C1-C5.....	<i>fruitless</i> common exons 1 to 5
Cas9.....	<i>Streptococcus pyogenes</i> CRISPR-associated protein 9
cDNA	complementary DNA
<i>CG17821</i>	candidate gene 17821
<i>CG5946</i>	candidate gene 5946
CHC	cuticular hydrocarbon
CIP	calf intestinal phosphatase
CNS.....	central nervous system
CO ₂	carbon dioxide
CRISPR.....	clustered regularly interspaced palindromic repeats
CS.....	Canton-S
<i>D. guttifera</i>	<i>Drosophila guttifera</i>
<i>D. melanogaster</i>	<i>Drosophila melanogaster</i>
<i>D. novamexicana</i>	<i>Drosophila novamexicana</i>
<i>D. pseudoobscura</i>	<i>Drosophila pseudoobscura</i>
<i>D. simulans</i>	<i>Drosophila simulans</i>
<i>D. texana</i>	<i>Drosophila texana</i>
<i>D. virilis</i>	<i>Drosophila virilis</i>
DBD	DNA binding domain

DGRC Drosophila Genomics Resource Center
 dm6 *Drosophila melanogaster* Release 6 reference genome
 DMSO dimethyl sulfoxide
 DPBS Dulbecco's phosphate-buffered saline
 DSB double-strand break
dsx *doublesex*
E. coli *Escherichia coli*
 E/I balance excitatory and inhibitory balance
ey *eyeless*
 F₀ parental generation
 F₁ offspring of parental generation
fru *fruitless*
 Fru *fruitless* protein product
fru^{COM} non-sex-specific *fruitless* transcripts
fru^F female-specific *fruitless* transcript starting from P1 exon
fru^M male-specific *fruitless* transcript starting from P1 exon
fru^{P1}-*fru*^{P5} alternatively spliced *fruitless* transcripts
 G₀ injection survivor
 G₁ offspring of injection survivor
GAL4 *Saccharomyces cerevisiae GAL4*
 Gal4 *Saccharomyces cerevisiae GAL4* protein product
GAL80 *Saccharomyces cerevisiae GAL80*
 Gal80 *Saccharomyces cerevisiae GAL80* protein product
 gDNA genomic DNA
 GFP green fluorescent protein
 GRASP general receptor for phosphoinositides 1-associated scaffold protein
 HA homology arm
 HDR homology directed repair
Hsp70 heat shock protein 70
Hsp70pA heat shock protein 70 transcriptional terminator
 IPI inter-pulse interval

K_{ir}2.1 potassium inwardly rectifying channel subfamily J member 2
 L1-L3 lamina monopolar neurons 1 to 3
 LB lysogeny broth
 LC10 lobula columnar 10
 LRGC London Regional Genomics Centre
 mCD8 *Mus musculus* cluster of differentiation 8
 ME756 *fruitless* microexon 756
 mRNA messenger RNA
 NEB New England Biolabs
 NHEJ non-homologous end joining
nonA *no-on-transientA*
 P1-P7 *fruitless* first exons 1 to 7
 p65-AD p65-activating domain
 PAM protospacer adjacent motif
 Pax6 paired box 6
per *period*
pgFAR fatty acyl-CoA reductase gene
ppk *pickpocket*
 QTL quantitative trait locus
 RFP red fluorescent protein
 RNAseq RNA sequencing
RpL32 60S ribosomal protein L32
 S *fruitless* sex specific exon
 S^F *fruitless* sex specific exon, female splicing
 S^M *fruitless* sex specific exon, male splicing
 SA splice acceptor
 SAG sex peptide abdominal ganglion
shibire^{ts} dynamin mutant (temperature sensitive shibire allele 1)
 Shibire^{ts} dynamin mutant (temperature sensitive shibire allele 1) protein product
 SOG suboesophageal ganglion
 SP sex peptide

spin *spinster*
 SPR sex peptide receptor
 SPSN sex peptide sensory neuron
 STE sodium-chloride-Tris-EDTA
SV40 simian vacuolating virus 40
SV40pA simian vacuolating virus 40 transcriptional terminator
 T-GEM Trojan-GAL4 expression module
 T2A *Thosea asigna* 2A-like peptide
 TeTxLC tetanus toxin light chain
tim *timeless*
tra *transformer*
tra-2 *transformer-2*
 TrpA1 transient receptor potential cation channel subfamily A member 1
TβH tyramine-beta-hydroxylase gene
 U6 type III RNA polymerase III promoter
 UAS upstream activation site
 VNC ventral nerve cord
 vpoDN vaginal plate opening descending neuron
 vpoEN vaginal plate opening excitatory neuron
 ZF zinc finger
 φC31 *Streptomyces* phage phiC31 integrase

List of symbols

Hz.....	hertz
°C.....	degrees Celsius
% RH.....	percent relative humidity
% V/V.....	percent volume by volume
PSI.....	pounds per square inch
RCF.....	relative centrifugal force
µg.....	microgram
µL.....	microliter
mL.....	milliliter
µm.....	micrometer
mm.....	millimeter
bp.....	base pairs
kb.....	kilobases
♂.....	male
♀.....	female

Molecular biology nomenclature

Genes

Italic font..... e.g. *gene*, *Gene*, *GENE*

Protein products of genes

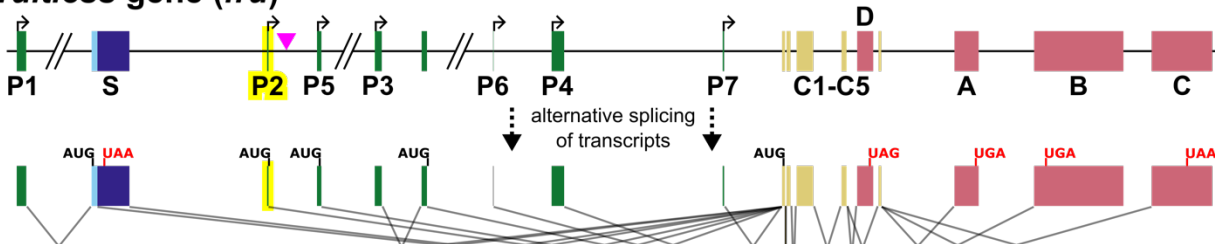
First letter capitalized, normal font..... e.g. Gene, GENE

Plasmid names

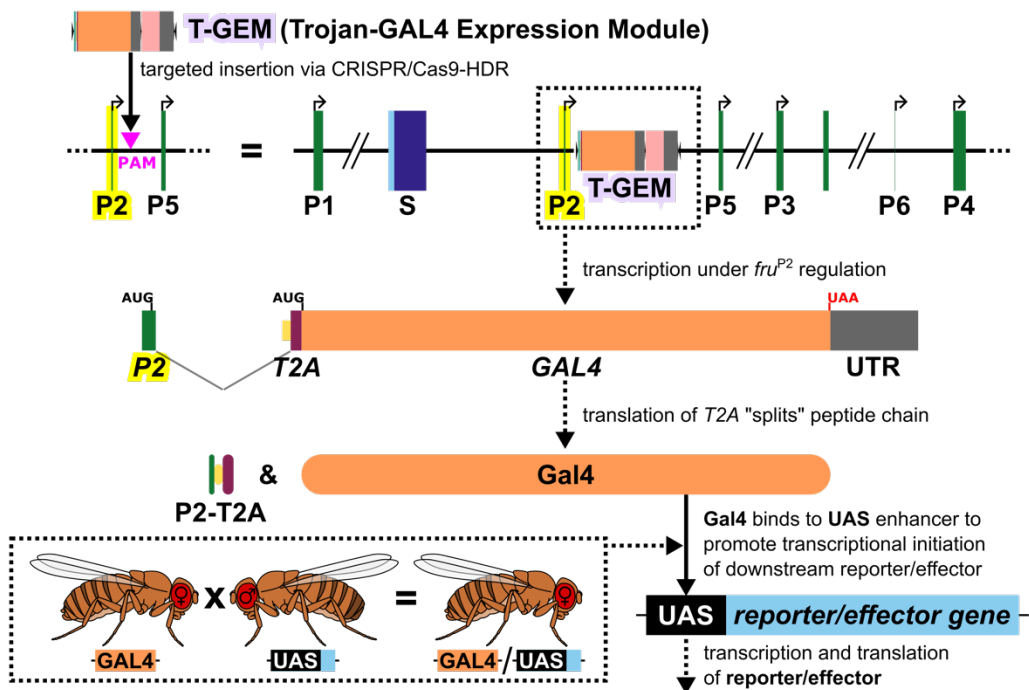
Lowercase p followed by plasmid contents of interest..... e.g. pContents-of-Interest

Graphical Overview

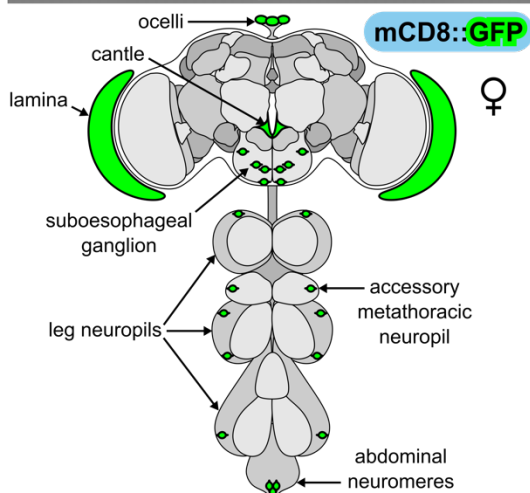
fruitless gene (*fru*)



Creating a transgenic line for genetic manipulation of *fru*^{P2}-expressing cells



What cells express *fru*^{P2} transcripts; do they modulate female receptivity?



- TrpA1** Hyperactivation of *fru*^{P2}-neurons significantly reduces female receptivity.
- Kir2.1** Constitutive, but not inducible, silencing of *fru*^{P2}-neurons significantly reduces female receptivity.
- TeTxLC**
- Shibire^{ts}**
- Reaper** Ablation of *fru*^{P2}-cells does not affect female receptivity and may not abolish mate rejection.

Conclusion *fru*^{P2} transcripts are expressed in neural tissues and have a role in modulating female mate receptivity in response to courting conspecific males.

1 Introduction

Species are broadly described as a distinctly recognizable group of organisms, but the criteria used to distinguish and define an organismal group as a species have been highly debated in speciation biology (Claridge, 2009; Coyne & Orr, 2004). Historically, Carl Linnaeus defined species by observable anatomical characteristics in the *Systema Naturae* (Claridge, 2009; Linné, 1735). In contemporary literature, many species concepts have been proposed and use various criteria for defining species (Coyne & Orr, 2004). Some species concepts from the twentieth century have defined a species as: a group of organisms sharing a single evolutionary lineage (Evolutionary Species Concept; Wiley, 1978), a group of organisms with adaptations for an exact ecological niche (Ecological Species Concept; Van Valen, 1976), a group of organisms capable of exchanging genetic material (Cohesion Species Concept; Templeton, 1989), a group of organisms with a common fertilization system that recognize each other as potential mates (Recognition Species Concept; Paterson, 1985), a group of organisms genetically and/or morphologically discrete from other such groups (Genotypic Cluster Species Concept; Mallet, 1995), or a group of organisms that viably interbreed and are reproductively isolated from other such groups (Biological Species Concept; Mayr, 1942). It is important to recognize that no single species concept should be taken as more objectively correct than others, and that usage of a particular species concept can vary depending on purpose and context (Coyne & Orr, 2004). However, for sexually reproducing organisms, the Biological Species Concept is the prevalent species concept used in recent biological literature and will be used to operationalize “species” in this project.

1.1 Speciation

Speciation is the divergence of one species into two or more reproductively isolated species, and is the process that largely underlies the formation of biodiversity on Earth (Matute & Cooper, 2021). Isolating barriers, also referred to as isolating mechanisms, are a critical aspect of speciation that prevent or greatly reduce genetic exchange (gene flow) between two populations and can lead to reproductive isolation (Coyne & Orr, 2004; Dobzhansky, 1937). Isolating barriers are often categorized into two groups contingent on prevention of gene flow before or after the fusion of male and female gametes to form a zygote, and are aptly termed pre-zygotic and post-zygotic isolating barriers (Coyne & Orr, 2004; Matute & Cooper, 2021). Post-zygotic barriers inhibit gene flow by decreasing hybrid offspring fitness through emergence of one or more maladaptive phenotypes, including behavioural and developmental deficits, sterility, and inviability (Coyne & Orr, 2004; Matute & Cooper, 2021). Pre-zygotic barriers inhibit gene flow by preventing successful copulation with heterospecific (different species) individuals and/or by preventing successful zygote formation (Coyne & Orr, 2004; Matute & Cooper, 2021). The reinforcement hypothesis proposes that natural selection should favour the evolution of pre-zygotic barriers in instances where post-zygotic barriers exist in order to avoid the fitness cost of producing maladaptive hybrids (Coyne & Orr, 1997; Matute & Cooper, 2021). However, experimental evidence has shown that pre-zygotic barriers evolve faster in some speciating groups while post-zygotic barriers evolve at the same rate, or faster, in other speciating groups; and it is likely that the evolutionary order of pre- and post-zygotic barriers varies across groups undergoing speciation (reviewed in Matute & Cooper, 2021). For example, in *Drosophila*, meta-analyses (Coyne & Orr, 1989, 1997) and quantification of isolating barriers in interspecific

crosses (Turissini et al., 2018) predict that, compared to post-zygotic barriers, pre-zygotic barriers evolve faster and are stronger inhibitors of gene flow.

1.2 Pre-zygotic isolating barriers

Pre-zygotic isolating barriers include gametic isolation, mechanical isolation, ecological isolation, and behavioural isolation. Each of these acts through a different mechanism that prevents fertilization from occurring. Gametic isolation occurs when gametes from isolated groups are unable to fuse to form a zygote (Coyne & Orr, 2004). Several steps must occur for motile sperm cells to fertilize an immotile egg; including movement through the female reproductive tract to reach the egg, enzymatic destruction of the egg envelope by action of acrosomal proteins, and membrane fusion with the egg (reviewed in Lobov et al., 2019). Factors that could cause gametic isolation include insufficient sperm motility for reaching the egg, incompatibility between egg membrane ligands and sperm receptors that causes failure for exocytosis of egg membrane-degrading acrosomal proteins, insufficient degradation of the egg membrane, and incompatibilities (currently unidentified) preventing membrane fusion (Lobov et al., 2019). Mechanical isolation occurs when reproductive organs from isolated groups are structurally incompatible or are unable to make physical contact, resulting in prevention of copulation and inability to transfer gametes (Coyne & Orr, 2004). Mismatching genital morphology can prevent genital coupling, as per the lock and key hypothesis (reviewed in Masly, 2011). Differences in gross morphology can also prevent coupling of otherwise compatible genitalia. Ecological isolation occurs when isolated groups are allopatric (geographically isolated), have temporal variance in reproductive maturity or activity (temporally isolated), or are dependent on different vectors for the transfer of gametes (e.g. pollinator isolation; reviewed in Coyne & Orr, 2004). Groups that cannot interact due to geographic features, such as mountain

ranges or oceans, are geographically isolated. Groups that reproduce in different seasons without temporal overlap are temporally isolated. In pollinator isolation, flower species that rely on different pollinating species (such as birds, bees, and butterflies) are reproductively isolated.

1.3 Behavioural isolation

Behavioural isolation, also referred to as ethological or sexual isolation, includes all behavioural differences between isolated groups that prevent the initiation or completion of copulation, and is thought to arise early in the speciation process (reviewed in Coyne & Orr, 1997). The mate recognition underlying behavioural isolation is important in preventing maladaptive heterospecific mating events between sympatric (not geographically isolated) groups (Gunst et al., 2018), especially in groups that are not fully reproductively isolated. Behavioural isolation can include differences in mating rituals and differences in mate preferences. Mating rituals are highly complex, and often species-specific, behaviours that provide conspicuous and intentional multimodal signals for drawing the attention and attraction of appropriate conspecific (same species) mates (Mitoyen et al., 2019). For example, *Schizocosa roverni* and *S. ocreata* (wolf spiders) are not mechanically or post-zygotically isolated, but are behaviourally isolated by differences in male courtship rituals (Stratton & Uetz, 1981). However, components other than the active performance of mating ritual behaviours can also elicit mate preference responses. For example, sympatric *Plethodon* (salamander) species, which share a common courtship ritual, are behaviourally isolated by their preference for conspecific odors (Dawley, 1986). Sexually selected traits can arise rapidly (Lande, 1981) and the co-evolution of these traits and corresponding preferences for these traits can lead to behavioural isolation (Coyne & Orr, 2004; Moehring & Boughman, 2019). The energy expenditure required for

reproduction is often not equal between males and females, and has typically resulted in the sexual selection of traits in males and mate preferences in females (Chenoweth & Blows, 2006).

1.3.1 Genetic basis of behavioural isolation

The genetic bases of behavioural isolation can be examined from two perspectives: the genes underlying the traits and signals that elicit mate preference, and those underlying mate preference itself. In *Ostrinia nubilalis* (corn borer moths) races, allelic differences in the *pgFAR* gene have been identified to influence pheromonal profiles responsible for intra-specific behavioural isolation (Lassance et al., 2010). Research in *Heliconius* butterflies has identified a single quantitative trait locus (QTL) responsible for both production of, and preference for, wing colouration (Merrill et al., 2011). Other research in *Heliconius* has identified the *wingless* gene to influence wing colour pattern traits that are important for discrimination of conspecifics and heterospecifics (Kronforst et al., 2006). In *Gasterosteus aculeatus* (sticklebacks), two QTLs have been identified to be associated with female mate preference for male morphology (Bay et al., 2017). The literature on the genetic basis of behavioural isolation is fairly scarce in many species, primarily due to limitations imposed by genetic toolkit availability.

1.4 *Drosophila* as a model organism for behavioural isolation

The benefits of *Drosophila* as a model organism, relative to vertebrate model organisms, are in cost, time, and space efficacy. *Drosophila* have a small housing footprint, allowing for maintenance of large sample sizes in a cost-effective manner. They also have short generation times, with development from embryogenesis to reproductive maturity requiring as little as nine days at standard ambient temperature (Hales et al., 2015). Their high fecundity allows production of numerous offspring per parent, for which offspring rearing is unnecessary, permitting rapid expansion of populations in an artificial setting (Hales et al., 2015).

Species in the *Drosophila* genus are reproductively isolated from one another at varying degrees and through differing combinations of isolation barriers (reviewed in Nanda & Singh, 2012), making *Drosophila* a popular model organism in speciation biology. Many *Drosophila* sister species pairs are not fully reproductively isolated and can be interbred to produce viable offspring (Carracedo et al., 2000). *Drosophila* species exhibit well-defined, complex, and robust behaviours (defined as the coordinated response to internal and/or external stimuli [Levitis et al., 2009]), making them popular model organisms in behavioural research (Sokolowski, 2001). Additionally, full genome sequencing and genetic toolkits are available in some *Drosophila* species, which are notably expansive in *D. melanogaster*. The combination of these characteristics has made the *Drosophila* genus a prevalent model organism for studying behavioural isolation.

1.4.1 Male reproductive behaviour

To maximize odds of successful copulation, male *Drosophila* must discriminate the species and sexual receptiveness of a potential mate. Both volatile and non-volatile pheromones are used to determine conspecific status and receptivity of a female, and upon sensing a suitable mating partner the male initiates a set of behaviours that are collectively called the courtship ritual (reviewed in Dickson, 2008). The courtship ritual begins with acquiring physical proximity to the potential female mate, usually on a food source (Hall, 1994). The male then physically orients itself toward the female, taps her abdomen using his tarsi, and begins to follow her (Hall, 1994). The male unilaterally extends and vibrates a wing to perform ‘wing song’ that consists of pulses and extended tones (pulse song and sine song, respectively; Shirangi et al., 2013). Performance of the pulse song has been shown to be plastic, and can be adjusted to optimize mating success based on the female’s responding movement speed (Coen et al., 2014). In *D.*

melanogaster the sine song resonates at ~160 Hz (Shorey, 1962). If the female slows locomotion in response to the male's behaviours, he licks the female's genitalia with his extended proboscis (Hall, 1994). This provides the male gustatory input for detection of non-volatile pheromones that can convey information about a female's receptivity. Last, the male bends his abdomen and attempts to copulate with the female (Hall, 1994).

1.4.2 Female reproductive behaviour

In response to a male's courtship ritual the female must gather information to assess her own internal state and to assess whether the male is conspecific and desirable as a mate (Aranha & Vasconcelos, 2018). If the female has not yet reached sexual maturity (several days post-eclosion), she exhibits rejection behaviours (Manning, 1967). If a female has recently mated, has not depleted the stored sperm from a previous mating, or determines that the courting male is not a suitable mate, she also exhibits rejection behaviours (reviewed in Dickson, 2008). These rejection behaviours can include increased locomotion, fending (lateral extension of a leg toward the courting male), ovipositor extrusion, and wing flicking and kicking to decamp a male attempting to mount (Cook & Connolly, 1973). If she determines that the courting male is a suitable mate, she is said to become receptive and slows locomotion, increases abdominal grooming, and assumes a posture where her external genitalia are positioned appropriately for copulation (Aranha & Vasconcelos, 2018; Hall, 1994). This positioning includes the opening of the wings and vaginal plates to physically permit genital contact (Kimura et al., 2008). Following copulation, the female performs a series of post-mating behaviours for 8-10 days that prevent further copulation until their reproductive tract has depleted the deposited sperm (Manning, 1967). Post-mating behaviour are initiated by the transfer of sex peptide (SP) from the male through ejaculatory contents (Liu & Kubli, 2003). The female undergoes several transient

behavioural changes, including changed food preference (Ribeiro & Dickson, 2010), increased aggression (Bath et al., 2017), and unwillingness to copulate.

1.4.3 Female mate preferences and their neural bases in *Drosophila*

Mate preference for conspecifics acts to behaviourally isolate species by preventing maladaptive mating with heterospecific populations, thereby decreasing interspecific gene flow. In *Drosophila* species, it is observed that males are more likely to court heterospecific females than females are willing to become receptive to heterospecific males (Laturney & Moehring, 2012), highlighting the importance of female mate preference and receptivity in behavioural isolation. There is extensive literature on signals that can affect female mate preference and receptivity within and between *Drosophila* species that include visual cues, the male courtship song, and cuticular hydrocarbon (CHC) pheromonal profiles. Recent research has begun to identify the neural architecture underlying perception and processing of these signals (Vaughan et al., 2014; Vijayan et al., 2014; Wang et al., 2021).

Visual signals, such as general locomotive behaviours and conspicuous traits, vary across *Drosophila* species and may contribute to mate preferences (Ferveur, 2010). Previous research has found that *D. simulans* does not mate in darkness while the *D. melanogaster* sister species does (Sakai et al., 2002), implying varying importance of visual cues between *Drosophila* species. It has been found that *D. guttifera* females prefer conspecific males with conspecific wing replacements over conspecifics with *D. melanogaster* wing replacements (Niida & Koshikawa, 2021). In *D. melanogaster*, increased saturation and hue of male wing coloration is associated with decreased copulation latency (Katayama et al., 2014), indicating female preference for wing phenotypes. However, there is virtually no literature on the neural basis of vision-mediated female preference. In males, research has identified that the lobula columnar 10

(LC10) visual projection neurons respond to dynamic visual stimuli with size and movement trajectory resembling other flies, and that silencing of these neurons results in an inability to orient towards a female during courtship (Ribeiro et al., 2018). The LC10 neurons have shared morphology and function between sexes (Ribeiro et al., 2018) and thus may also have a role in female mate preferences and receptivity, but this has yet to be explored.

The courtship song performed during male courtship has species-specific inter-pulse intervals (Shorey, 1962) that females of some species use to determine if a male is conspecific (Ewing & Bennet-Clark, 1968; Talyn & Dowse, 2004). A number of experiments have been conducted to test the importance of courtship song conspecificity using mute (wingless) males. In a study that paired *D. melanogaster* or *D. simulans* females with mute conspecific males, it was found that playing artificial heterospecific song increased mating latency but did not fully impede mating (Ritchie et al., 1999). Likewise, pairing mute *D. simulans* males with *D. melanogaster* females in the presence of artificial *D. melanogaster* courtship song increased heterospecific mating (Immonen & Ritchie, 2012). Research has revealed several neural tracts that underlie auditory-mediated female receptivity. Silencing the antennal mechanosensory and motor center projection neuron aPN1 and/or GABAergic local interneuron aLN(al) decreases response to conspecific courtship song, resulting in decreased female receptivity (Vaughan et al., 2014). In the same study, activity levels of the aPN1 are dependent on the inter-pulse interval (IPI) of artificial courtship songs played (Vaughan et al., 2014), indicating tuning of this single neuron for recognizing species-specific IPI. Recent research has identified the vaginal plate opening excitatory neurons (vpoEN) and descending neurons (vpoDN) as influencing courtship song-mediated female receptivity (Wang et al., 2021). The auditory vpoENs in the brain are

finely tuned to respond to courtship songs of conspecific IPI, and provided excitatory signalling to vpoDNs in the ventral nerve cord (VNC) to control vaginal plate opening (Wang et al., 2021).

Cuticular hydrocarbon pheromonal profiles vary by species across the *Drosophila* genus (Jallon & David, 1987), implying their role as a behavioural isolation barrier. However, *Drosophila* courtship is initiated by males and so the majority of the literature focuses on male mate preferences for female CHC profiles. Male *D. melanogaster* and *D. simulans* distinguish between female conspecifics and heterospecifics based on CHC profiles (Jallon, 1984). Male *D. simulans* flies preferentially court mosaic female *D. melanogaster* flies with a male abdomen, which expresses a CHC profile resembling *D. simulans* females (Coyne & Oyama, 1995). In research on conspecific mate preference, *D. melanogaster* males preferentially court mutant females lacking CHCs in comparison to normal females (Billeter et al., 2009). Variation in *D. melanogaster* male preference for conspecific female CHC profiles has also been observed (Pischedda et al., 2014), indicating that CHC preferences may be dynamic. The literature suggests that CHC profiles are important for male recognition of conspecifics and preferences for CHC profiles may rapidly evolve. There is some information on the neurogenetic basis of gustation-mediated female receptivity. It has been found that silencing gustatory neurons on the legs expressing cation channels *pickpocket 23* (*ppk23*) or *pickpocket 25* (*ppk25*) decrease female receptivity to conspecific males when the most distal antennal segment is absent, indicating that pheromonal cues detected by both the antennae and legs modulate female receptivity (Vijayan et al., 2014).

1.4.4 Genes underlying heterospecific mate preferences in *Drosophila*

Several genes have been identified as candidates for influencing and contributing to behavioural isolation in *Drosophila* species. Since CHC pheromonal profiles have been found to

vary across species and are used to discriminate between conspecifics and heterospecifics, changes in genetic architecture underlying CHC biosynthesis may contribute to behavioural isolation. Perfuming *D. novamexicana* males with *D. texana* males resulted in abolishment of mate rejection by *D. texana* females, and that the *CG17821* candidate gene likely underlies variation in the chemical structure of predominant CHCs in both species (Davis et al., 2021). Recently, the *CG5946* gene was identified to differentially influence production of 7-trisosene (7-T) and 7,11-heptacosadiene (7,11-HD) in *D. melanogaster* and *D. simulans* females (Ward & Moehring, 2021). Hybrid females carrying disrupted *D. melanogaster* *CG5946* (resulting in “unmasked” expression of *D. simulans* *CG5946*) were found to have increased 7-T and decreased 7,11-HD compared to hybrids not carrying the disruption, a CHC profile which more closely resembles that of *D. simulans* females (Ward & Moehring, 2021).

Several circadian genes have been implicated in species-specific behaviours that may contribute to behavioural isolation. The *period* (*per*) and *timeless* (*tim*) genes encode species-specific rhythms that affect courtship song and circadian locomotor activities. Transgenic insertion of *D. pseudoobscura* *per* into *D. melanogaster* flies carrying *per* deficiencies restored rhythmic deficiencies and produced a circadian rhythm and courtship song phenotype resembling that of *D. pseudoobscura* (Petersen et al., 1988). *Drosophila melanogaster* carrying a deficient *tim* allele had rescued, but altered, activity period rhythms after transgenesis of *D. pseudoobscura* *tim* (Noreen et al., 2018). Similarly, insertion of *D. simulans* *per* into *D. melanogaster* *per* deficient mutants resulted in recovery of arrhythmicity and produced flies with courtship songs performed in period lengths resembling *D. simulans* (Wheeler et al., 1991). The *no-on-transientA* (*nonA*) gene has also been identified to encode species-specific information for phase and IPI of courtship song. Transgenic insertion of *D. virilis* *nonA* into *D. melanogaster*

with deleted *nonA* was found to flies that perform courtship songs with phase and IPI similar to *D. virilis* (Campesan et al., 2001).

1.4.5 Neurogenetic basis of conspecific mate preference in *Drosophila*

Several genes have been identified that may influence female receptivity from the male “sender” side. However, there is little information on the genetic architecture underlying female mate preferences from the “receiver” side. Examination of genes and the associated neural processes that influence conspecific female receptivity can provide insight into the neurogenetic basis underlying female discrimination of heterospecific males.

The *spinster* (*spin*) locus influences intraspecific female receptivity (Suzuki et al., 1997). Sexually mature virgin female *spin* mutants had strongly decreased receptivity compared to CS flies and their receptivity was observed to peak two days post-eclosion before rapidly declining (Suzuki et al., 1997). The *spin* gene products are alternatively spliced to produce five splice variants, two of which can be used to rescue the low receptivity observed *spin* mutants (Nakano et al., 2001). Expression of *spin* was found in central nervous system (CNS) surface glial cells and ovarian follicle cells (Nakano et al., 2001). Mosaic analysis of *spin* in the central brain revealed two interneuron clusters, *spin-A* in the suboesophageal ganglion (SOG) and *spin-D* consisting of second-order olfactory neurons, that induced the low receptivity phenotype when homozygous for a *spin* mutant allele (Sakurai et al., 2013). Further, Sakurai et al. (2013) found that knock down of *spin* in olfactory receptor Or47b-expressing neurons, which are known to detect CHCs, partially decreased female receptivity; and that the *spin* neurons in the SOG, which receive gustatory input from the mouthparts and proboscis (Stocker & Schorderet, 1981), may form circuitry with *pickpocket* (*ppk*) neurons that have a role in activating post-mating behaviours (Sakurai et al., 2013).

The genetic and neural bases underlying SP-mediated post-mating behaviours also provides insights into the modulation of female receptivity. Sex peptide receptor (SPR), encoded by the *SPR* gene, is a receptor specific for SP that reduces female receptivity when knocked down (Yapici et al., 2008). A population of eight sex peptide sensory neurons (SPSNs) that co-express (*fruitless*) *fru* and *ppk* are necessary and sufficient for activating post-mating behaviours, and induce post-mating behaviours when silenced (Häsemeyer et al., 2009; Yang et al., 2009). Six of these *fru* and *ppk* co-expressing SPSNs also express *doublesex* (*dsx*; Rezával et al., 2012), a gene important in the sex-determination pathway that is also implicated in modulating post-mating behaviours. Silencing all *dsx*-expressing neurons in females results in their inability to perform post-mating behaviours after successful mating (Rideout et al., 2010). The neurons connecting SPSNs to the brain have been identified as SP abdominal ganglion (SAG) neurons, which are *dsx*-expressing and project into the dorsal protocerebrum in the central brain (Feng et al., 2014). The SAG neurons have a strong role in female receptivity; silencing them in virgin females results in almost complete unreceptivity, while hyperactivating them in recently-mated females increases receptivity (Feng et al., 2014). The vpoDNs identified to induce vaginal plate opening in response to conspecific courtship song were also found to express *dsx*, and it was proposed that signals originating from vpoENs and SPSNs integrate at vpoDNs to modulate receptivity depending on courtship song IPI and a female's internal state (Wang et al., 2021).

In summary, neurons expressing *spin*, *ppk*, *dsx*, and/or *fru* appear to form complex circuitry that integrates olfaction, gustation, and audition to modulate female mate preference and receptivity.

1.5 The *fruitless* gene

The *fru* locus was first identified to influence mating behaviours in x-ray mutagenized flies, of which male flies homozygous for the mutant *fru* allele were observed to court males while unable to successfully copulate with females (Gill, 1963; Hall, 1978). These seminal findings have led to research on the *fru* gene from a primarily male-centric viewpoint for several decades. In recent years, there is increasing evidence that the *fru* gene is also implicated in female receptivity. The observed expression of *fru* in the SP neural circuit implies a potential role in female receptivity, as described above, and recent research from our laboratory has demonstrated that *fru* directly influences both inter- and intra-specific female receptivity (Chowdhury et al., 2020).

The *fru* gene is remarkably complex; it is an expansive 131 kb in size that is alternatively spliced to include two variable regions and encodes for at least 15 different putative zinc-finger transcription factors, some of which are sex-specifically expressed (Figure 1; Goodwin et al., 2000). The variable first exons included in *fru* transcripts are referred to as the “promotor” exons (exons P1 to P7). Transcripts starting with P1 in females also contain a sex-specifically spliced exon, referred to as the “S” exon. The variable first exons are followed by exons common to most *fru* transcripts (“common exons” C1 to C5) with exons C1 to C3 encoding a Broad-Complex, Tramtrack and Bric a brac (BTB; Howe et al., 2021) domain and exons C3 to C5 encoding a connector region. The variable last exons encode for zinc-finger (ZF) motifs (exons A to D). The *fru* splice variants are categorized into five groups based on the first exons included in mature transcripts (termed *fru*^{P1} to *fru*^{P5}; Ryner et al., 1996; Usui-Aoki et al., 2000). The *fru*^{P1} splice variants are sex-specifically spliced and referred to as *fru*^M and *fru*^F for the male-specific

and female-specific variants respectively, while the fru^{P2} to fru^{P5} splice variants are non-sex-specifically spliced and collectively referred to as fru^{COM} (Sato, Goto, et al., 2019).

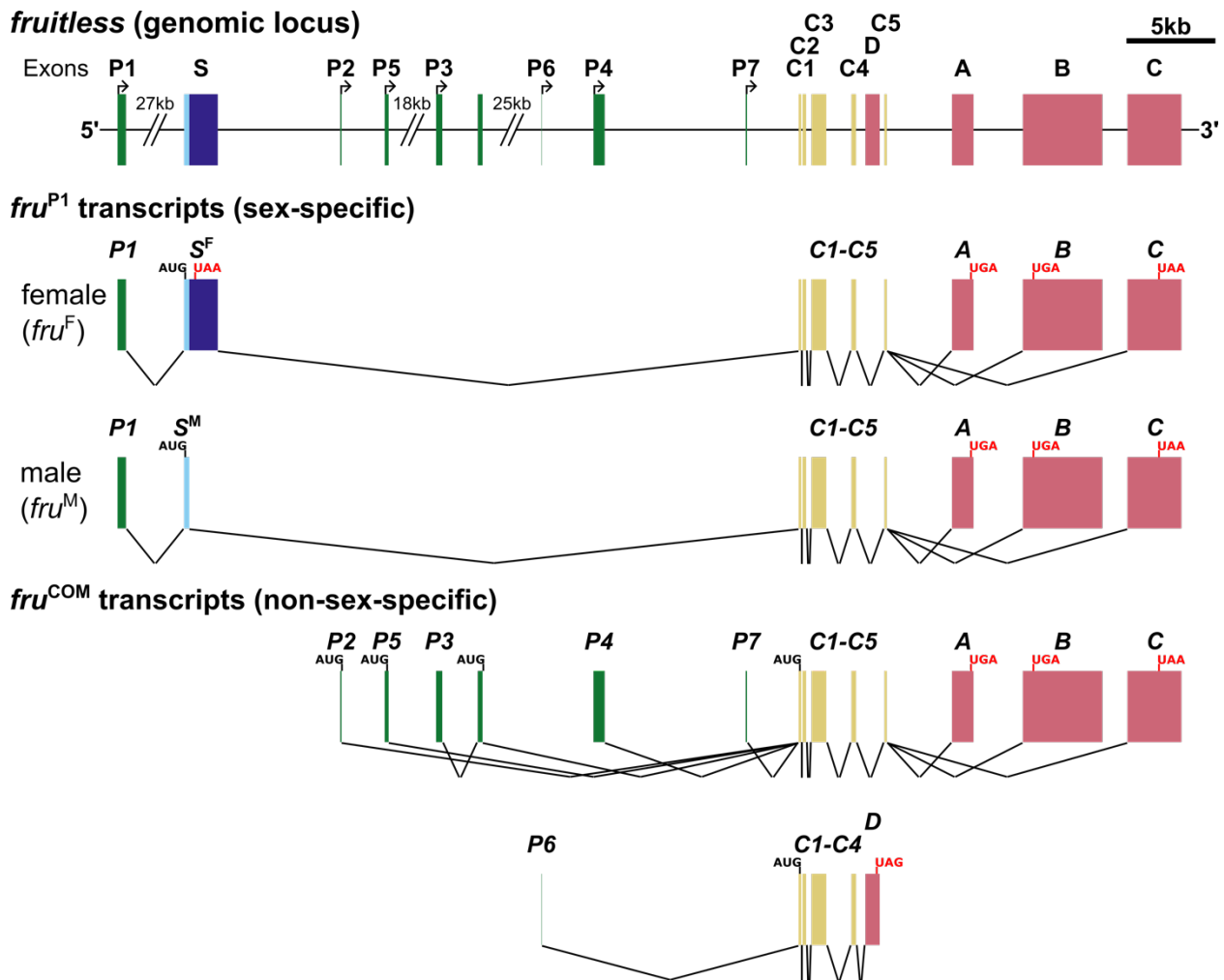


Figure 1. Schematics of *fruitless* genomic locus and alternatively spliced transcripts. Exons are categorized by colour: green (P1-P7) represents the variable first exon(s); blue (S) represents the sex-specifically spliced exon, where the dark blue exon is spliced out in males; yellow (C1-C5) represents the common exons (C1-C3 encodes for the BTB domain); and red (A-D) represents the variable last exon, encoding for a zinc finger domain. Transcriptional start sites are shown as black arrows in the genomic locus schematic. Translational start and stop site codons are denoted in black and red above exons in the transcript schematics. Lines connecting exons in the transcript schematics represent possible splice patterns. Schematics produced using the Release 6 reference genome (Hoskins et al., 2015) and gene product annotation data from FlyBase (Larkin et al., 2021; Matthews et al., 2015).

1.5.1 Sex-specific splice variants of *fru*

The fru^{P1} transcripts are the most thoroughly investigated group of *fru* splice variants and are important in the sex determination pathway and in male courtship ritual behaviours (Stockinger et al., 2005). The immature fru^{P1} transcripts are sex-specifically spliced to produce

male-specific *fru*^M and female-specific *fru*^F by action of *transformer* (*tra*) and *transformer-2* (*tra-2*) protein products (reviewed in Billeter et al., 2006). The *fru*^M splice variant is necessary for formation of the Muscle of Lawrence and male-specific neural circuitry (Nojima et al., 2010; Stockinger et al., 2005), and that *fru*^M is both necessary and sufficient for male courtship behaviours (Stockinger et al., 2005). Cells expressing *fru*^M have also been found to have a role in the regulation of sleep and reproductive behaviours, and are considered decision-making cells for the initiation of courtship ritual behaviours (Chen et al., 2017; Kimura et al., 2008). Spatially, *fru*^M is only expressed in neural tissues (Sato et al., 2019), with high expression in optic lobe neurons that innervate central brain regions associated with visual processes (Stockinger et al., 2005). The LC10 neuronal subgroup has been found to express *fru*^M, and is suspected to facilitate directing of courtship behaviours towards a female target (Ribeiro et al., 2018).

While *fru*^M has been found to have critical roles in the development of male reproductive anatomy and in male courtship behaviours, the female equivalent has not been observed for *fru*^F. In females, Tra and Tra-2 bind to *tra/tra-2* repeat elements located within the S exon to cause female-specific splicing, resulting in transcription of a full-length S exon (S^F), while males do not express *tra*, resulting in male-specific splicing that omits the 3' end of the S exon (S^M; Heinrichs et al., 1998). The full S exon in *fru*^F contains a translational stop that presumably prevents formation of a full peptide containing the BTB, connector, and ZF motifs (Stockinger et al., 2005). Although *fru*^F expression is detectable in adult females (Usui-Aoki et al., 2000), it is not currently known whether *fru*^F transcripts, or their peptide products, have any biological function.

1.5.2 Non-sex-specific splice variants of *fru*

The non-sex-specific *fru*^{COM} splice variants have received far less attention in the literature compared to the sex-specific transcripts. The *fru*^{P3} splice variants have been reported to serve a vital role in development (Anand et al., 2001) and high throughput RNA sequencing (RNAseq) data has shown that the P3 exon is highly expressed in the CNS during larval stages (Leader et al., 2018). It is suspected that these transcripts have a role in guiding motor neuron arborization to muscular tissues, as disruption of these splice variants causes lethality in late-pupal stages due to developmental and locomotor deficits preventing eclosion from the pupal casing (Anand et al., 2001). Little is known about the function of *fru*^{P4} and *fru*^{P5} splice variants, but high throughput RNAseq data has provided some insight on their expected spatial and temporal expression patterns; the P4 exon is expressed in the head, eyes, brain, and ventral nerve cord of both adult males and females, and in the CNS during larval stages; the P5 exon expressed in the head, eyes, brain, and ventral nerve cord of adult males and females as well as in male testis (Leader et al., 2018). The *fru*^{P6} and *fru*^{P7} transcripts have not currently been identified in the literature, but high throughput RNAseq data reports that the P6 exon is expressed in the head, eyes, brain, and ventral nerve cord of both adult males and females, and in the CNS during larval stages; and the P7 exon is expressed in the adult female eyes, brain, VNC, and in the adult male testis (Leader et al., 2018).

The *fru*^{P2} transcripts had no known biological functions until Chowdhury et al. (2020) identified this transcript as playing a key role in both inter- and intra-specific female receptivity. In this work, various disruptions within *fru* were paired with functional *fru* alleles to test for their influence on female receptivity through deficiency mapping in interspecies hybrids. *D. melanogaster* females containing disrupted *fru* (either deletions or disrupting insertions) were

crossed to *D. simulans* males to produce hybrids carrying disrupted *D. melanogaster fru* and normal *D. simulans fru*. Since *D. melanogaster* female preference is dominant over that of *D. simulans*, the removal of the *D. melanogaster* allele in hybrids “unmasks” the expression of *D. simulans fru* at the region homologous to the *D. melanogaster* disruption (Chowdhury et al., 2020). Hybrids carrying variously sized and positioned *D. melanogaster fru* disruptions were used to assess the effect of different genetic regions within *fru* on female receptivity to *D. melanogaster* males (Chowdhury et al., 2020). This research ultimately revealed that hybrid females carrying *D. melanogaster fru* disruptions located on, or near, the P2 exon (therefore expressing *D. simulans fru* at that locus) had decreased receptivity to *D. melanogaster* males in comparison to hybrids carrying no disruptions, signifying that the P2 exon influences heterospecific mate preference (Chowdhury et al., 2020). Further, pure *D. melanogaster* females homozygous for a precise P2 exon deletion exhibited decreased receptivity to conspecific males, signifying that the P2 exon also influences conspecific mate preference (Chowdhury et al., 2020). The spatial expression of *fru*^{P2} transcripts, or their protein products, have not been individually assessed. However, high-throughput RNAseq data has identified expression of the P2 exon in the head, eyes, brain, and ventral nerve cord of adult males and females, but not during development (Leader et al., 2018), implying that *fru*^{P2} is primarily expressed in mature neural tissues.

The *fru* gene was previously studied extensively for its role in the sex differentiation pathway and formation of the male-specific neural circuitry that modulates courtship behaviour, but the research conducted by Chowdhury et al., (2020) is the first to reveal that *fru* can influence female receptivity and is the first to reveal any biological effects of the P2 exon. These findings warrant further investigation of *fru* for its role in female receptivity.

1.6 Genetic tools in *Drosophila melanogaster* for investigating *fru*^{P2}

Drosophila melanogaster was one of the first model organisms to have its genome fully sequenced and annotated (Adams, 2000). An expansive genetic toolkit was developed and made publicly available for *D. melanogaster*, making it one of the most versatile organisms for genetic research. An important aspect of genetic research is the ability to perform genomic modifications to target genes of interest. Historically, transposable elements such as *P*-elements have been extensively used for creating mutant and transgenic lines, and have allowed for much of the seminal work in *Drosophila* genetics to be accomplished (McCullers & Steiniger, 2017). One of the major caveats of *P*-element-mediated transformations is that insertions are random, resulting in the inability to target specific genomic loci and a laborious process of screening transformants to only potentially find one that targets a locus of interest, and only rarely targets it in an ideal location. This is particularly problematic for highly alternatively-spliced genes such as *fru*, where the desired location of insertion is a specific exon rather than the entire gene, and where even insertions into the correct exon may not be ideal if they disrupt regulation of other splice variants. Recent developments in genetic engineering have permitted for high-specificity and high-efficiency genomic modifications, which have been translated for usage in *D. melanogaster*, and can be used to insert genetic constructs that facilitate expression of reporter and effector genes under regulation of endogenous genes of interest.

1.6.1 CRISPR/Cas9 targeted gene editing

Targeted gene editing involves the induction of a DNA double-strand break (DSB) at a specific genetic locus via nuclease activity, followed by hijacking of endogenous DSB-DNA repair systems (Li et al., 2020). One of the predominant systems for targeted gene editing is clustered regularly interspaced short palindromic repeat (CRISPR)/CRISPR-associated protein 9

(Cas9; Li et al., 2020). In a gene editing context, the CRISPR/Cas9 system uses two genetically engineered components, a single-stranded guide RNA (gRNA) that binds to a specific DNA sequence and a Cas9 that creates a DSB through nuclease activity (Li et al., 2020). The Cas9 complexes with a DNA-bound gRNA and, if a protospacer adjacent motif (PAM) is present downstream of the sequence bound by the gRNA, creates a DSB three bases upstream of the PAM (Li et al., 2020). Endogenous DSB-DNA repair mechanisms, including non-homologous end-joining (NHEJ) or homology directed repair (HDR), are then hijacked to either delete genomic material or insert foreign genetic material (Li et al., 2020). NHEJ repair involves ligation of DNA strands via DNA ligase 4 activity and is often used for targeted deletions, while HDR repair involves the ‘copying in’ of genetic information from a template (in a natural setting, often the homologous chromosome) via DNA polymerase activity to repair a damaged DNA strand and is often used for targeted insertions (reviewed in Featherstone & Jackson, 1999). Repair of DNA-DSBs by NHEJ is more efficient but also more prone to errors compared to HDR in both natural and gene editing contexts (Bassett & Liu, 2014). It can produce indels (addition or deletion of several bases) at the repair site(s), can reinsert an intentionally excised DNA fragment, and can insert DNA fragments in either forward or reverse orientations (Bassett & Liu, 2014). In a gene editing context HDR is often used, despite lower efficiency compared to NHEJ, as it does not produce indels and can be used for insertion of large transgenes in the desired orientation (Bassett & Liu, 2014). For HDR-mediated deletions, one DSB can be induced and a template containing homology regions (homology arms) flanking the deletion site can be introduced for repair via HDR. For HDR-mediated insertions, one DSB can be induced and a template containing the insert flanked by homology regions upstream and downstream of the DSB can be introduced for repair via HDR.

Targeted gene editing permits high-fidelity and high-specificity transgenesis, which is crucial when targeting loci-of-interest that are small or closely situated to other genomic elements. The *fru* P2 exon is one example of such a locus. It is 69 bp in length and is 2.4 kb upstream of the adjacent P5 exon, with the *fru*^{P5} regulatory elements (unidentified) presumably located within 2.4 kb. Using CRISPR/Cas9-mediated HDR, the P2 locus can be specifically targeted for transgenesis while minimizing the risk of producing unintended effects.

1.6.2 Gal4-UAS binary expression system

The *fru* P2 exon affects female receptivity (Chowdhury et al., 2020) and is predicted to be expressed in adult neural tissues (Leader et al., 2018). Therefore, both neuroanatomical mapping and neuronal manipulation of *fru*^{P2}-neurons may reveal key insights into the neural circuitry that underlies female receptivity. To efficiently study tissues-of-interest using multiple transgenic reporters and effectors, modular expression systems can be used. The Gal4-UAS system is a powerful modular tool that is commonly used in *D. melanogaster* for targeted expression of transgenes in tissues of interest. The Gal4 protein is a transcription factor endogenous to *Saccharomyces* that recognizes and binds an upstream activation site (UAS) enhancer to promote transcriptional initiation (Brand & Perrimon, 1993). This system has been incorporated into *D. melanogaster* as a tool for targeted gene expression (Brand & Perrimon, 1993) and generally requires three steps. First, the *GAL4* gene is inserted into the *D. melanogaster* genome downstream of the regulatory elements of a gene of interest, resulting in Gal4 expression in tissues that express the gene of interest. Second, a UAS construct containing an effector/reporter gene downstream and adjacent to the UAS enhancer is produced and inserted into the *D. melanogaster* genome. Third, the *GAL4* transgenic line is crossed to the UAS construct transgenic line to produce offspring that carry both *GAL4* and the UAS construct. The resulting

offspring express Gal4 in tissues of interest, which promotes expression of the effector/reporter gene from the UAS in those tissues. This system is highly versatile for several reasons. Many transgenic lines carrying *GAL4* or UAS constructs have been produced and are readily available from *Drosophila* stock centers. The Bloomington Drosophila Stock Center (BDSC) alone currently houses over 8000 *GAL4* lines and over 7000 UAS construct lines. The *GAL4* and UAS constructs can also be located anywhere in the genome, and combinations of multiple *GAL4* and UAS constructs can be used to simultaneously drive multiple effectors and/or reporters. In the individual *GAL4* and UAS construct lines, basal expression is low or non-existent since neither *GAL4* nor UAS are endogenous to *D. melanogaster*.

There are three methods of producing *GAL4* expression in the pattern of a specific gene of interest: *GAL4* can be inserted into the regulatory regions of the gene, *GAL4* can be inserted into the translational start site of the gene (Diao & White, 2012), or the regulatory region of a gene can be cloned and placed upstream of *GAL4* for transgenic insertion into the genome. There are caveats to these approaches. Insertion of *GAL4* into the regulatory regions of a gene may result in *GAL4* expression patterns not fully matching those of the gene, either due to disruption of the regulatory regions or placement of the *GAL4*, such that it cannot be expressed by the full regulatory region. Insertion of *GAL4* into the translational start site of a gene can fully capture the endogenous regulation of the gene of interest; however, it must be precisely inserted to avoid both frameshifts and inclusion of extraneous bases that, once translated, could potentially cause changes to Gal4 conformation that alter or hinder function. Expression of *GAL4* with a cloned regulatory region also may not capture all regulatory elements or may suppressed expression due to positional effects resulting from heterochromatin juxtaposition (Elgin & Reuter, 2013). High specificity insertion of *GAL4* is possible using gene editing strategies, such as the CRISPR/Cas9

system, but is dependent on the presence of PAM motifs and target sequences with minimal possible off-targeting. Targeting a splice variant of an alternatively spliced gene adds further complication; the region downstream of the translational start site may be extremely short, or the translational start site may be located in an exon that is common to multiple splice variant transcripts.

1.6.3 Trojan-GAL4 for targeting alternatively spliced genes

In alternatively spliced genes, an artificial exon containing a splice acceptor (SA) and *GAL4* can be inserted into a coding intron (an intron included in the transcript prior to splicing) to force inclusion of the *GAL4* into the mature transcript. However, splicing-in an artificial exon containing *GAL4* results in fusion of the Gal4 protein within the gene of interest protein product, which can hinder Gal4 function. The solution is to include a viral '2A-like' peptide upstream of the *GAL4*. Translation of a 2A-like sequence causes ribosomal 'skipping' between two particular codons that results in omission of peptide bonding between those corresponding amino acids; importantly, this does not trigger translational termination and the ribosome continues translation after the skipping activity (Diao & White, 2012; González et al., 2011). Translation of the *Thosea asigna* 2A-like peptide (T2A) has been demonstrated to cause ribosomal skipping in *Drosophila* (González et al., 2011), and has been used to produce a Trojan-GAL4 construct that permits expression of Gal4 as a separate protein (Diao & White, 2012). Insertion of an artificial exon containing Trojan-GAL4 into the coding intron immediately downstream of the P2 exon would cause expression of non-fusion Gal4 under full regulation of *fru*^{P2}, which can then be used to drive expression of UAS constructs containing fluorescent reporters or neuronal effectors to neuroanatomically map and manipulate *fru*^{P2} neurons.

1.7 Experimental objectives

The *fru* P2 exon was the first *fru* transcript identified to influence female receptivity to courting males (Chowdhury et al., 2020) and while high throughput RNAseq data predicts expression of the P2 exon in neural tissues, the spatial expression patterns and function of *fru*^{P2}-expressing neurons remain unknown. Here, I expanded on the *fru*^{P2} and behavioural neuroscience research by creating a transgenic model used to anatomically map *fru*^{P2}-neurons and to assess their role in female receptivity in *D. melanogaster*. First, I inserted a Trojan-GAL4 construct into the coding intron downstream of the P2 exon to produce a transgenic line that expresses Gal4 in all *fru*^{P2}-expressing cells. Second, I used this line to drive a fluorescent reporter for anatomical mapping of *fru*^{P2}-expressing tissues. Third, I used this line to drive effector proteins that hyperactivate or silence *fru*^{P2}-neurons to assess their role in modulating female receptivity.

1.7.1 Hypotheses and predictions

I hypothesized that *fru*^{P2} is expressed in neural tissues, and that tissues expressing *fru*^{P2} modulate female receptivity. In females, *fru*^{P2} is predominantly expressed in neural tissues with highest expression in the eyes (Leader et al., 2018). Higher expression in sensory organs relative to the brain suggests that *fru*^{P2} neurons in the eyes afferently synapse non-*fru*^{P2} expressing brain regions to modulate receptivity behaviour. Thus, I predicted that *fru*^{P2} neurons are localized in photoreceptor neurons, optic lobe tissues, and their connecting afferent tracts; and that hyperactivation or silencing of *fru*^{P2} neurons results in altered sexual receptivity to courting conspecific males.

2 Materials and Methods

2.1 *Drosophila* husbandry and stocks

All *Drosophila* stocks were maintained on standard recipe cornmeal food media (BDSC) in Fisherbrand™ AS-273 vials under a 14 hour light/10 hour dark cycle at 25 °C and 70% relative humidity (% RH). Virgin flies were obtained by sexing and collecting flies in late-pupal stage. Female pupae were identified by screening for absence of sex combs (Figure S1), followed by verification of sex post-eclosion. All anesthetic treatment was performed on CO₂ pads with ~30 PSI flow rate. See Table S1 for a comprehensive list of *Drosophila* stocks with full genotypes obtained from BDSC for this project. Balancer chromosomes are an invaluable tool in *Drosophila* genetic research; they are used to suppress recombination events and maintain heterozygosity of their homologous chromosome through lethality of recombinant products (Miller et al., 2019). A general use balancer line was obtained (BDSC #3703) and crossed with Canton-S (CS) wildtype flies to produce balancers lines carrying wildtype chromosomes (bal-w⁺ and bal-3; Table S2).

2.1.1 Genetic crosses

Virgin F₀ (parental) female flies and F₀ male flies of desired genotypes were obtained and aged for 2-7 days. For general crosses, F₀ flies were paired (1-5 females, 1-5 males) in fresh food vials and removed when late-stage pupae were observed. For propagation of flies for behavioural assaying, pairings consisted of 2 females and 3 males to ensure consistent larval density. Cotton plug was positioned approximately 30 mm from surface of the food for the first 3-5 days to promote interactions between flies, after which the cotton was repositioned to the top of the vial. After 7-10 days, F₀ flies were removed to prevent mating between F₀ and F₁ (offspring) flies.

2.2 General molecular and microbiological methods

All reagents and kits obtained from a scientific supplier were used as per manufacturer protocols, unless otherwise specified. The *Drosophila melanogaster* Release 6 (dm6; Hoskins et al., 2015) was used as the reference genome for this project. All Sanger sequencing was performed by the London Regional Genomics Centre and alignments were performed using Benchling Biology Software (2021). See Figure S2 for chromatogram legend for interpretation of supplementary Sanger sequencing chromatogram figures.

2.2.1 Genomic DNA extraction

Tissue(s) of interest were homogenized in sodium-chloride-Tris-EDTA (STE) buffer with 0.2 mg mL⁻¹ proteinase K and incubated in a BioRad MyCycler™ Thermal Cycler at 37 °C for 30 minutes, followed by incubation at 95 °C for 3 minutes for heat inactivation of proteinase K.

2.2.2 Bacterial propagation

Bacterial stock (permanent culture, working culture, or overnight culture) was quadrant streaked on 100 µg mL⁻¹ ampicillin lysogeny broth (LB) agar plates and incubated overnight at 37 °C. Single colonies were picked and used to inoculate LB broth with 100 µg mL⁻¹ ampicillin, followed by overnight incubation at 37 °C with orbital rotation or rocking. Sterile technique was used for all steps.

2.3 Transgenesis of T-GEM using CRISPR/Cas9-mediated HDR

CRISPR/Cas9-mediated HDR was used for targeted insertion of the T-GEM construct (Figure 2; Diao et al., 2015) into the first coding intron downstream of the P2 exon (Figure 3). The T-GEM construct encodes for an artificial exon containing a splice acceptor (SA), a linker region to compensate for frameshifts resulting from splice phasing, Trojan-GAL4 (*T2A* and *GAL4*), and an *Hsp70* polyadenylation terminator (*Hsp70pA*). Transcripts containing this

artificial exon are translated to produce Gal4 as a non-fusion protein, which drives transcription of UAS-constructs for expression of effector and/or reporter proteins. T-GEM also encodes for artificially multimerized paired box 6 (Pax6) homeodomain binding site P3/RSC1 (3xP3; (Bischof et al., 2007; Sheng et al., 1997) promoted expression of red fluorescent protein (RFP) in tissues that express *eyeless* (*ey*, a *Pax6* homolog), which in adults includes photoreceptors (Sheng et al., 1997) and various brain regions (Callaerts et al., 2001); proceeded by a *SV40* polyadenylation terminator (*SV40pA*). The 3xP3-promoted *RFP-SV40pA* is expressed in a pattern independent of the Trojan-GAL4 and acts solely as a visible marker (red fluorescence in the eyes) for T-GEM for detecting presence in the genome and for indicating successful transgenesis.

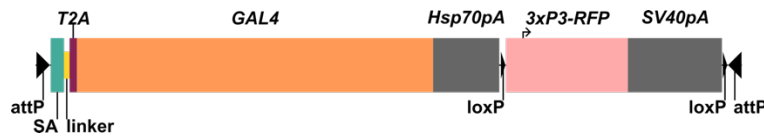


Figure 2. Schematic of the T-GEM construct. T-GEM includes inverted attP sites at the 5'- and 3'-ends for ϕ C31 integrase-mediated cassette exchange to replace T-GEM contents other genetic constructs, splice acceptor (SA) for incorporating linker-*T2A-GAL4-Hsp70pA* into mature transcripts during alternative splicing, linker for correcting frameshifts to prevent transcription of *T2A-GAL4-Hsp70pA* in an incorrect reading frame, *T2A* for production of Gal4 as a separate protein through ribosomal skipping during translation, *GAL4* transcription factor for promoting transcriptional initiation at UAS sites, 3xP3-*RFP* as a visible marker for detecting presence of T-GEM in the genome and/or for detecting successful transgenesis of T-GEM (flanked by *loxP* sites for Cre recombinase mediated excision), and *Hsp70pA* and *SV40pA* terminators to signal transcriptional termination and polyadenylation of *GAL4* and *RFP* transcripts, respectively. Adapted from Diao et al. (2015).

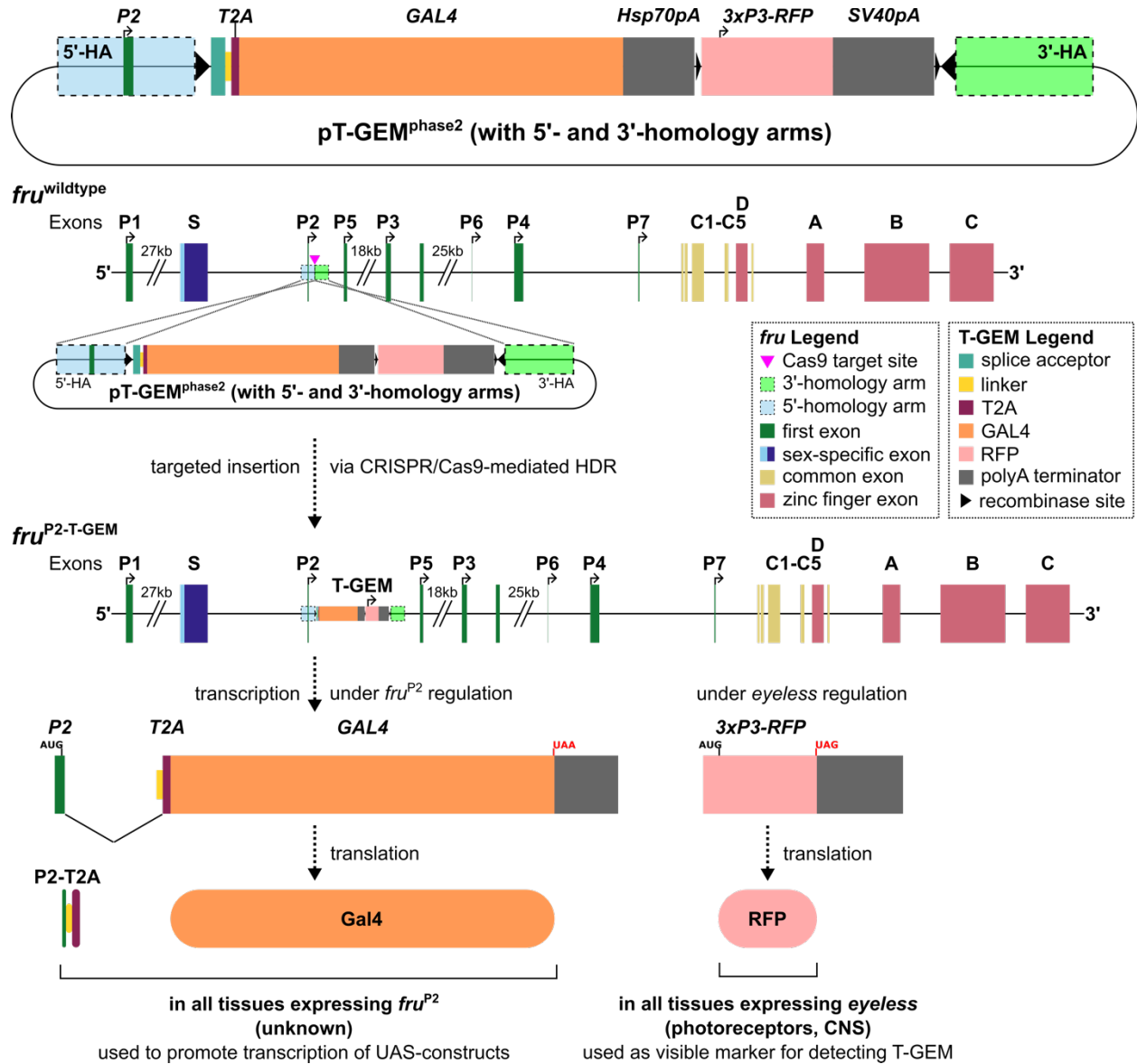


Figure 3. Method for producing a transgenic line expressing Gal4 under *fru*^{P2} regulation. The T-GEM construct is inserted into the coding intron downstream of the P2 exon using CRISPR/Cas9-mediated homology directed repair with the pT-GEM^{phase2} donor vector containing homology arms corresponding to regions flanking the Cas9 target site as a repair template, resulting in production of *fru*^{P2-T-GEM}. Transcription under *fru*^{P2} regulation produces a P2-linker-T2A-GAL4-Hsp70pA transcript, which is translated to produce non-fusion Gal4 in all *fru*^{P2}-expressing tissues for promoting transcription initiation at UAS sites. Transcription under *eyeless* regulation produces an RFP-SV40pA transcript, which is translated to produce RFP in photoreceptor and CNS tissues as a visible marker for detecting presence of T-GEM in the genome, indicating successful transgenesis.

2.3.1 Design of targeted insertion site

Potential target sequences 20 nucleotides in length with an NGG protospacer adjacent motif (PAM) within the first coding intron downstream of the P2 exon were accrued using the *CRISPR Optimal Target Finder* (Gratz et al., 2014). Targets with more than one predicted off-

target were excluded. The highest efficiency target was selected using *E-CRISP* (Heigwer et al., 2014), hereafter referred to as the Cas9 target (sequence 5'-GGCCGGGCCGTGTCATGGAA-3' with downstream PAM of TGG). A transgenic line ubiquitously expressing Cas9 and carrying a mutant *DNAIigase4* allele, to decrease NHEJ event occurrence, was obtained (BDSC #58492); hereafter referred to as the injection line. DNA was extracted from injection line flies and a region containing the Cas9 target was amplified using Invitrogen™ AccuPrime™ SuperMix II with primer set tgt_seq (Table S3). Amplicons were Sanger sequenced to confirm presence and fidelity of the Cas9 target in the injection line.

2.3.2 gRNA expression vector preparation

The pU6-3-gRNA expression vector (Gratz et al., 2014) was obtained as an *Escherichia coli* DMSO stock from the Drosophila Genomics Resource Center (DGRC) and propagated. Plasmids were extracted using an Invitrogen™ PureLink™ Quick Plasmid Miniprep Kit. Extracted pU6-3-gRNA was digested using BsaI (NEB), followed by phosphatase treatment using calf intestinal phosphatase (CIP; NEB). The fragment excised by digestion was removed through agarose gel electrophoresis and subsequent gel extraction using a Monarch® DNA Gel Extraction Kit. Sense and antisense oligos of the target sequence, including nucleotides for producing sticky ends complementing those produced by BsaI digestion of pU6-3-gRNA, were synthesized with 5'-phosphorylation by Eurofin (Table S4). Oligos were annealed by incubating at 95 °C for 5 min followed by decrement to 25 °C at a rate of 0.1 °C sec⁻¹ in 1X T4 DNA Ligase Reaction Buffer (NEB) in a BioRad Thermal Cycler. The produced double stranded target sequence oligonucleotide was ligated into the purified digested pU6-3-gRNA using T4 ligase (NEB) in a BioRad Thermal Cycler with the following program: 1x (25 °C for 30 minutes), 16x (16 °C for 15 minutes, 4 °C for 15 minutes), indefinite hold at 4 °C. The pU6-3-gRNA plasmid

with Cas9 target (hereafter referred to as “pU6-gRNA+target”) was transformed into NEB 10-beta competent *E. coli*. Potential transformant colonies were propagated and plasmids were extracted using a PureLink Miniprep Kit. Obtained plasmids were Sanger sequenced and aligned to a theoretical assembly of pU6-gRNA+target to verify successful cloning of the Cas9 target oligo into the gRNA scaffold vector. Successful transformants were propagated and stored in 50% V/V glycerol at -80 °C as permanent stocks, or at -20 °C as working stocks.

2.3.3 T-GEM donor vector preparation

Genomic regions approximately 1 kb upstream and downstream of the predicted Cas9 cut site were amplified from the injection line to produce homology arms (HAs) using Thermo Scientific™ Phusion™ High-Fidelity DNA Polymerase with primer sets 5arm and 3arm (Table S3). These primers contained additional bases at the 5'-ends for adding restriction enzyme sites and buffer bases (for optimizing restriction enzyme activity at the ends of linear DNA) to the HA amplicons. The HA amplicons were double digested (AgeI-HF [NEB] and NotI-HF [NEB] for the 5'-HA, and AscI [NEB] and SpeI [NEB] for the 3'-HA) to remove buffer bases and to produce sticky ends for cloning into the T-GEM construct plasmid, and column purified using a Monarch® PCR & DNA Cleanup Kit to remove excised fragments.

A plasmid containing the T-GEM construct for phase 2 splicing was obtained (pT-GEM^{phase2}; Diao et al., 2015) as an *E. coli* DMSO stock from DGRC, and propagated. Plasmids were extracted and double digested using AgeI-HF (NEB) and NotI-HF (NEB) for insertion of the 5'-HA, dephosphorylated with QuickCIP (NEB), and column purified with a Monarch Cleanup Kit to remove the small fragment excised by double-digestion. The prepared 5'-HA was ligated into the purified double-digested pT-GEM^{phase2} using T4 ligase (NEB) in a BioRad Thermal Cycler with the following program: 1x (25 °C for 30 minutes), 16x (16 °C for

15 minutes, 4 °C for 15 minutes), indefinite hold at 4 °C. The pT-GEM^{phase2} (with 5'-HA) was transformed into NEB 10-beta competent *E. coli* and potential transformant colonies were propagated. Plasmids were extracted from aliquots of potential transformant cultures using a PureLink Miniprep Kit, single-digested with NheI (NEB), resolved on a 0.5% agarose gel for verification of successful cloning by plasmid size, and further verified by Sanger sequencing and subsequent alignment to a theoretical assembly of pT-GEM^{phase2} (with 5'-HA). Successful transformants were propagated.

The pT-GEM^{phase2} (with 5'-HA) was extracted using a PureLink Miniprep Kit and double digested using AscI (NEB) and SpeI (NEB) for 3'-HA insertion, dephosphorylated with QuickCIP (NEB), and column purified with a Monarch Cleanup Kit to remove the small fragment excised by double-digestion. The prepared 3'-HA was ligated into the purified double-digested pT-GEM^{phase2} (with 5'-HA) using T4 ligase (NEB) in a BioRad Thermal Cycler with the following program: 1x (25 °C for 30 minutes), 16x (16 °C for 15 minutes, 4 °C for 15 minutes), indefinite hold at 4 °C. The pT-GEM^{phase2} (with 5'-HA and 3'-HA) was transformed into NEB 10-beta competent *E. coli* and potential transformant colonies were propagated. Plasmids were extracted from aliquots of potential transformant cultures using a PureLink Miniprep Kit, single-digested with NheI (NEB), resolved on a 0.5% agarose gel for verification of successful cloning by plasmid size, and further verified by Sanger sequencing and subsequent alignment to a theoretical assembly of pT-GEM^{phase2} (with 5'-HA and 3'-HA). Successful transformants were propagated and stored in 50% V/V glycerol at -80 °C as permanent stocks, or at -20°C as working stocks.

2.3.4 Microinjection preparation and protocol

The pU6-gRNA+target and pT-GEM^{phase2} (with 5'-HA and 3'-HA) *E. coli* cultures were both propagated, and plasmids were extracted using a PureLink Miniprep Kit using 3 mL of liquid culture per miniprep. The plasmids were concentrated using a Qiagen® QIAprep® Spin Miniprep Kit by binding >30 µg of purified plasmid to a spin column using PB buffer, followed by wash steps as per manufacturer protocol and elution with Invitrogen™ UltraPure™ DNase/RNase-Free Distilled Water. Generic blue food dye was filter-sterilized using a Whatman® Puradisc™ 0.2 µm filter and an autoclave-sterilized glass syringe. A microinjection mix comprised of pU6-gRNA+target, pT-GEM^{phase2} (with 5'-HA and 3'-HA), filter-sterilized food dye, and Ultrapure Water was made (see Table S5 for full recipe), gently vortexed, and centrifuged at 16000 RCF for 15 minutes to pellet any solids. The supernatant was decanted, aliquoted, and stored at -20 °C until used for microinjection.

A novel embryo collection apparatus was crafted from a Falcon 50 mL conical tube (as funnel and holder) and synthetic sheer ribbon (as filter; Figure S3). Loading needles were prepared by heating and hand stretching 1.0 mm inner diameter borosilicate capillary tubes (FHC) over a Bunsen burner. Injection needles were prepared from 0.75 mm ID borosilicate capillary tubes (FHC) using a Sutter Instrument Micropipette Puller P-97 (courtesy of Greg Gloor). The unstretched end a loading needle was inserted into a rubber bulb for aspiration of microinjection mix and subsequent transfer into injection needles. Approximately 1000 injection line flies were transferred into an embryo collection cage (Genesee Scientific) with active yeast paste smeared on an apple juice agar petri dish (hereafter referred to as apple yeast plate; see Table S6 for recipe). The apple yeast plates were changed to permit feeding ad libitum.

Prior to the first round of injection, the apple yeast plate in the embryo collection cage was replaced every 20 minutes for an hour prior to acclimate the flies to plate changing. Following this acclimation period, plates were changed 30 minutes prior to the next injection round. A wash bottle containing deionized water was used to dislodge and wash embryos from the previous apple yeast plate into the embryo collection basket apparatus (Figure S3). Embryos were collected from the basket using a fine synthetic paintbrush and aligned on a 22 x 22 mm glass coverslip, with embryos positioned laterally adjacent to neighboring embryos and with posterior ends facing one edge of the coverslip (Figure S4). Embryos that had visibly reached cellularization, the developmental change from a single multinucleate cell into a multicellular blastoderm (Lecuit & Wieschaus, 2000), were excluded. The coverslip with aligned embryos was air desiccated for approximately 5 minutes to evaporate excess water and to allow adhesion of the embryos to the coverslip surface. During this time, an injection needle was filled with the prepared microinjection mix using a loading needle and installed into a Sutter Instrument ZenoWorks Digital Microinjector. Following desiccation, the embryos were coated with generic extra-virgin olive oil and positioned for injection under a Nikon SMZ1500 stereoscopic microscope. The injection needle was opened and injection mix was injected into the posterior end of each embryo (Figure S4). Microinjector settings were adjusted to prevent backflow but varied for each round of injection due to variability in the gauge of injection needle tips. Embryos observed to have reached cellularization prior to injection were sacrificed and removed.

Olive oil was gently rinsed off of the injected embryos using deionized water from a wash bottle, and excess water was wicked using Kimtech Science™ Kimwipes™ Delicate Task Wipers. The cover slip was placed into a standard cornmeal food vial with anterior ends of the embryos oriented towards the food and positioned 1-2 mm from the food surface. Vials

containing embryos were incubated under a 14-hour light/10-hour dark cycle at 25 °C with 70% RH until reaching late-pupal stage. At late-pupal stage, the microinjection survivor (G_0) pupae were sexed and separated into individual vials to ensure virginity.

2.3.5 Screening for successful T-GEM transgenesis

The G_0 pupae that survived until adulthood were crossed to BDSC #3703 balancer flies to introduce third chromosome balancers for preventing possible loss of the integrated T-GEM construct. The resulting G_1 progeny were phenotypically screened at late-pupal stage for presence of the T-GEM visible marker 3xP3-RFP (RFP in the eyes) using a Zeiss StereoLumar V12 fluorescent dissecting microscope (Figure S5). Populations with ~50% RFP⁺ individuals were maintained for further verification of successful transgenesis. Successful insertion of the T-GEM construct into the targeted genomic locus was verified via PCR using Invitrogen™ Platinum™ SuperFi II PCR Master Mix with primer set ins_ver (Table S3) and subsequent agarose gel electrophoresis, and further verified with Sanger sequencing and subsequent alignment to a theoretical assembly of *fru* with T-GEM. Transgenic flies were backcrossed to bal-3 balancer flies to produce the genotype +; +; TI{*RFP*^{3xP3.PB=T-GEM}}*fru*^{P2-TG4.2/TM6B}, *Tb*¹ (hereafter referred to as *fru*^{P2-T-GEM}). The *fru*^{P2-T-GEM} flies were crossed to flies carrying UAS-linked nuclear green fluorescent protein (BDSC #4775) for preliminary verification of Gal4 functionality (Figure S6).

Virgin *fru*^{P2-T-GEM} and CS wildtype flies were sexed, collected, and aged for 3-5 days for RNA extraction. RNA extractions were performed in an RNase-free environment; surfaces, gloves, and pipettes were treated with Thermo Scientific™ RNase AWAY™ Surface Decontaminant. All centrifugation steps were performed at 12000 RCF in a 4 °C environment. Flies were placed in a 1.5 mL microcentrifuge tube, flash frozen using liquid nitrogen, and

homogenized in 1 mL Invitrogen™ TRIzol™ Reagent using a sterile microcentrifuge tube pestle. Tissue was pelleted by centrifugation for 10 minutes. The supernatant was decanted into a new microcentrifuge tube, incubated at room temperature for 5 minutes, and 200 µL of chloroform (Sigma Aldrich) was added. Samples were mixed by shaking, followed by incubation at room temperature for 3 minutes. The liquid phases were separated by centrifugation for 15 minutes. The colourless aqueous phase containing RNA was retained, 500 µL of anhydrous isopropanol was added to precipitate the RNA, and samples were mixed by inverting. Following incubation at room temperature for 10 minutes, the RNA was pelleted by centrifugation for 10 minutes and the supernatant was discarded. The nucleic acid pellet was washed with 1 mL of 75% V/V ethanol, re-pelleted by centrifugation for 5 minutes, and the supernatant was discarded. The RNA pellet was air desiccated in a fume hood, reconstituted in Ultrapure Water, and stored at -80 °C.

The extracted RNA was used for reverse transcription PCR (RT-PCR; PCR amplification of cDNA products). Complementary DNA (cDNA) was synthesized from total messenger RNA (mRNA) using a Thermo Scientific™ Maxima H Minus First Strand cDNA Synthesis Kit or an Invitrogen™ SuperScript™ IV First-Strand Synthesis System kit, with Thermo Scientific™ dsDNase treatment and Oligo(dT)₂₀ primers in a BioRad Thermal Cycler. The cDNA was PCR amplified using SuperFi II PCR Master Mix with forward primers binding to the P1, SS, or P2 exons (primer names P1, SS, and P2, respectively) and reverse primers binding to *GAL4* or the C3 exon (primer names GAL4 and COM3, respectively). Amplification of the 60S ribosomal protein L32 gene (*RpL32*) using primers spanning an exon-exon junction (primer names RpL32 Forward and RpL32 Reverse, respectively) was also performed as a type II error control and for detection of genomic DNA (gDNA) contamination (99 bp band indicates amplification of mRNA, 161 bp band indicates amplification of gDNA). See Table S7 for full list of RT-PCR

primers used. RT-PCR amplicons were visualized by agarose gel electrophoresis and bands were extracted using a Monarch Gel Extraction Kit. Extracted bands were Sanger sequenced and aligned to a theoretical assembly of *fru*^{P2-T-GEM} to verify in-frame inclusion of *T2A-GAL4* into *fru* transcripts and to analyze splicing of unexpected transcripts (see Results, below).

2.4 Imaging techniques

The *fru*^{P2} spatial expression patterns were characterized by crossing *fru*^{P2-T-GEM} females to BDSC #5137 males to drive expression of a membrane-bound green fluorescent protein (mCD8::GFP) in *fru*^{P2}-expressing tissues. Whole CNSes were extracted by microdissection and visualized with epi-fluorescent microscopy to determine the localization of *fru*^{P2}-expressing tissues.

2.4.1 Microdissection for extraction of whole central nervous systems

SYLGARD™ 184 Silicone Elastomer was prepared according to manufacturer instructions and used to coat the round well of a 75 x 44 x 6 mm glass slide (Figure S7). The silicone elastomer was cured in a fume hood for >48 hours. The dissection pad was filled with cold 1x DPBS. Adult flies were anesthetized on a CO₂ pad followed by cuticle dewaxing in 80% V/V ethanol for 3-5 seconds. Flies were briefly rinsed in cold 1x DPBS, then placed on the dissection pad. Dissections were performed using two pairs of Dumont No. 5 forceps. All non-CNS tissues, including trachea, were removed. Full dissections were performed within a 20-minute period for immediate downstream epi-fluorescent imaging.

2.4.2 Epi-fluorescent compound microscopy

Two 22 x 22 mm glass cover slips were affixed to a glass slide approximately 10 mm apart with clear nail varnish (Figure S8A), hereafter referred to as the bridging cover slips. Nail varnish was allowed to dry for >24 hours. A microdissected adult CNS (brain and ventral nerve

cord) was transferred from dissection pad to the area in between bridging cover slips on the prepared mounting slide by grasping the cervical connective using a pair of Dumont No. 5 forceps. An 18 x 18 mm cover slip was placed on top of the bridging cover slips to ensure no direct contact with the CNS (Figure S8B). Cold 1x DPBS was pipetted under the 18 x 18 mm cover slip to submerge the CNS (Figure S8C). All epi-fluorescent imaging was done using a Nikon Eclipse Ci-L microscope with Nikon CI-FL epi-fluorescence attachment (GFP-B/FITC-B and TRITC/CY3-G fluorescent filter cubes for GFP and RFP imaging, respectively), Lumencore Sola SM5-LCR-SA Light Engine, and Nikon C-PH Phase Contrast Turret Condenser. Nikon DS-U2 camera control unit, Nikon DS-Fi1 camera, and *Nikon Elements-Documentation* software was used to capture raw images. Image capturing was standardized with the following parameters: 1.0x gain, 2.0 sec exposure, and 0 neutral-density (ND). All images were processed using *Fiji/ImageJ* and annotated in *Microsoft Word* or *Inkscape*. See Figure 4 for schematic of *Drosophila* CNS anatomy used to map fluorescent expression.

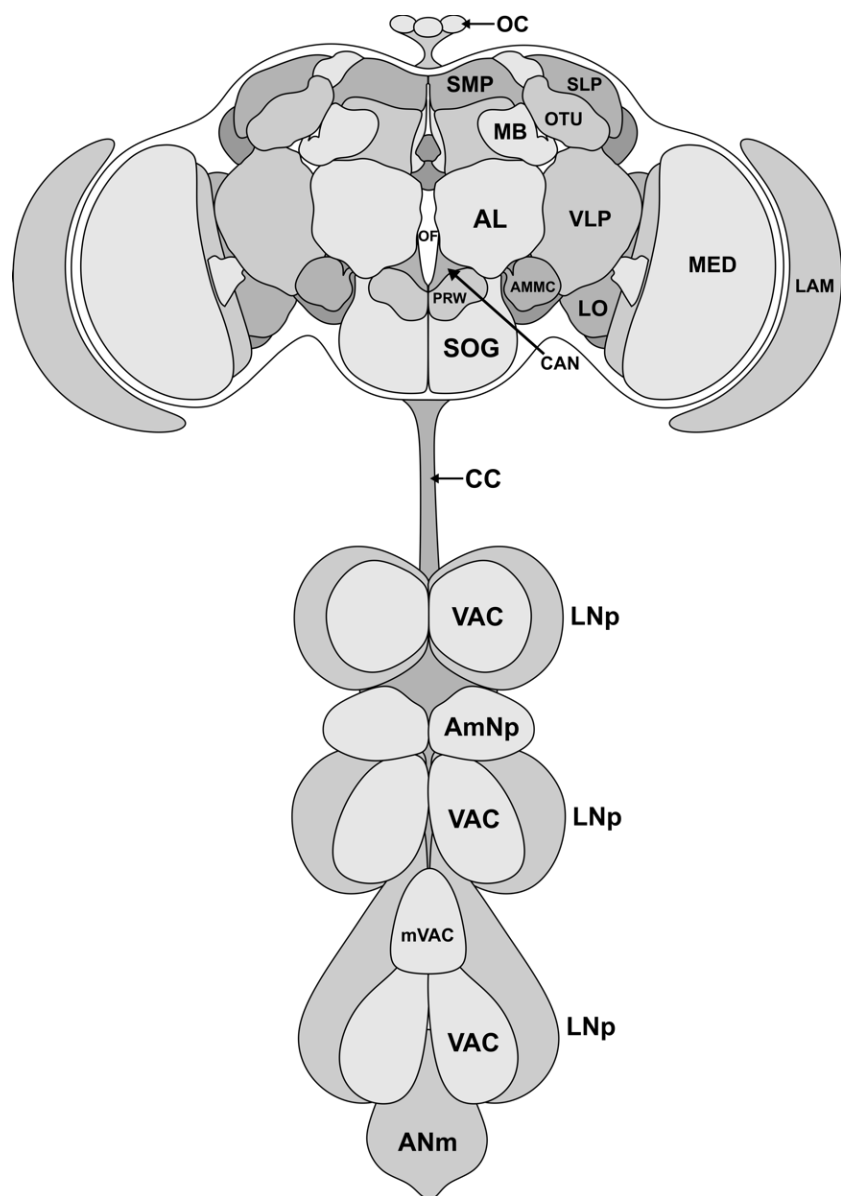


Figure 4. Schematic of *Drosophila* CNS anatomy. Central brain and VNC displayed in anterior view. Labels: AL) antennal lobe, AMMC) antennal mechanosensory and motor center, AmNp) accessory metathoracic neuropil, ANm) abdominal neuromeres, CAN) candle, CC) cervical connective, LAM) lamina, LNp) leg neuropil, LO) lobula, MB) mushroom body, MED) medulla, mVAC) medial ventral association center, OC) ocelli, OF) oesophageal foramen, OTU) optic tubercle, PRW) prow, SLP) superior lateral protocerebrum, SMP) superior medial protocerebrum, SOG) suboesophageal ganglion, VAC) ventral association center, VLP) ventrolateral protocerebrum. Schematic produced using brain nomenclature data in Jenett et al. (2012) and VNC nomenclature data in Court et al. (2020).

2.5 Behavioural assay methods

The role of *fru*^{P2}-neurons in modulating female receptivity was assessed by crossing *fru*^{P2-T-GEM} to BDSC #26263 to drive expression of a temperature-sensitive neuronal hyperactivator (TrpA1), to BDSC #44222 to drive expression of a temperature sensitive neuronal silencer (*Shibire*^{ts}), to BDSC #6596 or #28838 to drive expression of constitutive neuronal silencers (*K_{ir}2.1* or *TeTxLC*, respectively), or to BDSC #5824 to drive expression of an anti-apoptotic inhibitor (*Reaper*). Mating assays were performed to assess the effect of

hyperactivation, silencing, or ablation of *fru*^{P2}-expressing neurons on female receptivity in response to courting conspecific males.

2.5.1 Mating assays

Mating assays were performed using mating assay apparatuses (Figure 5; designed by Jamie Kramer) that permit temporally controlled interaction between paired flies. The apparatus contains 18 cylindrical 10 mm inner diameter chambers with a removable partition that separates each chamber into two sub-chambers for inhibiting interactions between flies, allowing for a maximum capacity of 36 individually separated flies (18 mating pairs). Mating assay apparatuses were washed with dish soap, triple rinsed with tap water and deionized water, and air-dried prior to conductance of each mating assay. All mating assays were conducted with virgin male CS wildtype flies as mating partners. All assayed female flies were collected during late-pupal stage to ensure virgin-status and aged 4-7 days post-eclosion to allow maturation to reproductive age prior to assaying. Equal numbers of experimental and control genotype groups (per experimental temperature) were assayed in each apparatus to control for external environmental effects such as atmospheric pressure (Austin et al., 2014). All assays were performed in a temperature-controlled Sanyo MIR-154 incubator with a water basin to maintain humidity and performed within 4 hours of the start of the light cycle to ensure maximum reproductive activity. Prior to experimental time zero, paired flies were acclimated to the incubator conditions for 30 minutes with partition in place to block within-pair interactions. At experimental time zero, video recording was initiated and partitions were removed to permit pairwise interactions for 30 minutes (Figure 5). Video recording was performed using an Apple iPad Mini with white-balance and focus locked to prevent lens auto-adjustment.

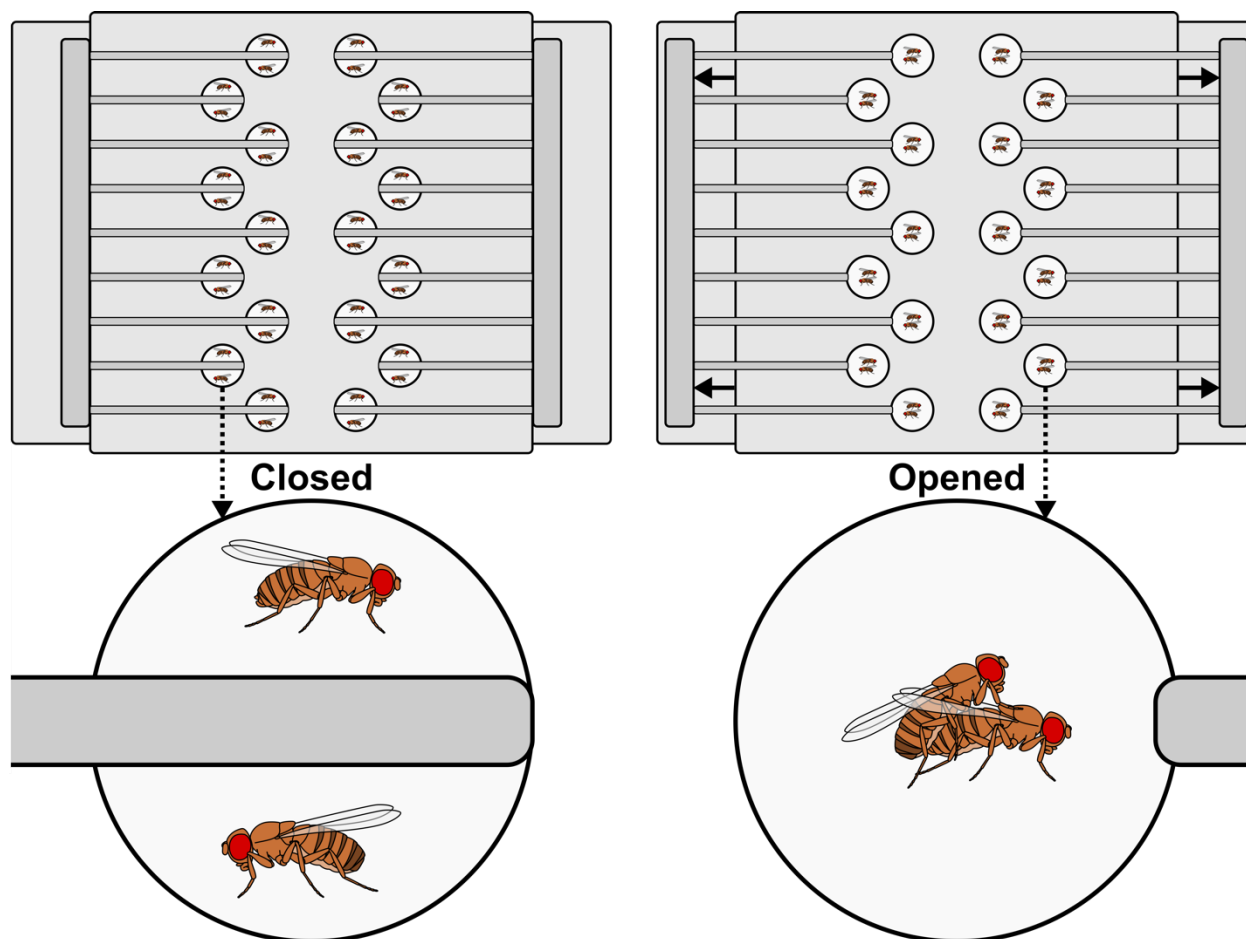


Figure 5. Schematic of mating assay apparatus. Apparatus contains 18 cylindrical 10 mm inner diameter chambers, allowing for a maximum capacity of 18 mating pairs. In closed position, partition blocks interaction between flies. In opened position, partition is removed to permit interaction between flies. Schematic produced based on apparatus designed by Jamie Kramer.

2.5.2 Assay scoring and statistical analysis

Assays were scored categorically for copulation (“mated” or “not mated”), and proportion mated was calculated for experimental and control groups. All assay scoring was performed in *VLC Media Player* 3.0.10 at 400% playback speed. Scores for a mating pair were omitted from analysis if males that did not exhibit any courtship behaviours (following, wing song, etc.) within the 30-minute assay period. Fisher's exact test with Freeman-Halton extension (2x3 contingency table) was conducted for each behavioural experiment. For statistically significant results, Fisher's exact test (2x2 contingency table) was used for post hoc testing. All

statistical analyses and graphical representation of behavioural data was performed using *R* 4.1.0 interfaced in *RStudio* 1.4.1717.

3 Results

3.1 Generation of a transgenic line expressing Gal4 in *fru*^{P2}-expressing tissues

To create flies that express Gal4 in *fru*^{P2} expressing tissues, CRISPR/Cas9-mediated HDR was used to insert the T-GEM construct into the coding intron immediately downstream of the *fru*^{P2} first exon (P2 exon; overviewed in Figure 3). A Cas9 target in the intron immediately downstream of the P2 exon was identified, verified for presence and fidelity in the injection line by Sanger sequencing (Figure S9), synthesized (Table S4), and cloned into the gRNA expression vector; successful cloning was verified by Sanger sequencing (Figure S10). Homology arms were amplified from the injection line and cloned into pT-GEM^{phase2}, and successful cloning was verified by agarose gel electrophoresis (Figure 6) and by Sanger sequencing (Figure S11).

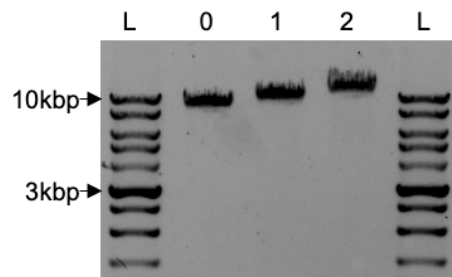
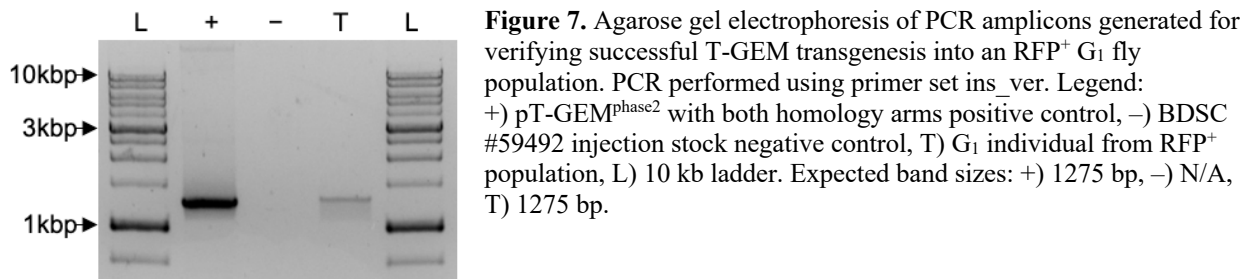


Figure 6. Agarose gel electrophoresis of digested (single cut) pT-GEM^{phase2} plasmids for verification of homology arm insertions into T-GEM donor vector. Legend: 0) pT-GEM^{phase2}, 1) pT-GEM^{phase2} with 5'-homology arm inserted, 2) pT-GEM^{phase2} with 5'-homology arm and 3'-homology arm inserted, L) 10 kb molecular ladder. Expected band sizes, calculated from pT-GEM^{phase2} sequence and homology arm sequences from dm6 reference genome: 0) 8124 bp, 1) 9055 bp, 2) 9986 bp.

An injection mix was prepared (Table S5) and microinjected into 885 embryos; 306 embryos survived embryogenesis and developed to sexual maturity (G₀ flies). The G₀ adults were individually crossed to the BDSC #3703 balancer line to produce independent populations, from which G₁ individuals (progeny of G₀ x BDSC #3703) were phenotypically screened for successful T-GEM transgenesis; 19 G₁ populations expressing RFP in the eyes (Figures S5-S6) were obtained. Behavioural sterility was observed in the G₁ males, which was resolved by backcrossing RFP⁺ G₁ females to either bal-3 or bal-w⁺ balancer flies. The resulting final

transgenic genotype was +; +; TI{*RFP*^{3xP3.PB=T-GEM}}*fru*^{P2-TG4.2/TM6B}, *Tb*¹ and is hereafter referred to as *fru*^{P2-T-GEM}. PCR amplification of *fru*^{P2-T-GEM} gDNA was used to verify insertion of the T-GEM construct into the Cas9 target, via agarose gel electrophoresis (Figure 7) and by Sanger sequencing (Figure S12).



The *fru*^{P2-T-GEM} line was expected to express transcripts containing *P2-linker-T2A-GAL4-Hsp70polyA* under control of *fru*^{P2} regulatory regions. RT-PCR amplification of total mRNA from *fru*^{P2-T-GEM} was performed to assess inclusion of *GAL4* into *fru* transcripts; agarose gel electrophoresis of RT-PCR amplicons revealed expression of *fru*^{P1} and *fru*^{P2} transcripts containing *GAL4* in males, and only *fru*^{P2} transcripts containing *GAL4* in females (Figure 8). Multiple *fru*^{P2} transcripts were observed in both genotypes for both sexes (see Discussion). Sanger sequencing of the extracted gel bands verified in-frame *T2A-GAL4* inclusion in female *fru*^{P2} transcripts, male *fru*^{P2} transcripts, and male *fru*^{P1} transcripts (Figures S13-S15). Sanger sequencing of the unexpected *fru*^{P2} gel band revealed partial inclusion of the intron downstream of the P2 exon, which contains the *fru* microexon 756 (ME756; Pang et al., 2021), and two open reading frames containing translation stop codons preceding the T-GEM construct (Figure S16).

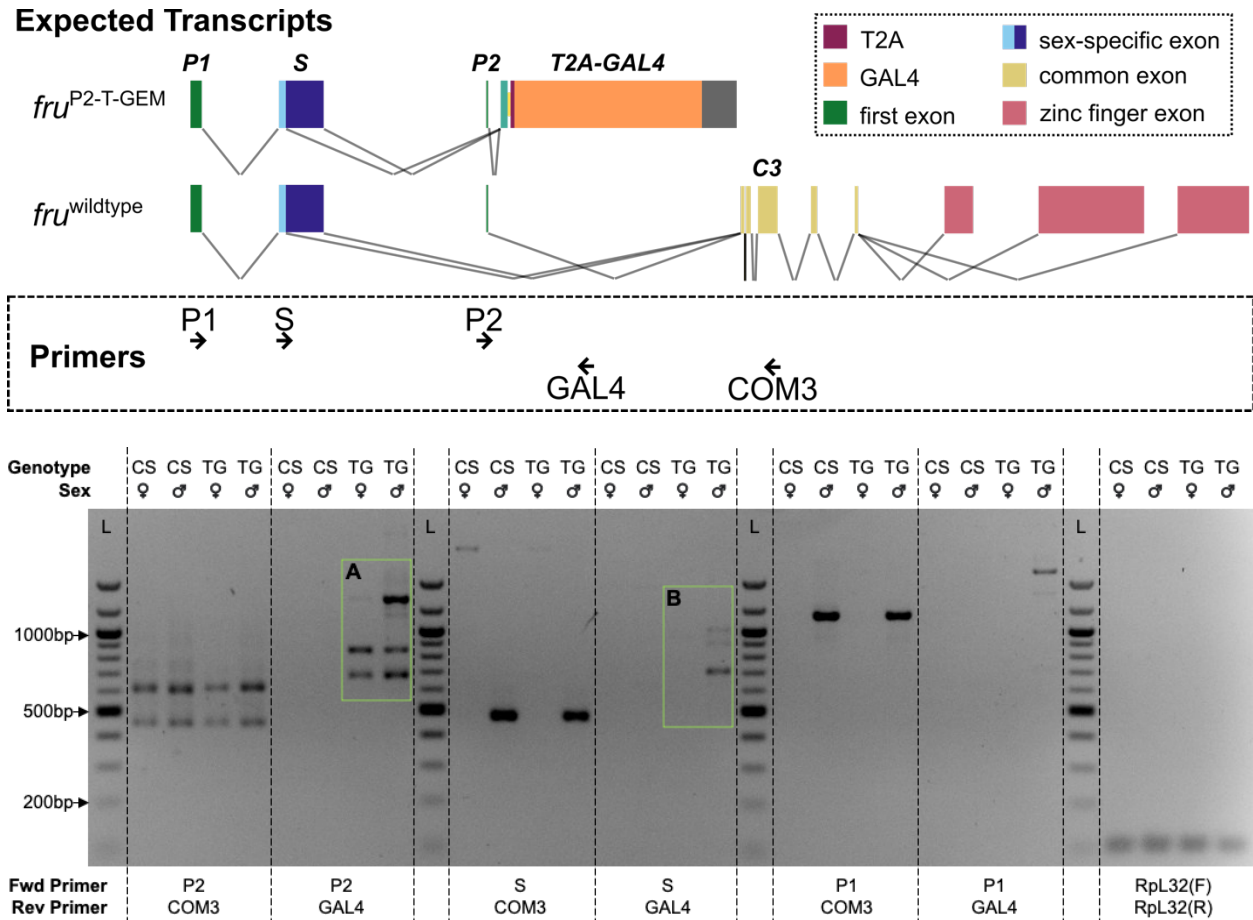


Figure 8. Agarose gel electrophoresis of RT-PCR amplicons generated from *fru* transcripts. Top schematic overviews predicted wildtype *fru*^{P2} (*fru*^{wildtype}) and *fru*^{P2-T-GEM} transcripts with primers used for RT-PCR. Green boxes denote amplicons that were Sanger sequenced. Agarose gel legend: CS) Canton-S wildtype, TG) *fru*^{P2-T-GEM}/*TM6B*, *Tb*¹, L) 1 kb molecular ladder. Green box A denotes bands extracted for Sanger sequencing using P2 forward primer. Green box B denotes bands extracted for Sanger sequencing using S forward primer.

3.2 *fru*^{P2} is expressed in female neural tissues

The *fru*^{P2-T-GEM} line was used to drive membrane-bound GFP (mCD8::GFP) to determine the expression pattern of *fru*^{P2}-expressing cells. *fru*^{P2-T-GEM} flies were crossed to UAS-*mCD8::GFP* flies to produce experimental flies (UAS-*mCD8::GFP*/+; *fru*^{P2-T-GEM}/+). *fru*^{P2-T-GEM} and UAS-*mCD8::GFP* flies were each crossed to CS wildtype flies to produce genetic controls (UAS-*mCD8::GFP*/+; +/+ and +/+; *fru*^{P2-T-GEM}/+, respectively). *fru*^{P1-GAL4} (expressing Gal4 in *fru*^{P1} tissues) flies were crossed to UAS-*mCD8::GFP* flies to produce *fru*^{P1} controls (UAS-*mCD8::GFP*/+; *fru*^{P1-GAL4}/+). Full CNS dissections were performed and epi-fluorescent imaging

was conducted (Figures 9, S17, S18). The T-GEM visible marker (RFP), which is expressed in a pattern independent of *fru*^{P2} expression, was observed only in flies carrying *fru*^{P2-T-GEM} (Figures 9A, 9D, S17, S18). Expression of GFP was not observed in the genetic controls (Figure S17). In male experimental flies, GFP was observed in *fru*^{P1}-expressing neural circuitry (lateral protocerebral complex and tritocerebral loop, Figure 10), partially resembling the male *fru*^{P1} control flies (Figure 9E-F). In female experimental flies, GFP expression was observed in the ocelli, lamina, central brain, and ventral nerve cord (Figure 9B), and was not observed to resemble the female *fru*^{P1} control flies (Figure 9C). In the central brain, GFP was observed in cell bodies within the suboesophageal ganglion and in the cantle (ventral oesophageal foramen; Figure 11). In the ventral nerve cord, GFP was observed in cell bodies within the abdominal neuromeres and the leg neuropils (Figure 9B).

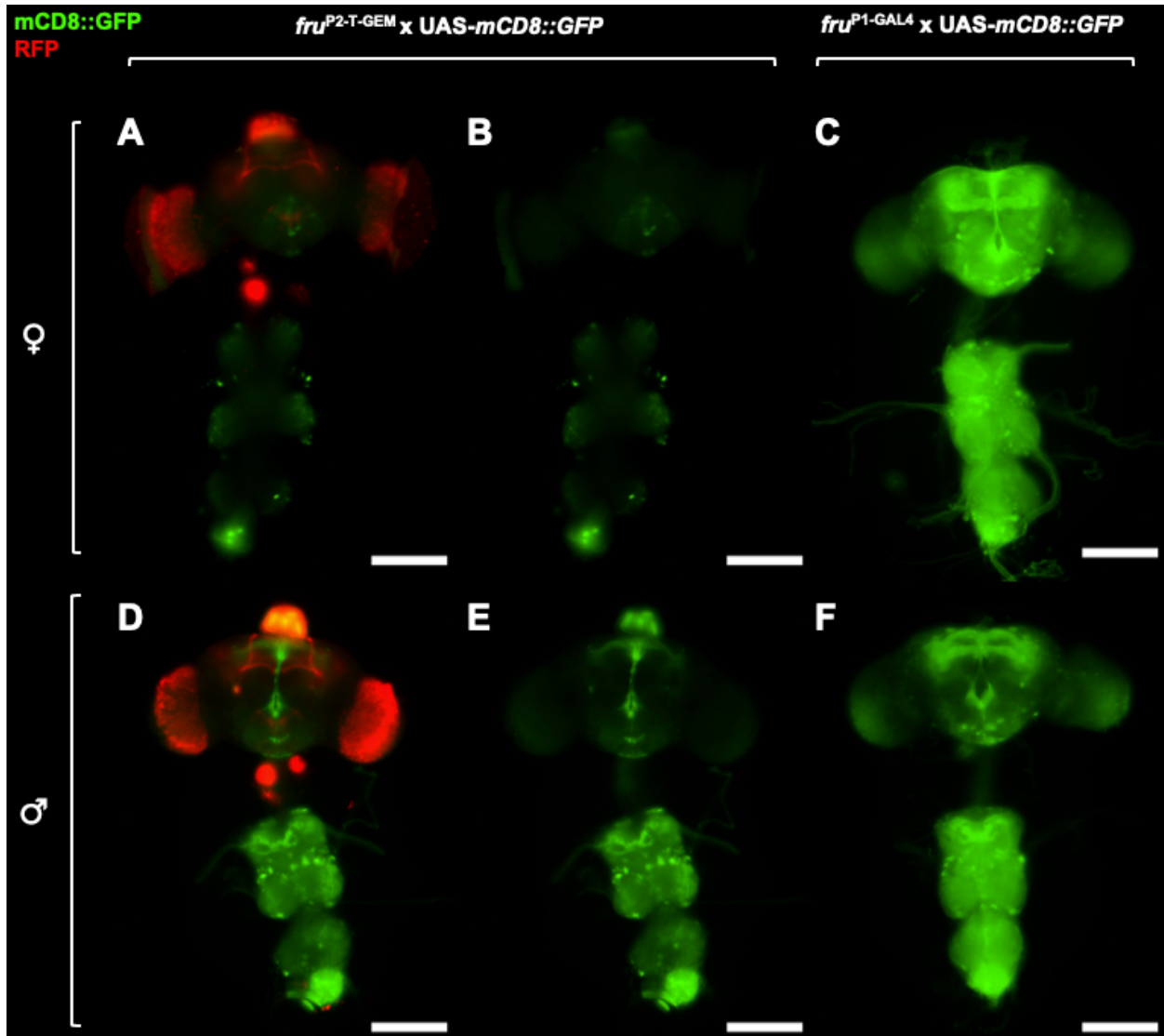


Figure 9. Epi-fluorescent imaging of whole-mounted adult female and male CNSes expressing mCD8::GFP under fru^{P2} and fru^{P1} regulation. The top tissue in each image for each sex is the brain, while the bottom tissue is the ventral nerve cord, shown in anterior view. Subfigures: (A,D) $fru^{T-GEM} \times UAS-mCD8::GFP$ imaging with merged RFP and GFP channels or (B,E) GFP channel only, and (C,F) $fru^{P1-GAL4} \times UAS-mCD8::GFP$ imaging with GFP channel only. $Fru^{T-GEM} \times UAS-mCD8::GFP$ expresses RFP (red fluorescence) in *eyeless*-expressing tissues as a visible marker indicating presence of the T-GEM construct, and membrane bound GFP (green fluorescence) in fru^{P2} -expressing tissues. $fru^{P1-GAL4} \times UAS-mCD8::GFP$ expresses membrane bound GFP in fru^{P1} -expressing tissues. All image capturing was performed at with standardized parameters (1.0x gain, 2.0 sec exposure, and 0 ND). All images were produced by z-stack (21 x 2 μ m). Scale bars represent 200 μ m.

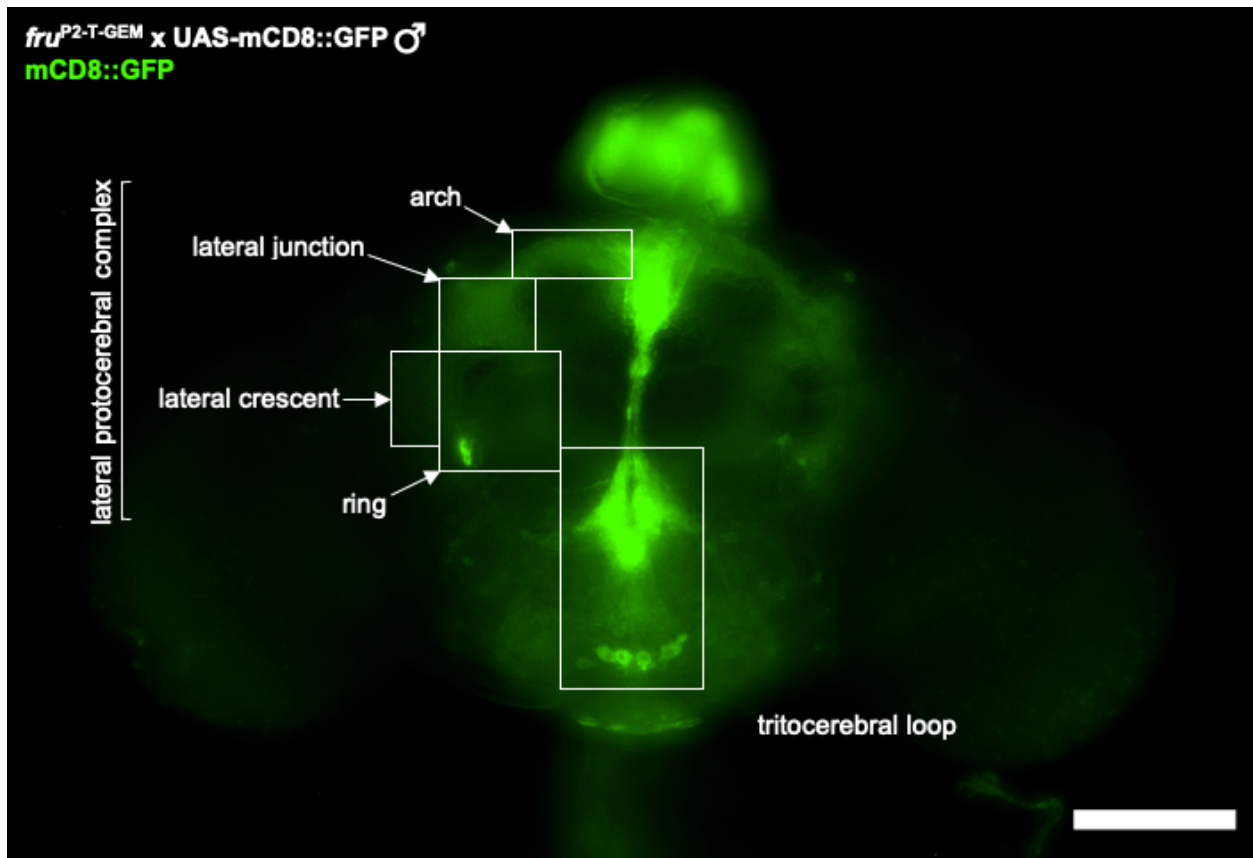


Figure 10. Epi-fluorescent imaging of whole-mounted adult male brain expressing mCD8::GFP under *fru*^{P2} and *fru*^{P1} regulation. Anterior view. In males, *fru*^{P2-T-GEM} drives membrane bound GFP (green fluorescence) in *fru*^M-expressing tissues and *fru*^{P2}-expressing tissues. Known *fru*^{P1}-expressing tissues (lateral protocerebral complex [arch, lateral junction, lateral crescent, ring] and tritocerebral loop) are labelled by white boxes and arrows. Image was produced by z-stack (21 x 2 μm). Scale bar represents 100 μm.

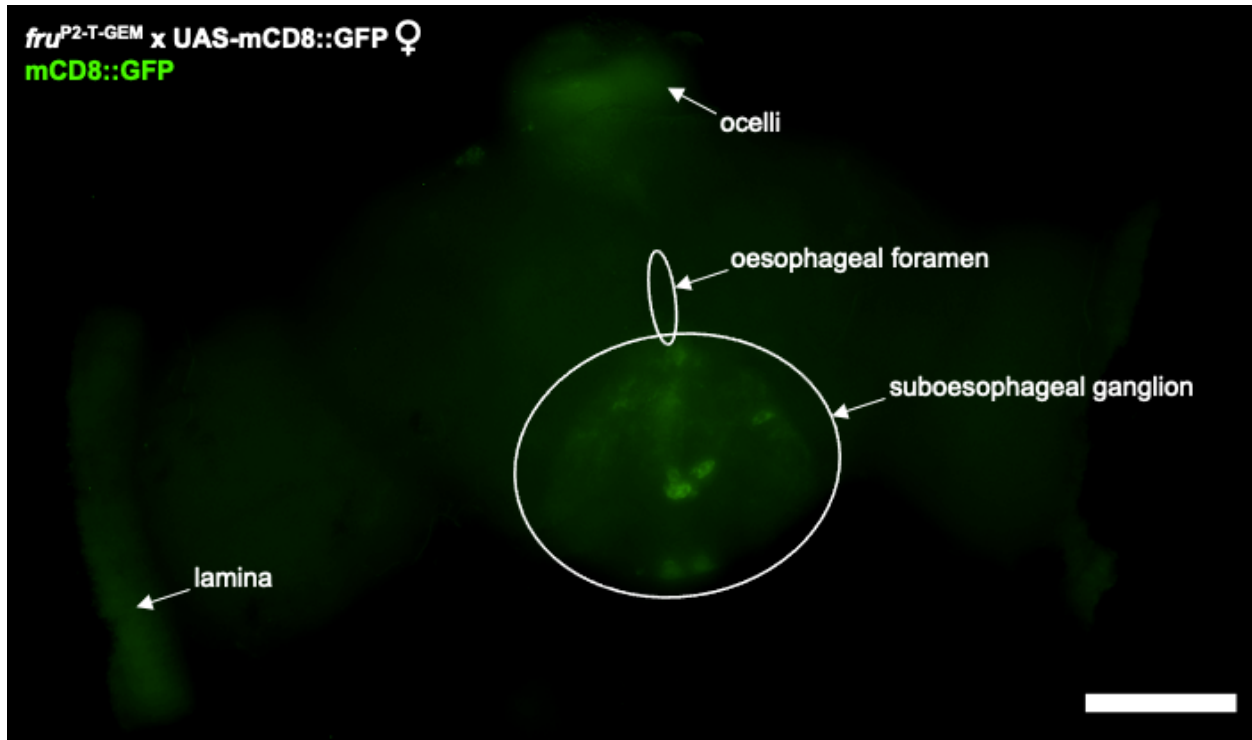


Figure 11. Epi-fluorescent imaging of whole-mounted adult female brain expressing mCD8::GFP under fru^{P2} regulation. Anterior view. In females, $fru^{P2-T-GEM}$ drives membrane bound GFP in fru^{P2} -expressing tissues, but not in fru^{P1} -expressing tissues. fru^{P2} -expressing tissues were identified in the ocelli, lamina, ventral oesophageal foramen, and suboesophageal ganglion; labelled by white circles and arrows. Image was produced by z-stack (21 x 2 μm intervals). Scale bar represents 100 μm .

3.3 fru^{P2} -expressing neurons modulate female receptivity

A temperature-sensitive cation channel (*TrpA1*), which causes neuronal depolarization at approximately 29 °C (Hamada et al., 2008; Pauls et al., 2015), was driven using $fru^{P2-T-GEM}$ to determine the effect of neuronal hyperactivation of fru^{P2} -expressing neurons. $fru^{P2-T-GEM}$ flies were crossed to *UAS-TrpA1* flies to produce female experimental flies (*UAS-TrpA1/+; fru^{P2-T-GEM}/+*). $fru^{P2-T-GEM}$ and *UAS-TrpA1* flies were each crossed to CS wildtype flies to produce female genetic control flies (*UAS-TrpA1/+; +/+* and *+/+; fru^{P2-T-GEM}/+*, respectively). Mating assays were performed, scored categorically for copulation, and mating proportions were calculated for each genotype. There was a significant difference in mating proportion across the three genotypes at 31 °C (Fisher's exact test with Freeman-Halton extension [2x3 contingency table], $p=1.151 \times 10^{-11}$; Figure 12). Post hoc testing revealed significantly lower mating proportion

for the experimental genotype compared to the *UAS-TrpA1* and *fru*^{P2-T-GEM} genetic controls (Fisher's exact tests [2x2 contingency tables]; $p=1.275 \times 10^{-8}$ and $p=7.645 \times 10^{-10}$, respectively), and no significant differences in mating proportion between the genetic controls (Fisher's exact test [2x2 contingency table], $p=0.7019$). The experimental female flies did not display abnormalities in rejection behaviours or locomotion, and were not observed to exhibit any headbutting, boxing, or tussling behaviours that would be indicative of abnormally high aggression. There was no significant difference in mating proportion across the three genotypes at 25 °C (Fisher's exact test with Freeman-Halton extension [2x3 contingency table], $p=0.3239$; Figure 12).

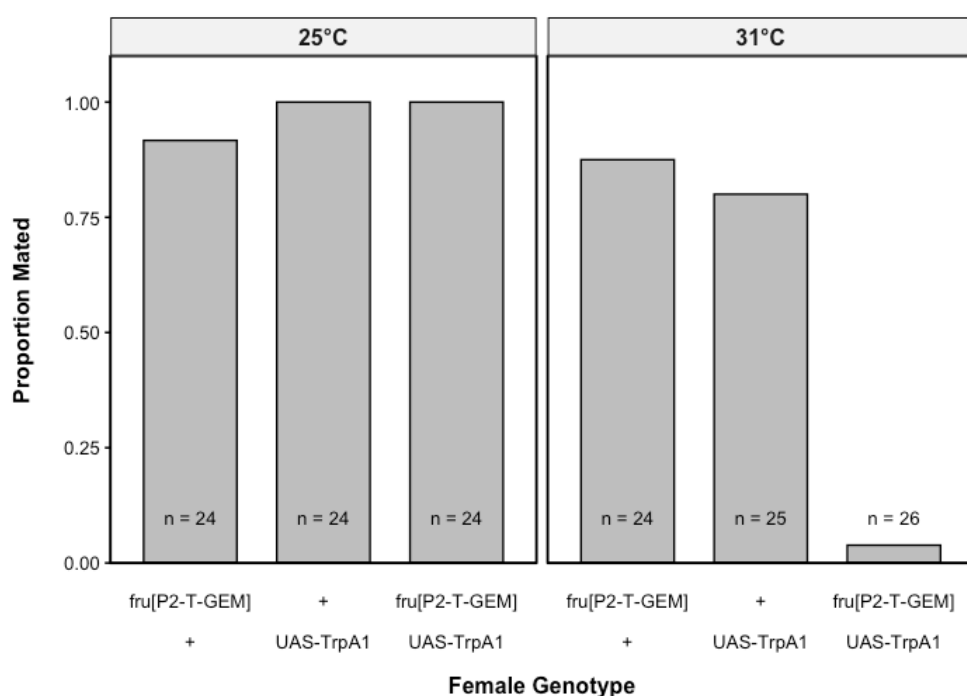


Figure 12. Proportion of pairs mated when hyperactivating *fru*^{P2}-expressing neurons using TrpA1. n = total number of pairs in each group. Females were paired with wildtype males. Hyperactivation of *fru*^{P2} neurons via TrpA1 significantly decreases female receptivity to courting conspecific males. Fisher's exact test with Freeman-Halton extension (2x3 contingency table) at 25 °C, $p=0.3239$; 31 °C, $p=1.151 \times 10^{-11}$.

The temperature-sensitive effector *Shibire*^{ts}, which causes inhibition of synaptic recycling through endocytic arrest at 30 °C (Kitamoto, 2001), was driven using *fru*^{P2-T-GEM} to determine the effect of neuronal silencing of *fru*^{P2}-expressing neurons. *fru*^{P2-T-GEM} flies were crossed to *UAS-shibire*^{ts} flies to produce female experimental flies (+/+; *fru*^{P2-T-GEM}/*UAS-shibire*^{ts}). *fru*^{P2-T-GEM}

and UAS-*shibire*^{ts} flies were each crossed to CS wildtype flies to produce female genetic controls (+/+; UAS-*shibire*^{ts}/+ and +/+; *fru*^{P2-T-GEM}/+, respectively). Mating assays were performed, scored categorically for copulation, and mating proportions were calculated for each genotype. There was no significant difference in mating proportion across the three genotypes at 31 °C (Freeman-Halton extension [2x3 contingency table], p=0.758; Figure 13) and no significant difference in mating proportion between the experimental genotype compared to the *fru*^{P2-T-GEM} genetic control (Fisher's exact test [2x2 contingency table], p=0.4783). Flies were not assayed at 25 °C.

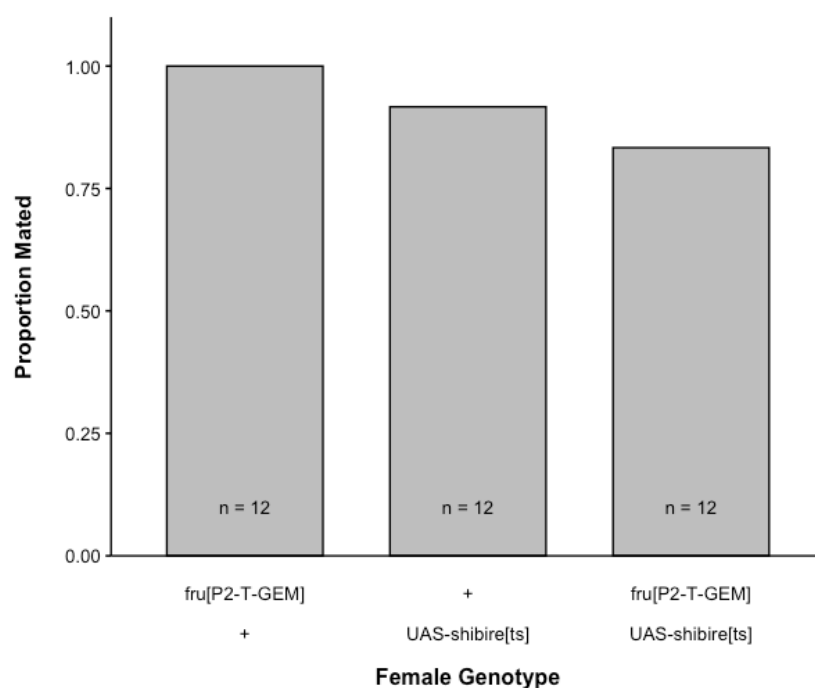


Figure 13. Proportion of pairs mated when silencing *fru*^{P2}-expressing neurons using *Shibire*^{ts}. n = total number of pairs in each group. Silencing of *fru*^{P2} neurons via *shibire*^{ts} at does not significantly affect female receptivity to courting conspecific males. Fisher's exact test with Freeman-Halton extension (2x3 contingency table), p=0.758.

An inward-rectifier potassium ion channel ($K_{ir2.1}$), which causes constitutive neuronal hyperpolarization (Pauls et al., 2015), was driven using *fru*^{P2-T-GEM} to determine the effect of neuronal silencing of *fru*^{P2}-expressing neurons. *fru*^{P2-T-GEM} flies were crossed to UAS-*K_{ir2.1}* flies to produce female experimental flies (UAS-*K_{ir2.1}*/+; *fru*^{P2-T-GEM}/+). *fru*^{P2-T-GEM} and UAS-*K_{ir2.1}* flies were each crossed to CS wildtype flies to produce female genetic controls (UAS-*K_{ir2.1}*/+; +/+ and +/+; *fru*^{P2-T-GEM}/+, respectively). Mating assays were performed, scored categorically for

copulation, and mating proportions were calculated for each genotype. There was a significant difference in mating proportion across the three genotypes (Freeman-Halton extension [2x3 contingency table], $p < 2.2 \times 10^{-16}$; Figure 14). Post hoc testing revealed significantly lower mating proportion for the experimental genotype compared to the UAS-*Kir2.1* and *fru*^{P2-T-GEM} genetic controls (Fisher's exact test [2x2 contingency tables]; $p = 9.904 \times 10^{-12}$ and $p = 1.551 \times 10^{-12}$, respectively), and no significant difference between the genetic controls (Fisher's exact test [2x2 contingency table], $p = 1.0$).

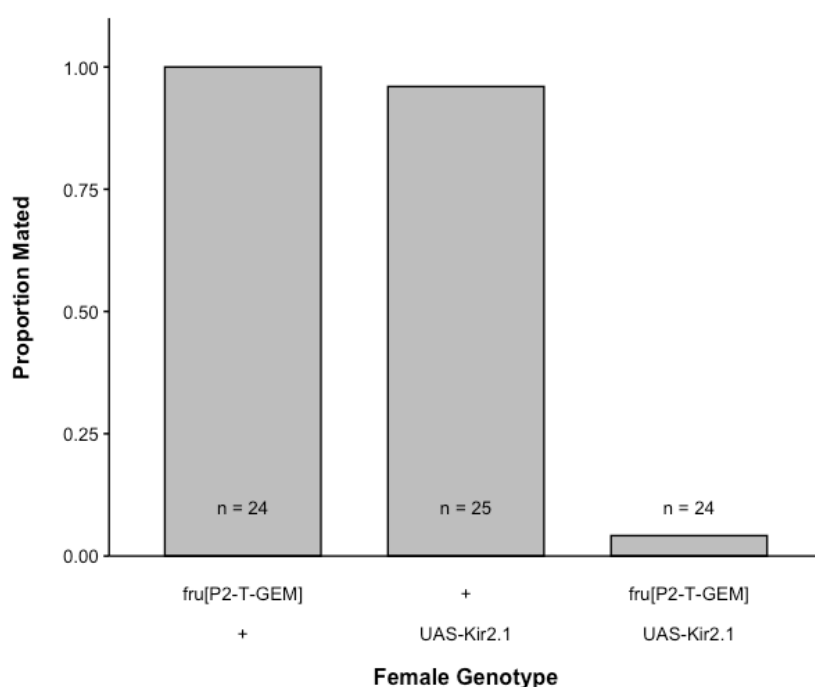


Figure 14. Proportion of pairs mated when silencing *fru*^{P2}-expressing neurons using *Kir2.1*. n = total number of pairs in each group. Hyperpolarization of *fru*^{P2} neurons via *Kir2.1* significantly decreases female receptivity to courting conspecific males. Fisher's exact test with Freeman-Halton extension (2x3 contingency table), $p < 2.2 \times 10^{-16}$.

The tetanus toxin light chain (TeTxLC), which catalyzes cleavage of synaptobrevin to inhibit synaptic vesicle exocytosis (Sweeney et al., 1995), was driven using *fru*^{P2-T-GEM} to determine the effect of neuronal silencing of *fru*^{P2}-expressing neurons. *fru*^{P2-T-GEM} flies were crossed to UAS-*TeTxLC* flies to produce female experimental flies (UAS-*TeTxLC*/+; *fru*^{P2-T-GEM}/+). *fru*^{P2-T-GEM} and UAS-*TeTxLC* flies were each crossed to CS wildtype flies to produce female genetic controls (UAS-*TeTxLC* /+; +/+ and +/+; *fru*^{P2-T-GEM}/+, respectively). Mating assays were performed, scored categorically for copulation, and mating proportions were

calculated for each genotype. There was a significant difference in mating proportion across the three genotypes (Fisher's exact test with Freeman-Halton extension [2x3 contingency table], $p=8.23 \times 10^{-10}$; Figure 15). Post hoc testing revealed significantly lower mating proportion for the experimental genotype compared to the UAS-*TeTxLC* and *fru*^{P2-T-GEM} genetic controls (Fisher's exact test [2x2 contingency tables]; $p=2.304 \times 10^{-8}$ and $p=1.426 \times 10^{-6}$, respectively), and no significant difference between the genetic controls (Fisher's exact test [2x2 contingency table], $p=0.6085$).

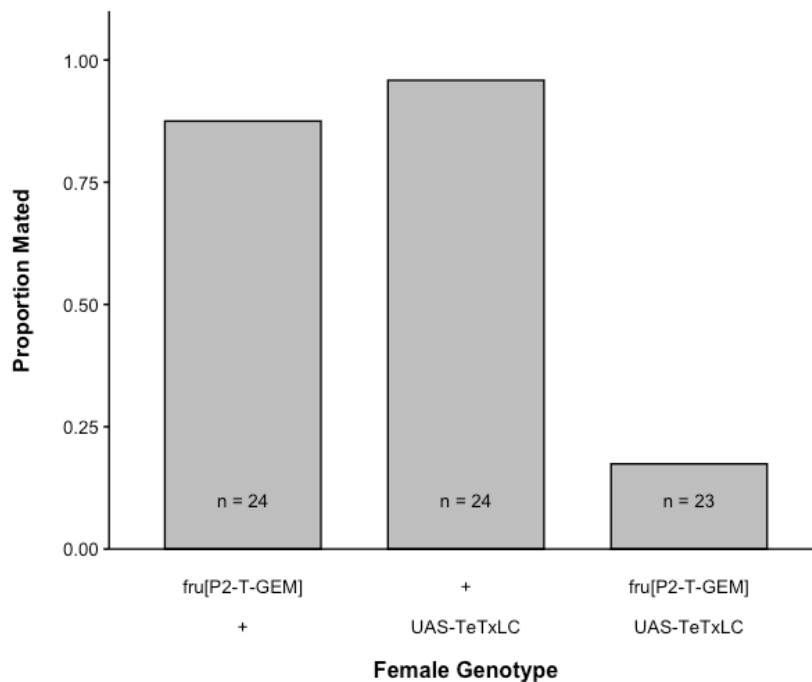


Figure 15. Proportion of pairs mated when silencing *fru*^{P2}-expressing neurons using *TeTxLC*. n = total number of pairs in each group. Inhibition of neurotransmitter exocytosis in *fru*^{P2} neurons via *TeTxLC* significantly decreases female receptivity to courting conspecific males. Fisher's exact test with Freeman-Halton extension (2x3 contingency table), $p=8.23 \times 10^{-10}$.

The Reaper protein, which inhibits anti-apoptotic activity and results in cell death (Goyal et al., 2000), was driven using *fru*^{P2-T-GEM} to determine whether *fru*^{P2}-expressing cells are necessary for eliciting either receptivity or rejection behaviours. *fru*^{P2-T-GEM} flies were crossed to UAS-*reaper* flies to produce female experimental flies (UAS-*reaper*/+; *fru*^{P2-T-GEM}/+). *fru*^{P2-T-GEM} and UAS-*reaper* flies were each crossed to CS wildtype flies to produce female genetic controls (UAS-*reaper*/+; +/+ and +/+; *fru*^{P2-T-GEM}/+, respectively). Mating assays were performed, scored

categorically for copulation, and mating proportions were calculated for each genotype. There was no significant difference in mating proportion across the three genotypes (Fisher's exact test with Freeman-Halton extension [2x3 contingency table], $p=0.3077$; Figure 16). Experimental female flies were qualitatively observed to exhibit rejection behaviours prior to and following copulation that included running, decamping, wing flicking, and kicking. No female flies of either experimental or control genotypes were qualitatively observed to re-mate during the 30-minute test period.

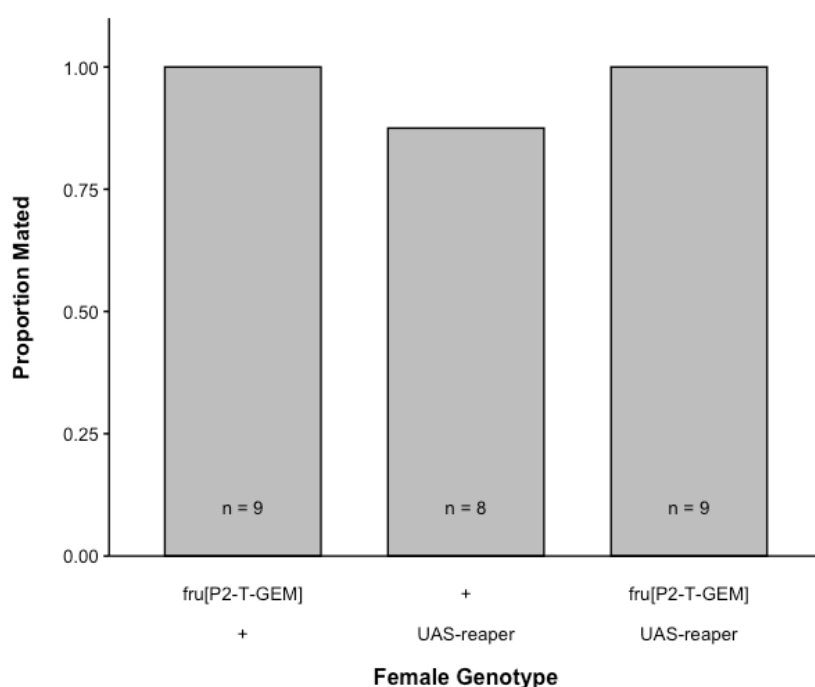


Figure 16. Proportion of pairs mated when ablating *fru*^{P2}-expressing neurons using Reaper. n = total number of pairs in each group. Ablation of *fru*^{P2} cells via *reaper* does not significantly affect female receptivity to courting conspecific males. Fisher's exact test with Freeman-Halton extension (2x3 contingency table), $p=0.3077$.

4 Discussion

In this project, CRISPR/Cas9-mediated HDR was used to create the novel *fru*^{P2-T-GEM} transgenic line that expresses Gal4 in all *fru*^{P2}-expressing tissues to anatomically map *fru*^{P2}-neurons and to assess their role in modulating female receptivity. It was hypothesized that *fru*^{P2} is expressed in neural tissues, and that tissues expressing *fru*^{P2} modulate female receptivity. It was predicted that *fru*^{P2} neurons would be localized in photoreceptor neurons, optic lobe tissues, and their connecting afferent tracts. The *fru*^{P2} neurons were observed in photoreceptor

tissues and afferent visual tissues, but not in the optic lobe tissues. It was also predicted that hyperactivation or silencing of these neurons would result in altered sexual receptivity to courting males. Female receptivity was indeed observed to significantly decrease upon hyperactivation or constitutive silencing.

4.1 Transgenic line caveats

The *fru*^{P2-T-GEM} line was successfully created and verified to express functional Gal4 in *fru*^{P2}-expressing tissues, however, there are several caveats with this line that must be addressed.

4.1.1 *fru*^{P2-T-GEM} captures both *fru*^{P1} and *fru*^{P2} expression in males

The T-GEM splice acceptor forces splicing-in of *T2A* and *GAL4* in all transcripts transcribed from regulatory regions upstream of T-GEM. Since the *fru*^{P1} regulatory regions are positioned upstream of T-GEM, *fru*^{P1} transcripts may also contain the artificial exon containing *T2A-GAL4*. Therefore, the *fru*^{P2-T-GEM} line may express *T2A-GAL4* under *fru*^M and *fru*^F regulation in addition to *fru*^{P2} regulation.

Previous research that generated a *GAL4* line expressing Gal4 under *fru*^{P1} regulation (*fru*^{P1-GAL4}) was shown to label *fru*^F in females (Stockinger et al., 2005), which was verified in this project (Figure 9C). *fru*^F transcripts were not detected through RT-PCR with primers P1 or S in combination with GAL4 or COM3 (Figure 8). This was confirmed by using the *fru*^{P1-GAL4} line to drive expression of membrane-bound GFP under *fru*^F regulation, which revealed extensive GFP labelling in the central brain and VNC (Figure 9C) that was not observed when driving membrane bound GFP using the *fru*^{P2-T-GEM} line (Figure 9B). This implies that inclusion of *T2A-GAL4* in *fru*^F transcripts does not result in expression of Gal4 under *fru*^F regulation, presumably due to the presence of multiple in-frame stop codons in the female splicing of the S exon that

causes translational termination prior to translation of *T2A-GAL4*. It was concluded that the *fru*^{P2-T-GEM} line expresses Gal4 in *fru*^{P2} tissues, but not *fru*^{P1} tissues, for females.

Inclusion of *T2A* and *GAL4* in male *fru*^{P1} transcripts was verified by RT-PCR (Figure 8), Sanger sequencing (Figure S15), and was supported by the imaging data (Figure 9E-F). Driving membrane-bound GFP using *fru*^{P2-T-GEM} resulted in labelling of previously identified *fru*^M neural circuitry, including the lateral protocerebral complex and the tritocerebral loop (Figure 10), congruent to previous immunohistochemistry (IHC) labelling of Fru^M (Yu et al., 2010). Driving membrane-bound GFP using *fru*^{P1-GAL4} (Figure 9F) labelled a larger population of *fru*^M-neurons compared to both IHC labelling of Fru^M (Yu et al., 2010) and *fru*^{P2-T-GEM}-driven GFP labelling (Figure 9E), making it difficult to identify cells or regions that may be *fru*^{P1}-negative and *fru*^{P2}-positive. Expression of Fru^{COM} is more discreet than that of Fru^M (Lee et al., 2000), and is expressed in the lateral protocerebral complex and tritocerebral loop similar to labelling by *fru*^{P2-T-GEM} (Figure 10). It is possible that *fru*^M and *fru*^{P2} are co-expressed in these cells or that separate *fru*^M- and *fru*^{P2}-neurons have similar expression patterns and/or share neural circuitry, but further investigation is needed. The major implication for observed differences in GFP labelling between the *fru*^{P1-GAL4} and *fru*^{P2-T-GEM} lines is that the traditional *GAL4* may less specifically capture *fru*^M expression compared to a Trojan-Gal4 approach. The *fru*^{P1-GAL4} line was observed to label *fru*^{P2-T-GEM}-labelled regions and additionally the mushroom body, which has a role in the olfactory learning and memory processes that contribute to modulation of male courtship behaviours (Montague & Baker, 2016). It is possible that previous research using the *fru*^{P1-GAL4} line to drive reporters and/or effectors have targeted non-*fru*^M tissues, and thus it may be beneficial to produce a transgenic line for expressing Trojan-Gal4 under control of *fru*^{P1} regulation to revisit *fru*^M expression and role in male courtship behaviours.

With the imaging data, in combination with the RT-PCR amplification of *fru* transcripts (Figure 8) and subsequent Sanger sequencing (Figures S14-S15), it can be concluded that *fru*^{P2-T-GEM} expresses Gal4 under control of both *fru*^{P1} and *fru*^{P2} regulation in males. This makes *fru*^{P2-T-GEM} currently unusable for assessment of *fru*^{P2} in males due to the genetic confound of capturing expression of *fru*^{P1}; this is particularly so in the case of *fru*^M since it is known to be expressed in adult neural tissues (Lee et al., 2000; Stockinger et al., 2005). There are several ways that this issue can be resolved for usage of this line for investigation of *fru*^{P2} in males: 1) a custom Trojan-Gal4 construct could be created for in-frame insertion directly into the P2 exon, 2) an early stop codon could be introduced directly into the P1 exon or male-transcribed portion of the S exon via gene editing, 3) an early stop codon preceded by a splice acceptor could be inserted into the coding intron downstream of the P1 exon via gene editing, 4) the chromosome containing *fru*^{P2-T-GEM} could be recombined with a pre-existing *fru*^{ΔP1} chromosome to introduce a deleted P1 exon locus, or 5) the P1 exon could be deleted from the chromosome containing *fru*^{P2-T-GEM} through gene editing methods. Insertion of *T2A-GAL4* (not as an artificial exon) directly into the P2 exon would circumvent the issue of capturing *fru* transcripts with regulatory regions located upstream of the P2 locus but would also have less versatility for downstream applications in contrast to using the T-GEM construct. The T-GEM construct contains recombination sites for simple replacement of both *T2A-GAL4* and *3xP3-RFP* with other transgenic constructs (see Future directions). Deletion of the P1 exon may be the optimal approach since early termination of *fru*^M may cause formation of a short Fru^M peptide that resembles Fru^F, and it is not currently known whether Fru^F peptides have any biological function. Of the two P1 exon deletion methods proposed, deletion via gene editing is preferred

over the recombination approach since the T-GEM construct is large (>5 kb) and it is possible that the T-GEM construct may also be partially or fully recombined out.

4.1.2 *fru*^{P2-T-GEM} may feminize Fru^M proteins in males

Splicing-in of the *T2A-GAL4* results in truncation of the peptide during translation at the T2A auto-cleavage site. In the case of *fru*^M transcripts this would cause truncation of the peptide prior to the common exons, resulting in formation of a peptide resembling Fru^F. In the process of making this genetic line, G₁ transformant male flies were found to be behaviourally sterile and did not produce offspring when paired with CS wildtype, BDSC #3703 balancer, or *fru*^{P2-T-GEM} females. This suggests that the truncated Fru^M peptide could have unintended effects resulting in behavioural sterility. Interestingly, this was observed in flies even when heterozygous for the transgenic chromosome, implying that truncation of Fru^M results in a gain-of-function effect. However, this behavioural sterility was resolved once the sex chromosomes were backcrossed out using bal-3 or bal-w⁺ balancer lines carrying CS wildtype sex chromosomes. These observations suggest that there may be interaction effect(s) between the *fru*^{P2-T-GEM} chromosome and sex chromosome(s) donated from BDSC #3703 balancer line, or with the sex chromosome(s) from the BDSC #58492 injection line. The X chromosome from the BDSC #3703 balancer line (w¹¹¹⁸) contains a white mutation, resulting in decreased production of drosopterin and ommochrome (eye pigments) and subsequent impairment of visual acuity (Ferreiro et al., 2018; Nolte, 1952). *fru*^M is vital for male reproductive behaviours and is expressed in neural tissues of the visual pathway (Stockinger et al., 2005), so it is possible that feminization of Fru^M in combination with impaired visual acuity may have caused the observed gain-of-function behavioural sterility, but further investigation is needed. If feminization of Fru^M does have

unintended consequences, it can be resolved by deleting the P1 exon from the *fru*^{P2-T-GEM} chromosome as described in the prior section.

4.1.3 *fru*^{P2-T-GEM} captures expression of an identified *fru*^{P2} transcript in both sexes

RT-PCR amplification of *fru*^{P2-T-GEM} total mRNA revealed three amplicons produced with primers P2 and GAL4, two of which were unexpected (Figure 8, box A). The gel band for the largest amplicon was observed to be much stronger for males than females, and Sanger sequencing revealed that this amplicon contained the full intron between the P2 exon and the splice acceptor. It is likely that this amplicon is produced from *fru*^{P1} and *fru*^{P2} pre-mRNA that have not undergone splicing. The literature on polyadenylation and splicing suggests that the presence of an exon containing polyadenylation sites, when preceded by an intron containing splicing sites at the 3' end, causes the rate at which polyadenylation occurs to increase and results in RNA intermediates that are polyadenylated but not spliced (Niwa et al., 1990). The transcripts produced by *fru*^{P2-T-GEM} fit these criteria, as the T-GEM artificial exon contains a splice acceptor at the 5' end that is not included in the transcripts (effectively becoming part of 3' end of the upstream intron) and also contains the *Hsp70* polyadenylation signal. Therefore, these amplicons may be produced by amplification of *fru*^{P1} transcripts that have been polyadenylated but have not yet undergone splicing to remove the P2 exon. In support of this idea, the relative gel band strength of amplicons produced by primers P1 or SS in combination with GAL4 or COM3 were undetectable or weak in females but strong in males, which is mirrored in the largest amplicon produced by primers P2 and GAL4.

The second unexpected band, however, was likely to be amplified from mature mRNA. Sanger sequencing revealed that this amplicon contained a portion of the intron between the P2 exon and the T-GEM construct, and thus the transcript from which this amplicon was produced is

likely to have already undergone splicing. This extended *fru*^{P2} transcript includes an additional 165 bp of the intronic region immediately downstream of the P2 exon. Interestingly, the 3'-end of this extended region aligns precisely with the *fru* microexon 756 (ME756; Figure S16) that was recently identified (Pang et al., 2021). This *fru*^{P2} transcript was found to have two open reading frames within the extended P2 exon that each encode for an in-frame translational stop site. Therefore, I predict that translation of these transcripts does not produce functional Gal4, similar to how Fru^F expression is not captured due to an early translational stop in the female-specifically spliced S exon. It is possible that this extended *fru*^{P2} transcript has some non-coding functions, but this has yet to be examined. It is also possible that this extended *fru*^{P2} transcript previously did not contain stop codons and produced biologically functional products, and later changes to this locus rendered it non-functional. Future work with this transcript may include investigation of possible non-coding RNA functions and assessment for functional orthologs including this extended region in Dipteran species.

4.1.4 *fru*^{P2-T-GEM} may disrupt regulation of downstream *fru* transcripts

After recovering the behavioural sterility, male flies carrying *fru*^{P2-T-GEM} were able to mate with female flies carrying *fru*^{P2-T-GEM} to produce progeny homozygous for *fru*^{P2-T-GEM}. These individuals were observed to have viability issues at late-pupal stages due to locomotor defects, an effect similar to deletion of the P3 exon or knockdown of *fru*^{P3} transcripts (Moehring laboratory, unpublished data; Anand et al., 2001). Additionally, it is known that P2 does not serve a vital role (Anand et al., 2001) and that precise deletion of the P2 exon is homozygous viable (*fru*^{ΔP2} line; Chowdhury et al., 2020). This suggests that insertion of the T-GEM construct into the intronic region downstream of the P2 exon may be directly disrupting regulatory elements of downstream *fru* transcripts that have vital functions. Although the lethal phenotype of

homozygous *fru*^{P2-T-GEM} appears to mirror the P3 knockdown/deletion lethal phenotype, the P5 exon is spatially closer to the P2 exon than the P3 exon (2.4 kb for P5 vs 25.8 kb for P3). However, high throughput RNAseq data has not observed expression of the P5 exon during development (Leader et al., 2018), making it unlikely that this disruption of P5 would cause developmental lethality. The large size of the T-GEM construct (5.2 kb) therefore likely produces positional effects that disrupt expression of the downstream *fru*^{P3} splice variants. If so, a potential solution could be to excise the 3xP3-*RFP* visible marker from the *fru*^{P2-T-GEM} transgenic chromosome via Cre-recombinase activity to shorten the insertion by approximately 1.4 kb. Further work is needed to determine the mechanism by which *fru*^{P2-T-GEM} is causing homozygous lethality in late developmental stages.

4.1.5 CRISPR/Cas9 off-targeting

The possibility of off-target insertion(s) of the T-GEM construct resulting from off-target Cas9 nuclease activity cannot be ruled out. However, based on the Cas9 target design, no strong off-targets were predicted on any other chromosome. Any potential off-targets on the same chromosome matched a maximum of 14 bases to the Cas9 target sequence and NGG PAMs necessary for Cas9 nuclease activity were not identified in any immediately adjacent regions, and all other chromosomes were crossed out after transgenic insertion. It remains possible that variation between the BDSC #58492 injection line genome and the dm6 reference genome could have caused missed identification of off-targets. Despite this, the HDR-mediated insertion of T-GEM utilized homology arms approximately 1 kb in length each, and it is unlikely that any regions adjacent to the potential off-targets exhibit sufficient homology to permit usage of the T-GEM donor plasmid as a DNA-DSB repair template.

4.2 Female neuroanatomy of *fru*^{P2}-expressing tissues

Using the *fru*^{P2-T-GEM} transgenic line to drive a membrane bound GFP reporter in *fru*^{P2}-expressing tissues, *fru*^{P2} expression is identified in adult female optic tissues, the central brain, and the ventral nerve cord.

4.2.1 Female optic tissues express *fru*^{P2}

Previous high-throughput RNAseq data identified high levels of P2 exon expression occurring in female eyes (Leader et al., 2018). Here, I have experimentally characterized the spatial expression of *fru*^{P2} in optic tissues to a higher specificity. From the epi-fluorescent imaging, *fru*^{P2}-expressing tissues were identified in the ocelli and the lamina. *fru*^{P2} expression was identified in all three ocelli. The *Drosophila* ocelli are simple eye structures that exhibit peak activity in response to light in the ultraviolet to blue range (Pollock & Benzer, 1988). Light in this frequency range may aid regulation of circadian rhythms for both locomotor activity (Rieger et al., 2003) and mating activity (Sakai et al., 2002; Sakai & Ishida, 2001). *Drosophila simulans* have an anti-phasic circadian rhythm for mating activity compared to *D. melanogaster*, which may contribute to the behavioural isolation between these species (Sakai & Ishida, 2001). It is possible that the ocelli provide feedback about environmental light levels for a female to determine whether it is an appropriate time to accept courtship attempts and perhaps, based on temporal alignment of courtship to the species-specific circadian rhythm for mating activity, whether a courting male is conspecific or heterospecific. *fru*^{P2} expression was also identified in the lamina. In *Drosophila*, the retinal photoreceptors arborize to monopolar cells in the lamina to form ‘cartridges’ that transmit descending visual information to the optic lobe medulla (Vogt & Desplan, 2007). The lamina L1 and L2 monopolar cells have been identified to relay back-to-front and front-to-back motion information about objects, while the L3 pathway provides object

orientation information (Rister et al., 2007). For copulation to occur, males must first display courtship behaviours for female assessment, often initiated by physical orienting towards and approaching/following a female. The lamina may relay such information in females and thus could be a primary signal for initiating the neural processes for copulatory decision-making.

4.2.2 Female central brain regions express *fru*^{P2}

The epi-fluorescent live imaging revealed that *fru*^{P2-T-GEM} drove expression of membrane-bound GFP in cell bodies within SOG and in the tissues surrounding the cante (ventral oesophageal foramen). Fru^{COM} products may be expressed in the brain, but the observed fluorescence was concluded to most likely be caused by antibody cross-reactivity (Lee et al., 2000). Interestingly, the IHC in Lee et al., (2000) seemed to label Fru^{COM} in at least one bilateral pair of cell bodies in the SOG (Lee et al., 2000) that display spatial similarity to the *fru*^{P2}-expressing neurons in the SOG, and thus it seems likely that they are the same cells.

Octopaminergic neurons have a role in modulating female receptivity through roles in post-mating responses, ovulation, and oviposition (Lee et al., 2003; Rezával et al., 2014), and recent research in our laboratory demonstrated that two bilateral pairs of octopaminergic neurons in the central brain modulate female receptivity (Moehring laboratory, unpublished data). The *fru*^{P2}-expressing neurons patterns resemble previously mapped octopaminergic circuitry in the central brain (Busch et al., 2009), with localization within the SOG and cante. It is possible that the *fru*^{P2}-expressing neurons in the central brain could be octopaminergic, but further investigation is required. There are also several studies that have identified small populations of neurons in the central brain that affect female receptivity and appear to have similar spatial expression patterns to the *fru*^{P2}-expressing neurons. The *spin-A* cluster of *spin* expressing neurons are suspected to receive gustatory input from the mouthparts and proboscis for modulation of female receptivity,

and has been observed in the SOG and cantle (or region surrounding the ventral oesophageal foramen) in a pattern that resembles that of *fru*^{P2}-expressing neurons (Sakurai et al., 2013). Although the *spin-A* neuron cluster does not express *fru*, it remains possible that *fru*^{P2}-expressing neurons form neural circuitry with *spin* neurons to modulate female receptivity. The *spin-A* neurons also form circuitry with *ppk*-expressing neurons (Sakurai et al., 2013) that have projections, but not cell bodies, in the SOG (Yang et al., 2009). These *ppk*-neuronal projections appear to densify at two to four locations in the SOG (Yang et al., 2009) that are spatially similar to the observed *fru*^{P2}-expressing neuron cell bodies. The *dsx*-expressing SAG neurons also relay SP signalling from *fru*, *ppk* and *dsx* co-expressing SPSNs to the SOG (Feng et al., 2014) and the *vpoDNs* to modulate initiation of post-mating behaviours (Wang et al., 2021). Localization of *fru*^{P2} neurons in the SOG may implicate them in SP-mediated post-mating behaviours, but further investigation is needed to determine if *fru*^{P2} neurons form circuitry with these *spin*, *ppk*, and/or *dsx* neurons.

4.2.3 Female ventral nerve cord regions express *fru*^{P2}

From the epi-fluorescent imaging, *fru*^{P2} expression was identified in multiple loci within the ventral nerve cord, including all six neuropils, the accessory metathoracic neuropils (AmNp), and the abdominal neuromeres. While the brain is the more likely location of neurons directly affecting behaviours, there also are several ways that the VNC could be impacting female receptivity. The VNC is a relay center for both sensory and motor signalling from internal and external organs, however it is unlikely that the *fru*^{P2} tissues observed in the VNC are part of motor pathways. Hyperactivation or silencing of the *fru*^{P2}-expressing neurons was not qualitatively observed to increase or decrease general locomotion, nor to cause seizures or paralysis, which might be expected if *fru*^{P2} is expressed in motor neurons.

Instead, there is a possibility that the *fru*^{P2} expression in the leg neuropils and AmNp could impact female receptivity through efferent sensory signalling pathways from gustatory receptors on the legs and wings. The AmNp is known to receive afferent sensory signalling from the wings (Venkatasubramanian & Mann, 2019), and the legs express *ppk23* and *ppk25* gustatory neurons that decrease female receptivity upon silencing (Vijayan et al., 2014). Notably, *ppk23* and *ppk25* neurons only affected female receptivity when the third antennal segment was absent (Vijayan et al., 2014), implying the legs have a secondary role in pheromonal detection. Thus, *fru*^{P2} neurons relaying afferent gustatory signalling from the wings and legs could contribute to, but likely not fully constitute, the pheromonal assessment of a courting male. Besides the pheromonal cues provided by a courting male, there are external factors that could influence female receptivity. Presence of olfactory and gustatory cues from yeast can indicate presence of high nutritional food sources and act to increase female receptivity (Gorter et al., 2016). The *fru*^{P2} neurons projecting from the legs and wings could afferently relay external information used to assess if the environment can sufficiently provide resources for egg production and offspring survival, which could contribute to modulating receptivity (Gorter et al., 2016).

Expression of *fru*^{P2} was also identified in the abdominal neuromeres, which has been highly implicated in the SP-mediated post-mating response. Neurons expressing *ppk* (Häsemeyer et al., 2009) and *dsx* (Rezával et al., 2012, 2014), and the vpoDNs (Wang et al., 2021) are implicated in post-mating responses and have projections to, and through, the abdominal neuromeres to relay both ascending SP signalling from SPSNs and descending signalling to control vaginal plate opening. Previous work has demonstrated that a population of approximately nine SP-signalling *dsx*-expressing neurons in the abdominal neuromeres are octopaminergic, and approximately four of these neurons have ascending projections terminating

in the SOG (Rezával et al., 2012, 2014). The expression of *fru*^{P2} in the SOG and abdominal neuromeres appears to mirror the general layout of the SP-signalling system, but further investigation is needed to determine if *fru*^{P2}-neurons shares circuitry with the SP network and how they contribute to SP-signalling.

4.3 Female receptivity is modulated by *fru*^{P2}-expressing neurons

In this project, hyperactivation or silencing of *fru*^{P2}-neurons significantly and robustly affect female receptivity. The data presented in this project is the first to demonstrate that any *fru*-neurons besides *fru*^{P1}-neurons can influence behaviour, and the first to demonstrate that *fru*^{COM} neurons modulate female receptivity.

4.3.1 Constitutive silencing of *fru*^{P2}-expressing neurons reduces receptivity

Neuronal silencing of the SPSNs in the female reproductive organs or the SAGs that transmit ascending SP-signalling to the SOG decrease female receptivity and promote post-mating behaviours (Feng et al., 2014; Häsemeyer et al., 2009; Rideout et al., 2010; Yang et al., 2009). The *fru*^{P2}-neurons have similarities in spatial expression patterns to SP-signalling neurons in both the SOG and abdominal neuromeres, and constitutive silencing of *fru*^{P2}-neurons caused a significant decrease in female receptivity. These results imply that *fru*^{P2}-neurons may have a direct role in, or have shared circuitry with, the ascending SP-signalling network. Constitutive silencing of *fru*^{P2}-neurons was not qualitatively observed to decrease locomotion or cause paralysis. This implies that silencing of these *fru*^{P2}-neurons is directly and specifically affecting female receptivity, perhaps through SP signalling.

Silencing *fru*^{P2}-neurons using the temperature-sensitive Shibire^{ts} resulted in a non-significant decrease in female receptivity compared to controls. It is possible that this was a type II error that resulted from insufficient experimental power due to low sample sizes, but silencing

through $K_{ir}2.1$ or TeTxLC significantly and robustly reduced female receptivity. This was surprising since *Shibire^{ts}* has previously been demonstrated to be as effective, if not more effective, than $K_{ir}2.1$ or TeTxLC as an effector for neuronal silencing (Pauls et al., 2015). However, the *Shibire^{ts}*, $K_{ir}2.1$, and TeTxLC effectors cause neuronal silencing by different mechanisms: *Shibire^{ts}* prevents recycling of synaptic vesicles at high temperatures, $K_{ir}2.1$ hyperpolarizes neurons constitutively, and TeTxLC cleaves synaptobrevin to prevent vesicular fusion to the pre-synaptic membrane (Pauls et al., 2015). The *shibire^{ts}* mutation rapidly inhibits neuronal signalling at high temperatures, causing full paralysis within two minutes and death after 12 hours if expressed pan-neurally (Grigliatti et al., 1973). Ectopic expression of *Shibire^{ts}* in cholinergic neurons also causes paralysis at similar rates (Kitamoto, 2001). In contrast to $K_{ir}2.1$ or TeTxLC, there is a temporal delay in the silencing effects of *Shibire^{ts}* since it requires depletion of synaptic vesicles rather than directly inhibiting neuronal depolarization or neurotransmitter release from the pre-synaptic terminal. Therefore, a sufficient amount of neuronal activation is required for neuronal silencing by *Shibire^{ts}*. Female rejection is an active behaviour, and it follows that activation of neurons that elicit female rejection are required for their silencing by *Shibire^{ts}*. The mating assays in this project used virgin females that were naïve to male courtship, and it is possible that the quantity of rejection behaviours exhibited before and after initial exposure to a courting male is insufficient for synaptic depletion of *fru^{P2}*-neurons despite the 30-minute acclimation period to the restrictive temperature. Alternatively, it could imply that *fru^{P2}*-neurons are specifically tuned for modulating behaviours that are not exhibited during the mating assays, such as rejection or feeding behaviours. Additionally, the *fru^{P2}*-neurons and their pre-synaptic partners could be extremely sensitive and have low activation thresholds, making it difficult to reach synaptic depletion before mating occurs.

4.3.2 Hyperactivation of *fru*^{P2}-expressing neurons reduces receptivity

Hyperactivation of *fru*^{P2}-neurons virtually eliminates receptivity to courting conspecific males. It is somewhat surprising that both hyperactivation and silencing of *fru*^{P2}-neurons cause significant decreases in female receptivity. This suggests that the neural circuitry for female copulatory decision-making is finely tuned such that deviation in activation levels disrupting a specific excitatory and inhibitory balance (E/I balance) triggers elicitation of rejection behaviours. Similarly, elicitation of male courtship by *fru*^M and *dsx* co-expressing neurons requires a specific E/I balance from afferent sensory neurons, which provide both excitatory and inhibitory signalling upon detection of female pheromones (Kallman et al., 2015). It is possible that the *fru*^{P2}-neurons could comprise separate populations of excitatory and inhibitory neurons that are integrated into a single neural circuit that modulates receptivity based on E/I balance. It is also possible that *fru*^{P2}-neurons are integrated into multiple neural circuits that are components of female receptivity as a whole. In either case, the wide distribution of *fru*^{P2}-neurons suggests that female receptivity is governed by highly complex combinations of multimodal external and internal signalling. These may include visual signalling from the optic tissues, gustatory or pheromonal signalling from external organs such as the legs and wings, and internal SP signalling from the reproductive organs.

The wide distribution of *fru*^{P2}-expression makes it difficult to disentangle the pathway(s) or mechanism(s) by which these tissues modulate female receptivity. In contrast to SP-signalling and the initiation of post-mating responses, the roles of visual, gustatory, and pheromonal signalling in modulation of female receptivity are not well characterized. If *fru*^{P2}-neurons have a role in SP-signalling, and silencing SP-signalling neurons results in decreased receptivity (Feng et al., 2014; Häsemeyer et al., 2009; Rideout et al., 2010; Yang et al., 2009), then it can be

inferred that hyperactivation of *fru*^{P2}-neurons independent of the SP-signalling pathway caused the observed decrease in female receptivity. Hyperactivation of the *fru*^{P2}-neurons strongly decreased female receptivity but was not qualitatively observed to cause increased locomotion or grooming, or to cause abnormally aggressive behaviours such as headbutting, boxing, or tussling; suggesting that these neurons are directly and specifically modulating female receptivity, perhaps through visual, pheromonal, and/or gustatory signalling. Characterization of the *fru*^{P2}-neurons causing decreased receptivity upon hyperactivation may provide insights into whether signalling independent of SP contributes to modulation of female receptivity, and if so, the types of signalling that are important. To approach this, *GAL80* constructs can be used to inhibit Gal4 activity in a tissue-specific manner, reducing the number of cells where Gal4 is active. For example, the *tshirt-GAL80* construct, which expresses Gal80 in the VNC, can be crossed into flies carrying *fru*^{P2-T-GEM} and UAS-*TrpA1* to create flies that only have hyperactivation of *fru*^{P2}-neurons in optic tissues and the central brain. Another approach for characterization of *fru*^{P2}-expressing neuronal subgroups is the split-*GAL4* system for intersectional expression of UAS-constructs (see Future directions, below).

4.3.3 Ablation of *fru*^{P2}-expressing tissues does not affect receptivity

Driving Reaper to ablate all *fru*^{P2}-expressing tissues was not observed to affect female receptivity. Although these experiments were preliminary and may have been insufficiently powered due to low sample sizes, the results provide possible insight on the role of *fru*^{P2}-neurons in female receptivity. Females with ablated *fru*^{P2}-expressing tissues were qualitatively observed to exhibit typical rejection behaviours in response to male courtship prior to copulation, including running, decamping, wing flicking, and kicking. During the 30-minute assays, females did not re-mate and were observed to reject all courtship following initial mating. These results

imply that *fru*^{P2}-neurons may not be necessary for initiating post-mating behaviours.

Approximately eight of the 34 SPSNs in the female reproductive tract express *fru*^{P1} (Rezával et al., 2012) and SAG neurons do not express *fru*^{P1} (Feng et al., 2014), but it remains unknown if these SP signalling neurons express *fru*^{P2}. The observation that females with ablated *fru*^{P2}-neurons do not re-mate suggests that, if *fru*^{P2} is expressed in the SP signalling network, they may not be necessary for SP-mediated post-mating behaviours. These observations also imply that *fru*^{P2}-neurons may not be necessary for performing rejection behaviours, thus it would be unlikely that *fru*^{P2}-neurons are modulating female receptivity by directly eliciting rejection behaviours; instead, it would be more likely that they provide afferent signalling to modulate upstream copulatory decision-making. Further extension on this experiment, including quantification of mating latency and specific rejection behaviours exhibited pre- and post-mating, is needed to determine if ablation of *fru*^{P2}-expressing tissues causes subtle changes in female receptivity that were undetectable in this preliminary experiment.

4.4 Future directions

In this project, the T-GEM construct inserted downstream of the P2 exon was used to screen for successful CRISPR/Cas9-HDR transgenesis and to drive expression of a non-fusion Gal4 under control of *fru*^{P2} regulation. However, the T-GEM construct is highly versatile, and the *fru*^{P2-T-GEM} line can be easily modified for future research. The most proximal and distal ends of the T-GEM construct include inverted attP sites for ϕ C31-mediated cassette exchange to allow for replacement of SA-T2A-GAL4-Hsp70pA and 3xP3-RFP-SV40pA with a different genetic construct. This can be done by crossing pre-existing lines that express ϕ C31-integrase and carry an inverted attB-flanked gene construct, or by microinjecting expression vectors containing those components. In short, *fru*^{P2-T-GEM} line can be used to generate further transgenic lines that express

genetic constructs under control of *fru*^{P2} regulation. For higher-resolution examination of *fru*^{P2}-neurons, the T-GEM contents could be exchanged for a split-*GAL4* hemidriver. The split-Gal4 system requires dimerization of split-Gal4 hemidrivers, consisting of a Gal4 DNA binding domain (Gal4-DBD) and p65 activation domain (p65-AD), within a cell for the formation of a functional GAL4 protein (Luan et al., 2006). Only tissues with both DBD and AD expression can promote transcriptional initiation from a UAS site (Luan et al., 2006). Using this approach, *fru*^{P2}-*GAL4-DBD* could be paired with *TβH-p65-AD* (expresses p65-AD in octopaminergic neurons) to drive expression of a UAS fluorescent reporter only in cells that co-express *fru*^{P2} and octopamine. This technique could also be applied to drive expression of neuronal hyperactivators or silencers in specific subsets of *fru*^{P2}-expressing cells, such as lamina tissue or ventral nerve cord tissue. Further, the expression pattern of individual *fru*^{COM} transcripts is currently unknown. The split-Gal4 system could be applied to examine individual transcripts within the *fru*^{P2} transcript group (for example, targeting of only *fru*^{P2} transcripts expressing the A exon). For anatomical mapping of neural architecture upstream and downstream of *fru*^{P2}-neurons, T-GEM could be exchanged for trans-Tango components for trans-synaptic circuit tracing (Talay et al., 2017) and, once potential synaptic connections have been determined, T-GEM could be exchanged for t-GRASP components to assess neural connectivity to specific neuronal subtypes (Shearin et al., 2018).

4.5 Final conclusions

In this project, I produced the *fru*^{P2-T-GEM} transgenic line and used it to reveal that *fru*^{P2}-neurons are localized in optic tissues, the central brain, and the ventral nerve cord. I found that these neurons have a strong modulating role in female receptivity and can exert this effect via both increased and decreased neural activity. Further examination of the non-sex-specific splice

variants and investigation from a female-centric point of view are critical to understanding the biological functions of the *fruitless* gene. This research highlights the exceptional complexity of decision-making processes that underlie a female's decision to mate. It is evident that there is much research that has yet to be performed in order to fully understand this scrutinized and yet understudied gene.

References

- Adams, M. D. (2000). The genome sequence of *Drosophila melanogaster*. *Science*, 287(5461), 2185–2195. <https://doi.org/10.1126/science.287.5461.2185>
- Anand, A., Vilella, A., Ryner, L. C., Carlo, T., Goodwin, S. F., Song, H.-J., Gailey, D. A., Morales, A., Hall, J. C., Baker, B. S., & Taylor, B. J. (2001). Molecular genetic dissection of the sex-specific and vital functions of the *Drosophila melanogaster* sex determination gene *fruitless*. *Genetics*, 158(4), 1569–1595. <https://doi.org/10.1093/genetics/158.4.1569>
- Aranha, M. M., & Vasconcelos, M. L. (2018). Deciphering *Drosophila* female innate behaviors. *Current Opinion in Neurobiology*, 52, 139–148. <https://doi.org/10.1016/j.conb.2018.06.005>
- Austin, C. J., Guglielmo, C. G., & Moehring, A. J. (2014). A direct test of the effects of changing atmospheric pressure on the mating behavior of *Drosophila melanogaster*. *Evolutionary Ecology*, 28(3), 535–544. <https://doi.org/10.1007/s10682-014-9689-8>
- Bassett, A. R., & Liu, J.-L. (2014). CRISPR/Cas9 and genome editing in *Drosophila*. *Journal of Genetics and Genomics*, 41(1), 7–19. <https://doi.org/10.1016/j.jgg.2013.12.004>
- Bath, E., Bowden, S., Peters, C., Reddy, A., Tobias, J. A., Easton-Calabria, E., Seddon, N., Goodwin, S. F., & Wigby, S. (2017). Sperm and sex peptide stimulate aggression in female *Drosophila*. *Nature Ecology & Evolution*, 1(6), 1–6. <https://doi.org/10.1038/s41559-017-0154>
- Bay, R. A., Arnegard, M. E., Conte, G. L., Best, J., Bedford, N. L., McCann, S. R., Dubin, M. E., Chan, Y. F., Jones, F. C., Kingsley, D. M., Schluter, D., & Peichel, C. L. (2017). Genetic coupling of female mate choice with polygenic ecological divergence facilitates stickleback speciation. *Current Biology*, 27(21), 3344–3349. <https://doi.org/10.1016/j.cub.2017.09.037>
- Benchling. (2021). *Biology software*. <https://benchling.com>
- Billeter, J.-C., Atallah, J., Krupp, J. J., Millar, J. G., & Levine, J. D. (2009). Specialized cells tag sexual and species identity in *Drosophila melanogaster*. *Nature*, 461(7266), 987–991. <https://doi.org/10.1038/nature08495>
- Billeter, J.-C., Rideout, E. J., Dornan, A. J., & Goodwin, S. F. (2006). Control of male sexual behavior in *Drosophila* by the sex determination pathway. *Current Biology*, 16(17), R766–776. <https://doi.org/10.1016/j.cub.2006.08.025>
- Bischof, J., Maeda, R. K., Hediger, M., Karch, F., & Basler, K. (2007). An optimized transgenesis system for *Drosophila* using germ-line-specific ϕ C31 integrases. *Proceedings of the National Academy of Sciences of the United States of America*, 104(9), 3312–3317. <https://doi.org/10.1073/pnas.0611511104>
- Brand, A. H., & Perrimon, N. (1993). Targeted gene expression as a means of altering cell fates and generating dominant phenotypes. *Development*, 118(2), 401–415. <https://doi.org/10.1242/dev.118.2.401>

- Busch, S., Selcho, M., Ito, K., & Tanimoto, H. (2009). A map of octopaminergic neurons in the *Drosophila* brain. *Journal of Comparative Neurology*, *513*(6), 643–667. <https://doi.org/10.1002/cne.21966>
- Callaerts, P., Leng, S., Clements, J., Benassayag, C., Cribbs, D., Kang, Y. Y., Walldorf, U., Fischbach, K.-F., & Strauss, R. (2001). *Drosophila* Pax-6/eyeless is essential for normal adult brain structure and function. *Journal of Neurobiology*, *46*(2), 73–88. [https://doi.org/10.1002/1097-4695\(20010205\)46:2<73::aid-neu10>3.0.co;2-n](https://doi.org/10.1002/1097-4695(20010205)46:2<73::aid-neu10>3.0.co;2-n)
- Campesan, S., Dubrova, Y., Hall, J. C., & Kyriacou, C. P. (2001). The *nonA* gene in *Drosophila* conveys species-specific behavioral characteristics. *Genetics*, *158*(4), 1535–1543.
- Carracedo, M. C., Suarez, C., & Casares, P. (2000). Sexual isolation between *Drosophila melanogaster*, *D. Simulans* and *D. Mauritiana*: Sex and species specific discrimination. *Genetica*, *108*(2), 155–162. <https://doi.org/10.1023/A:1004132414511>
- Chen, D., Sitaraman, D., Chen, N., Jin, X., Han, C., Chen, J., Sun, M., Baker, B. S., Nitabach, M. N., & Pan, Y. (2017). Genetic and neuronal mechanisms governing the sex-specific interaction between sleep and sexual behaviors in *Drosophila*. *Nature Communications*, *8*(1), 1–14. <https://doi.org/10.1038/s41467-017-00087-5>
- Chenoweth, S. F., & Blows, M. W. (2006). Dissecting the complex genetic basis of mate choice. *Nature Reviews Genetics*, *7*(9), 681–692. <https://doi.org/10.1038/nrg1924>
- Chowdhury, T., Calhoun, R. M., Bruch, K., & Moehring, A. J. (2020). The *fruitless* gene affects female receptivity and species isolation. *Proceedings of the Royal Society B: Biological Sciences*, *287*(1923), 20192765. <https://doi.org/10.1098/rspb.2019.2765>
- Claridge, M. F. (2009). Species are real biological entities. In F. J. Ayala & R. Arp (Eds.), *Contemporary Debates in Philosophy of Biology* (pp. 91–109). Wiley-Blackwell. <https://doi.org/10.1002/9781444314922.ch5>
- Coen, P., Clemens, J., Weinstein, A. J., Pacheco, D. A., Deng, Y., & Murthy, M. (2014). Dynamic sensory cues shape song structure in *Drosophila*. *Nature*, *507*(7491), 233–237. <https://doi.org/10.1038/nature13131>
- Cook, R., & Connolly, K. (1973). Rejection responses by female *Drosophila melanogaster*: Their ontogeny, causality and effects upon the behaviour of the courting male. *Behaviour*, *44*(1–2), 142–165. <https://doi.org/10.1163/156853973X00364>
- Court, R., Namiki, S., Armstrong, J. D., Börner, J., Card, G., Costa, M., Dickinson, M., Duch, C., Korff, W., Mann, R., Merritt, D., Murphey, R. K., Seeds, A. M., Shirangi, T., Simpson, J. H., Truman, J. W., Tuthill, J. C., Williams, D. W., & Shepherd, D. (2020). A systematic nomenclature for the *Drosophila* ventral nerve cord. *Neuron*, *107*(6), 1071–1079.e2. <https://doi.org/10.1016/j.neuron.2020.08.005>
- Coyne, J. A., & Orr, H. A. (1989). Patterns of speciation in *Drosophila*. *Evolution*, *43*(2), 362–381. <https://doi.org/10.1111/j.1558-5646.1989.tb04233.x>
- Coyne, J. A., & Orr, H. A. (1997). “Patterns of speciation in *Drosophila*” revisited. *Evolution*, *51*(1), 295–303. <https://doi.org/10.1111/j.1558-5646.1997.tb02412.x>
- Coyne, J. A., & Orr, H. A. (2004). *Speciation*. Sinauer Associates.

- Coyne, J. A., & Oyama, R. (1995). Localization of pheromonal sexual dimorphism in *Drosophila melanogaster* and its effect on sexual isolation. *Proceedings of the National Academy of Sciences of the United States of America*, *92*(21), 9505–9509.
<https://doi.org/10.1073/pnas.92.21.9505>
- Davis, J. S., Percy, M. J., Yew, J. Y., & Moyle, L. C. (2021). A shift to shorter cuticular hydrocarbons accompanies sexual isolation among *Drosophila americana* group populations. *Evolution Letters*. <https://doi.org/10.1002/evl3.246>
- Dawley, E. M. (1986). Behavioral isolating mechanisms in sympatric terrestrial salamanders. *Herpetologica*, *42*(2), 156–164.
- Diao, F., Ironfield, H., Luan, H., Diao, F., Shropshire, W. C., Ewer, J., Marr, E., Potter, C. J., Landgraf, M., & White, B. H. (2015). Plug-and-play genetic access to *Drosophila* cell types using exchangeable exon cassettes. *Cell Reports*, *10*(8), 1410–1421.
<https://doi.org/10.1016/j.celrep.2015.01.059>
- Diao, F., & White, B. H. (2012). A novel approach for directing transgene expression in *Drosophila*: T2A-Gal4 in-frame fusion. *Genetics*, *190*(3), 1139–1144.
<https://doi.org/10.1534/genetics.111.136291>
- Dickson, B. J. (2008). Wired for sex: The neurobiology of *Drosophila* mating decisions. *Science*, *322*(5903), 904–909. <https://doi.org/10.1126/science.1159276>
- Dobzhansky, T. (1937). Genetic nature of species differences. *The American Naturalist*, *71*(735), 404–420. <https://doi.org/10.1086/280726>
- Elgin, S. C. R., & Reuter, G. (2013). Position-effect variegation, heterochromatin formation, and gene silencing in *Drosophila*. *Cold Spring Harbor Perspectives in Biology*, *5*(8), a017780. <https://doi.org/10.1101/cshperspect.a017780>
- Ewing, A. W., & Bennet-Clark, H. C. (1968). The courtship songs of *Drosophila*. *Behaviour*, *31*(3–4), 288–301. <https://doi.org/10.1163/156853968X00298>
- Featherstone, C., & Jackson, S. P. (1999). DNA double-strand break repair. *Current Biology*, *9*(20), R759–R761. [https://doi.org/10.1016/S0960-9822\(00\)80005-6](https://doi.org/10.1016/S0960-9822(00)80005-6)
- Feng, K., Palfreyman, M. T., Häsemeyer, M., Talsma, A., & Dickson, B. J. (2014). Ascending SAG neurons control sexual receptivity of *Drosophila* females. *Neuron*, *83*(1), 135–148.
<https://doi.org/10.1016/j.neuron.2014.05.017>
- Ferreiro, M. J., Pérez, C., Marchesano, M., Ruiz, S., Caputi, A., Aguilera, P., Barrio, R., & Cantera, R. (2018). *Drosophila melanogaster* White Mutant *w1118* undergo retinal degeneration. *Frontiers in Neuroscience*, *11*, 732.
<https://doi.org/10.3389/fnins.2017.00732>
- Ferveur, J.-F. (2010). *Drosophila* female courtship and mating behaviors: Sensory signals, genes, neural structures and evolution. *Current Opinion in Neurobiology*, *20*(6), 764–769.
<https://doi.org/10.1016/j.conb.2010.09.007>
- Gill, K. S. (1963). A mutation causing abnormal mating behavior. *Drosophila Information Service*, *38*, 33.

- González, M., Martín-Ruiz, I., Jiménez, S., Pirone, L., Barrio, R., & Sutherland, J. D. (2011). Generation of stable *Drosophila* cell lines using multicistronic vectors. *Scientific Reports*, *1*(1), 75. <https://doi.org/10.1038/srep00075>
- Goodwin, S. F., Taylor, B. J., Vilella, A., Foss, M., Ryner, L. C., Baker, B. S., & Hall, J. C. (2000). Aberrant splicing and altered spatial expression patterns in *fruitless* mutants of *Drosophila melanogaster*. *Genetics*, *154*(2), 725–745. <https://doi.org/10.1093/genetics/154.2.725>
- Gorter, J. A., Jagadeesh, S., Gahr, C., Boonekamp, J. J., Levine, J. D., & Billeter, J.-C. (2016). The nutritional and hedonic value of food modulate sexual receptivity in *Drosophila melanogaster* females. *Scientific Reports*, *6*(1), 19441. <https://doi.org/10.1038/srep19441>
- Goyal, L., McCall, K., Agapite, J., Hartwig, E., & Steller, H. (2000). Induction of apoptosis by *Drosophila reaper*, *hid* and *grim* through inhibition of IAP function. *The EMBO Journal*, *19*(4), 589–597. <https://doi.org/10.1093/emboj/19.4.589>
- Gratz, S. J., Ukken, F. P., Rubinstein, C. D., Thiede, G., Donohue, L. K., Cummings, A. M., & O'Connor-Giles, K. M. (2014). Highly specific and efficient CRISPR/Cas9-catalyzed homology-directed repair in *Drosophila*. *Genetics*, *196*(4), 961–971. <https://doi.org/10.1534/genetics.113.160713>
- Grigliatti, T. A., Hall, L., Rosenbluth, R., & Suzuki, D. T. (1973). Temperature-sensitive mutations in *Drosophila melanogaster*. *Molecular and General Genetics*, *120*(2), 107–114. <https://doi.org/10.1007/BF00267238>
- Gunst, N., Vasey, P. L., & Leca, J.-B. (2018). Deer mates: A quantitative study of heterospecific sexual behaviors performed by Japanese macaques toward sika deer. *Archives of Sexual Behavior*, *47*(4), 847–856. <https://doi.org/10.1007/s10508-017-1129-8>
- Hales, K. G., Korey, C. A., Larracunte, A. M., & Roberts, D. M. (2015). Genetics on the fly: A primer on the *Drosophila* model system. *Genetics*, *201*(3), 815–842. <https://doi.org/10.1534/genetics.115.183392>
- Hall, J. C. (1978). Courtship among males due to a male-sterile mutation in *Drosophila melanogaster*. *Behavior Genetics*, *8*(2), 125–141. <https://doi.org/10.1007/BF01066870>
- Hall, J. C. (1994). The mating of a fly. *Science*, *264*(5166), 1702–1714. <https://doi.org/10.1126/science.8209251>
- Hamada, F. N., Rosenzweig, M., Kang, K., Pulver, S. R., Ghezzi, A., Jegla, T. J., & Garrity, P. A. (2008). An internal thermal sensor controlling temperature preference in *Drosophila*. *Nature*, *454*(7201), 217–220. <https://doi.org/10.1038/nature07001>
- Häsemeyer, M., Yapici, N., Heberlein, U., & Dickson, B. J. (2009). Sensory neurons in the *Drosophila* genital tract regulate female reproductive behavior. *Neuron*, *61*(4), 511–518. <https://doi.org/10.1016/j.neuron.2009.01.009>
- Heigwer, F., Kerr, G., & Boutros, M. (2014). E-CRISP: Fast CRISPR target site identification. *Nature Methods*, *11*(2), 122–123. <https://doi.org/10.1038/nmeth.2812>

- Heinrichs, V., Ryner, L. C., & Baker, B. S. (1998). Regulation of sex-specific selection of *fruitless* 5' splice sites by *transformer* and *transformer-2*. *Molecular and Cellular Biology*, *18*(1), 450–458. <https://doi.org/10.1128/MCB.18.1.450>
- Hoskins, R. A., Carlson, J. W., Wan, K. H., Park, S., Mendez, I., Galle, S. E., Booth, B. W., Pfeiffer, B. D., George, R. A., Svirskas, R., Krzywinski, M., Schein, J., Accardo, M. C., Damia, E., Messina, G., Méndez-Lago, M., de Pablos, B., Demakova, O. V., Andreyeva, E. N., ... Celniker, S. E. (2015). The Release 6 reference sequence of the *Drosophila melanogaster* genome. *Genome Research*, *25*(3), 445–458. <https://doi.org/10.1101/gr.185579.114>
- Howe, K. L., Achuthan, P., Allen, J., Allen, J., Alvarez-Jarreta, J., Amode, M. R., Armean, I. M., Azov, A. G., Bennett, R., Bhai, J., Billis, K., Boddu, S., Charkhchi, M., Cummins, C., Da Rin Fioretto, L., Davidson, C., Dodiya, K., El Houdaigui, B., Fatima, R., ... Flicek, P. (2021). Ensembl 2021. *Nucleic Acids Research*, *49*(Database Issue), D884–D891. <https://doi.org/10.1093/nar/gkaa942>
- Immonen, E., & Ritchie, M. G. (2012). The genomic response to courtship song stimulation in female *Drosophila melanogaster*. *Proceedings of the Royal Society B: Biological Sciences*, *279*(1732), 1359–1365. <https://doi.org/10.1098/rspb.2011.1644>
- Jallon, J.-M. (1984). A few chemical words exchanged by *Drosophila* during courtship and mating. *Behavior Genetics*, *14*(5), 441–478. <https://doi.org/10.1007/BF01065444>
- Jallon, J.-M., & David, J. R. (1987). Variations in cuticular hydrocarbons among the eight species of the *Drosophila Melanogaster* subgroup. *Evolution*, *41*(2), 294–302. <https://doi.org/10.1111/j.1558-5646.1987.tb05798.x>
- Jenett, A., Rubin, G. M., Ngo, T.-T. B., Shepherd, D., Murphy, C., Dionne, H., Pfeiffer, B. D., Cavallaro, A., Hall, D., Jeter, J., Iyer, N., Fetter, D., Hausenfluck, J. H., Peng, H., Trautman, E. T., Svirskas, R. R., Myers, E. W., Iwinski, Z. R., Aso, Y., ... Zugates, C. T. (2012). A GAL4-driver line resource for *Drosophila* neurobiology. *Cell Reports*, *2*(4), 991–1001. <https://doi.org/10.1016/j.celrep.2012.09.011>
- Kallman, B. R., Kim, H., & Scott, K. (2015). Excitation and inhibition onto central courtship neurons biases *Drosophila* mate choice. *ELife*, *4*, e11188. <https://doi.org/10.7554/eLife.11188>
- Katayama, N., Abbott, J. K., Kjærandsen, J., Takahashi, Y., & Svensson, E. I. (2014). Sexual selection on wing interference patterns in *Drosophila melanogaster*. *Proceedings of the National Academy of Sciences of the United States of America*, *111*(42), 15144–15148. <https://doi.org/10.1073/pnas.1407595111>
- Kimura, K., Hachiya, T., Koganezawa, M., Tazawa, T., & Yamamoto, D. (2008). *Fruitless* and *doublesex* coordinate to generate male-specific neurons that can initiate courtship. *Neuron*, *59*(5), 759–769. <https://doi.org/10.1016/j.neuron.2008.06.007>
- Kitamoto, T. (2001). Conditional modification of behavior in *Drosophila* by targeted expression of a temperature-sensitive *shibire* allele in defined neurons. *Journal of Neurobiology*, *47*(2), 81–92. <https://doi.org/10.1002/neu.1018>

- Kronforst, M. R., Young, L. G., Kapan, D. D., McNeely, C., O'Neill, R. J., & Gilbert, L. E. (2006). Linkage of butterfly mate preference and wing color preference cue at the genomic location of *wingless*. *Proceedings of the National Academy of Sciences of the United States of America*, *103*(17), 6575–6580. <https://doi.org/10.1073/pnas.0509685103>
- Lande, R. (1981). Models of speciation by sexual selection on polygenic traits. *Proceedings of the National Academy of Sciences*, *78*(6), 3721–3725. <https://doi.org/10.1073/pnas.78.6.3721>
- Larkin, A., Marygold, S. J., Antonazzo, G., Attrill, H., dos Santos, G., Garapati, P. V., Goodman, J. L., Gramates, L. S., Millburn, G., Strelets, V. B., Tabone, C. J., Thurmond, J., & FlyBase Consortium. (2021). FlyBase: Updates to the *Drosophila melanogaster* knowledge base. *Nucleic Acids Research*, *49*(D1), D899–D907. <https://doi.org/10.1093/nar/gkaa1026>
- Lassance, J.-M., Groot, A. T., Liénard, M. A., Antony, B., Borgwardt, C., Andersson, F., Hedenström, E., Heckel, D. G., & Löfstedt, C. (2010). Allelic variation in a fatty-acyl reductase gene causes divergence in moth sex pheromones. *Nature*, *466*(7305), 486–489. <https://doi.org/10.1038/nature09058>
- Laturney, M., & Moehring, A. J. (2012). The genetic basis of female mate preference and species isolation in *Drosophila*. *International Journal of Evolutionary Biology*, *2012*, 328392. <https://doi.org/10.1155/2012/328392>
- Leader, D. P., Krause, S. A., Pandit, A., Davies, S. A., & Dow, J. A. T. (2018). FlyAtlas 2: A new version of the *Drosophila melanogaster* expression atlas with RNA-Seq, miRNA-Seq and sex-specific data. *Nucleic Acids Research*, *46*(Database Issue), D809–D815. <https://doi.org/10.1093/nar/gkx976>
- Lecuit, T., & Wieschaus, E. (2000). Polarized insertion of new membrane from a cytoplasmic reservoir during cleavage of the *Drosophila* embryo. *Journal of Cell Biology*, *150*(4), 849–860. <https://doi.org/10.1083/jcb.150.4.849>
- Lee, G., Foss, M., Goodwin, S. F., Carlo, T., Taylor, B. J., & Hall, J. C. (2000). Spatial, temporal, and sexually dimorphic expression patterns of the *fruitless* gene in the *Drosophila* central nervous system. *Journal of Neurobiology*, *43*(4), 404–426. [https://doi.org/10.1002/1097-4695\(20000615\)43:4<404::aid-neu8>3.0.co;2-d](https://doi.org/10.1002/1097-4695(20000615)43:4<404::aid-neu8>3.0.co;2-d)
- Lee, H.-G., Seong, C.-S., Kim, Y.-C., Davis, R. L., & Han, K.-A. (2003). Octopamine receptor OAMB is required for ovulation in *Drosophila melanogaster*. *Developmental Biology*, *264*(1), 179–190. <https://doi.org/10.1016/j.ydbio.2003.07.018>
- Levitis, D. A., Lidicker, W. Z., & Freund, G. (2009). Behavioural biologists do not agree on what constitutes behaviour. *Animal Behaviour*, *78*(1), 103–110. <https://doi.org/10.1016/j.anbehav.2009.03.018>
- Li, H., Yang, Y., Hong, W., Huang, M., Wu, M., & Zhao, X. (2020). Applications of genome editing technology in the targeted therapy of human diseases: Mechanisms, advances and prospects. *Signal Transduction and Targeted Therapy*, *5*(1), 1–23. <https://doi.org/10.1038/s41392-019-0089-y>

- Linné, C. von. (1735). *Systema naturae*. Apud Theodorum Haak.
- Liu, H., & Kubli, E. (2003). Sex-peptide is the molecular basis of the sperm effect in *Drosophila melanogaster*. *Proceedings of the National Academy of Sciences of the United States of America*, *100*(17), 9929–9933. <https://doi.org/10.1073/pnas.1631700100>
- Lobov, A. A., Maltseva, A. L., Mikhailova, N. A., & Granovitch, A. I. (2019). The molecular mechanisms of gametic incompatibility in invertebrates. *Acta Naturae*, *11*(3), 4–15. <https://doi.org/10.32607/20758251-2019-11-3-4-15>
- Luan, H., Peabody, N. C., Vinson, C. R., & White, B. H. (2006). Refined spatial manipulation of neuronal function by combinatorial restriction of transgene expression. *Neuron*, *52*(3), 425–436. <https://doi.org/10.1016/j.neuron.2006.08.028>
- Mallet, J. (1995). A species definition for the modern synthesis. *Trends in Ecology & Evolution*, *10*(7), 294–299. [https://doi.org/10.1016/0169-5347\(95\)90031-4](https://doi.org/10.1016/0169-5347(95)90031-4)
- Manning, A. (1967). The control of sexual receptivity in female *Drosophila*. *Animal Behaviour*, *15*(2), 239–250. [https://doi.org/10.1016/0003-3472\(67\)90006-1](https://doi.org/10.1016/0003-3472(67)90006-1)
- Masly, J. P. (2011). 170 years of “lock-and-key”: Genital morphology and reproductive Isolation. *International Journal of Evolutionary Biology*, *2012*, e247352. <https://doi.org/10.1155/2012/247352>
- Matthews, B. B., Dos Santos, G., Crosby, M. A., Emmert, D. B., St Pierre, S. E., Gramates, L. S., Zhou, P., Schroeder, A. J., Falls, K., Strelets, V., Russo, S. M., Gelbart, W. M., & FlyBase Consortium. (2015). Gene model annotations for *Drosophila melanogaster*: Impact of high-throughput data. *G3 (Bethesda, Md.)*, *5*(8), 1721–1736. <https://doi.org/10.1534/g3.115.018929>
- Matute, D. R., & Cooper, B. S. (2021). Comparative studies on speciation: 30 years since Coyne and Orr. *Evolution*, *75*(4), 764–778. <https://doi.org/10.1111/evo.14181>
- Mayr, E. (1942). *Systematics and the origin of species*. Columbia University Press.
- McCullers, T. J., & Steiniger, M. (2017). Transposable elements in *Drosophila*. *Mobile Genetic Elements*, *7*(3), 1–18. <https://doi.org/10.1080/2159256X.2017.1318201>
- Merrill, R. M., Van Schooten, B., Scott, J. A., & Jiggins, C. D. (2011). Pervasive genetic associations between traits causing reproductive isolation in *Heliconius* butterflies. *Proceedings of the Royal Society B: Biological Sciences*, *278*(1705), 511–518. <https://doi.org/10.1098/rspb.2010.1493>
- Miller, D. E., Cook, K. R., & Hawley, R. S. (2019). The joy of balancers. *PLoS Genetics*, *15*(11). <https://doi.org/10.1371/journal.pgen.1008421>
- Mitoyen, C., Quigley, C., & Fusani, L. (2019). Evolution and function of multimodal courtship displays. *Ethology*, *125*(8), 503–515. <https://doi.org/10.1111/eth.12882>
- Moehring, A. J., & Boughman, J. W. (2019). Veiled preferences and cryptic female choice could underlie the origin of novel sexual traits. *Biology Letters*, *15*(2), 20180878. <https://doi.org/10.1098/rsbl.2018.0878>

- Montague, S. A., & Baker, B. S. (2016). Memory elicited by courtship conditioning requires mushroom body neuronal subsets similar to those utilized in appetitive memory. *PLOS ONE*, *11*(10), e0164516. <https://doi.org/10.1371/journal.pone.0164516>
- Nakano, Y., Fujitani, K., Kurihara, J., Ragan, J., Usui-Aoki, K., Shimoda, L., Lukacsovich, T., Suzuki, K., Sezaki, M., Sano, Y., Ueda, R., Awano, W., Kaneda, M., Umeda, M., & Yamamoto, D. (2001). Mutations in the novel membrane protein Spinster interfere with programmed cell death and cause neural degeneration in *Drosophila melanogaster*. *Molecular and Cellular Biology*, *21*(11), 3775–3788. <https://doi.org/10.1128/MCB.21.11.3775-3788.2001>
- Nanda, P., & Singh, B. N. (2012). Behavioural reproductive isolation and speciation in *Drosophila*. *Journal of Biosciences*, *37*(2), 359–374. <https://doi.org/10.1007/s12038-012-9193-7>
- Niida, T., & Koshikawa, S. (2021). No evidence for contribution of sexually monomorphic wing pigmentation pattern to mate choice in *Drosophila guttifera*. *Ethology*, *127*(7), 527–536. <https://doi.org/10.1111/eth.13157>
- Niwa, M., Rose, S. D., & Berget, S. M. (1990). In vitro polyadenylation is stimulated by the presence of an upstream intron. *Genes & Development*, *4*(9), 1552–1559. <https://doi.org/10.1101/gad.4.9.1552>
- Nojima, T., Kimura, K., Koganezawa, M., & Yamamoto, D. (2010). Neuronal synaptic outputs determine the sexual fate of postsynaptic targets. *Current Biology*, *20*(9), 836–840. <https://doi.org/10.1016/j.cub.2010.02.064>
- Nolte, D. J. (1952). The eye-pigmentary system of *Drosophila*. *Journal of Genetics*, *51*(1), 142. <https://doi.org/10.1007/BF02986712>
- Noreen, S., Pegoraro, M., Nouroz, F., Tauber, E., & Kyriacou, C. P. (2018). Interspecific studies of circadian genes *period* and *timeless* in *Drosophila*. *Gene*, *648*, 106–114. <https://doi.org/10.1016/j.gene.2018.01.020>
- Pang, T.-L., Ding, Z., Liang, S.-B., Li, L., Zhang, B., Zhang, Y., Fan, Y.-J., & Xu, Y.-Z. (2021). Comprehensive identification and alternative splicing of microexons in *Drosophila*. *Frontiers in Genetics*, *12*, 447. <https://doi.org/10.3389/fgene.2021.642602>
- Paterson, H. E. (1985). The recognition concept of species. In *Species and Speciation* (E. Vrba, Vol. 4).
- Pauls, D., von Essen, A., Lyutova, R., van Giesen, L., Rosner, R., Wegener, C., & Sprecher, S. G. (2015). Potency of transgenic effectors for neurogenetic manipulation in *Drosophila* larvae. *Genetics*, *199*(1), 25–37. <https://doi.org/10.1534/genetics.114.172023>
- Petersen, G., Hall, J. C., & Rosbash, M. (1988). The *period* gene of *Drosophila* carries species-specific behavioral instructions. *The EMBO Journal*, *7*(12), 3939–3947. <https://doi.org/10.1002/j.1460-2075.1988.tb03280.x>
- Pischedda, A., Shahandeh, M. P., Cochrane, W. G., Cochrane, V. A., & Turner, T. L. (2014). Natural variation in the strength and direction of male mating preferences for female

- pheromones in *Drosophila melanogaster*. *PLOS ONE*, 9(1), e87509.
<https://doi.org/10.1371/journal.pone.0087509>
- Pollock, J. A., & Benzer, S. (1988). Transcript localization of four opsin genes in the three visual organs of *Drosophila*; RH2 is ocellus specific. *Nature*, 333(6175), 779–782.
<https://doi.org/10.1038/333779a0>
- Rezával, C., Nojima, T., Neville, M. C., Lin, A. C., & Goodwin, S. F. (2014). Sexually dimorphic octopaminergic neurons modulate female postmating behaviors in *Drosophila*. *Current Biology*, 24(7), 725–730. <https://doi.org/10.1016/j.cub.2013.12.051>
- Rezával, C., Pavlou, H. J., Dornan, A. J., Chan, Y.-B., Kravitz, E. A., & Goodwin, S. F. (2012). Neural circuitry underlying drosophila *Drosophila* postmating behavioral responses. *Current Biology*, 22(13), 1155–1165. <https://doi.org/10.1016/j.cub.2012.04.062>
- Ribeiro, C., & Dickson, B. J. (2010). Sex peptide receptor and neuronal TOR/S6K signaling modulate nutrient balancing in *Drosophila*. *Current Biology*, 20(11), 1000–1005.
<https://doi.org/10.1016/j.cub.2010.03.061>
- Ribeiro, I. M. A., Drews, M., Bahl, A., Machacek, C., Borst, A., & Dickson, B. J. (2018). Visual projection neurons mediating directed courtship in *Drosophila*. *Cell*, 174(3), 607–621.
<https://doi.org/10.1016/j.cell.2018.06.020>
- Rideout, E. J., Dornan, A. J., Neville, M. C., Eadie, S., & Goodwin, S. F. (2010). Control of sexual differentiation and behavior by the *doublesex* gene in *Drosophila melanogaster*. *Nature Neuroscience*, 13(4), 458–466. <https://doi.org/10.1038/nn.2515>
- Rieger, D., Stanewsky, R., & Helfrich-Förster, C. (2003). Cryptochrome, compound eyes, Hofbauer-Buchner eyelets, and ocelli play different roles in the entrainment and masking pathway of the locomotor activity rhythm in the fruit fly *Drosophila melanogaster*. *Journal of Biological Rhythms*, 18(5), 377–391.
<https://doi.org/10.1177/0748730403256997>
- Rister, J., Pauls, D., Schnell, B., Ting, C.-Y., Lee, C.-H., Sinakevitch, I., Morante, J., Strausfeld, N. J., Ito, K., & Heisenberg, M. (2007). Dissection of the peripheral motion channel in the visual system of *Drosophila melanogaster*. *Neuron*, 56(1), 155–170.
<https://doi.org/10.1016/j.neuron.2007.09.014>
- Ritchie, M. G., Halsey, E. J., & Gleason, J. M. (1999). *Drosophila* song as a species-specific mating signal and the behavioural importance of Kyriacou & Hall cycles in *D. melanogaster* song. *Animal Behaviour*, 58(3), 649–657.
<https://doi.org/10.1006/anbe.1999.1167>
- Ryner, L. C., Goodwin, S. F., Castrillon, D. H., Anand, A., Vilella, A., Baker, B. S., Hall, J. C., Taylor, B. J., & Wasserman, S. A. (1996). Control of male sexual behavior and sexual orientation in *Drosophila* by the *fruitless* gene. *Cell*, 87(6), 1079–1089.
[https://doi.org/10.1016/S0092-8674\(00\)81802-4](https://doi.org/10.1016/S0092-8674(00)81802-4)
- Sakai, T., & Ishida, N. (2001). Circadian rhythms of female mating activity governed by clock genes in *Drosophila*. *Proceedings of the National Academy of Sciences of the United States of America*, 98(16), 9221–9225. <https://doi.org/10.1073/pnas.151443298>

- Sakai, T., Isono, K., Tomaru, M., Fukatami, A., & Oguma, Y. (2002). Light wavelength dependency of mating activity in the *Drosophila melanogaster* species subgroup. *Genes & Genetic Systems*, 77(3), 187–195. <https://doi.org/10.1266/ggs.77.187>
- Sakurai, A., Koganezawa, M., Yasunaga, K., Emoto, K., & Yamamoto, D. (2013). Select interneuron clusters determine female sexual receptivity in *Drosophila*. *Nature Communications*, 4(1), 1–9. <https://doi.org/10.1038/ncomms2837>
- Sato, K., Goto, J., & Yamamoto, D. (2019). Sex mysteries of the fly courtship master regulator *fruitless*. *Frontiers in Behavioral Neuroscience*, 13, 245. <https://doi.org/10.3389/fnbeh.2019.00245>
- Sato, K., Ito, H., Yokoyama, A., Toba, G., & Yamamoto, D. (2019). Partial proteasomal degradation of Lola triggers the male-to-female switch of a dimorphic courtship circuit. *Nature Communications*, 10(1), 1–15. <https://doi.org/10.1038/s41467-018-08146-1>
- Shearin, H. K., Quinn, C. D., Mackin, R. D., Macdonald, I. S., & Stowers, R. S. (2018). T-GRASP, a targeted GRASP for assessing neuronal connectivity. *Journal of Neuroscience Methods*, 306, 94–102. <https://doi.org/10.1016/j.jneumeth.2018.05.014>
- Sheng, G., Thouvenot, E., Schmucker, D., Wilson, D. S., & Desplan, C. (1997). Direct regulation of rhodopsin 1 by *Pax-6/eyeless* in *Drosophila*: Evidence for a conserved function in photoreceptors. *Genes & Development*, 11(9), 1122–1131. <https://doi.org/10.1101/gad.11.9.1122>
- Shirangi, T. R., Stern, D. L., & Truman, J. W. (2013). Motor control of *Drosophila* courtship song. *Cell Reports*, 5(3), 678–686. <https://doi.org/10.1016/j.celrep.2013.09.039>
- Shorey, H. H. (1962). Nature of the sound produced by *Drosophila melanogaster* during courtship. *Science*, 137(3531), 677–678. <https://doi.org/10.1126/science.137.3531.677>
- Sokolowski, M. B. (2001). *Drosophila*: Genetics meets behaviour. *Nature Reviews Genetics*, 2(11), 879–890. <https://doi.org/10.1038/35098592>
- Stocker, R. F., & Schorderet, M. (1981). Cobalt filling of sensory projections from internal and external mouthparts in *Drosophila*. *Cell and Tissue Research*, 216(3), 513–523. <https://doi.org/10.1007/BF00238648>
- Stockinger, P., Kvitsiani, D., Rotkopf, S., Tirián, L., & Dickson, B. J. (2005). Neural circuitry that governs *Drosophila* male courtship behavior. *Cell*, 121(5), 795–807. <https://doi.org/10.1016/j.cell.2005.04.026>
- Stratton, G. E., & Uetz, G. W. (1981). Acoustic communication and reproductive isolation in two species of wolf spiders. *Science*, 214(4520), 575–577. <https://doi.org/10.1126/science.214.4520.575>
- Suzuki, K., Juni, N., & Yamamoto, D. (1997). Enhanced mate refusal in female *Drosophila* induced by a mutation in the *spinster* locus. *Applied Entomology and Zoology*, 32(1), 235–243. <https://doi.org/10.1303/aez.32.235>
- Sweeney, S. T., Broadie, K., Keane, J., Niemann, H., & O’Kane, C. J. (1995). Targeted expression of tetanus toxin light chain in *Drosophila* specifically eliminates synaptic

- transmission and causes behavioral defects. *Neuron*, *14*(2), 341–351.
[https://doi.org/10.1016/0896-6273\(95\)90290-2](https://doi.org/10.1016/0896-6273(95)90290-2)
- Talay, M., Richman, E. B., Snell, N. J., Hartmann, G. G., Fisher, J. D., Sorkaç, A., Santoyo, J. F., Chou-Freed, C., Nair, N., Johnson, M., Szymanski, J. R., & Barnea, G. (2017). Transsynaptic mapping of second-order taste neurons in flies by trans-Tango. *Neuron*, *96*(4), 783–795. <https://doi.org/10.1016/j.neuron.2017.10.011>
- Talyn, B. C., & Dowse, H. B. (2004). The role of courtship song in sexual selection and species recognition by female *Drosophila melanogaster*. *Animal Behaviour*, *68*(5), 1165–1180. <https://doi.org/10.1016/j.anbehav.2003.11.023>
- Templeton, A. R. (1989). The meaning of species and speciation: A genetic perspective. In D. Otte & J. A. Endler (Eds.), *Speciation and its Consequences* (pp. 3–27).
- Turissini, D. A., McGirr, J. A., Patel, S. S., David, J. R., & Matute, D. R. (2018). The rate of evolution of postmating-prezygotic reproductive isolation in *Drosophila*. *Molecular Biology and Evolution*, *35*(2), 312–334. <https://doi.org/10.1093/molbev/msx271>
- Usui-Aoki, K., Ito, H., Ui-Tei, K., Takahashi, K., Lukacsovich, T., Awano, W., Nakata, H., Piao, Z. F., Nilsson, E. E., Tomida, J., & Yamamoto, D. (2000). Formation of the male-specific muscle in female *Drosophila* by ectopic *fruitless* expression. *Nature Cell Biology*, *2*(8), 500–506. <https://doi.org/10.1038/35019537>
- Van Valen, L. (1976). Ecological species, multispecies, and oaks. *Taxon*, *25*(2–3), 233–239. <https://doi.org/10.2307/1219444>
- Vaughan, A. G., Zhou, C., Manoli, D. S., & Baker, B. S. (2014). Neural pathways for the detection and discrimination of conspecific song in *D. melanogaster*. *Current Biology*, *24*(10), 1039–1049. <https://doi.org/10.1016/j.cub.2014.03.048>
- Venkatasubramanian, L., & Mann, R. S. (2019). The development and assembly of the *Drosophila* adult ventral nerve cord. *Current Opinion in Neurobiology*, *56*, 135–143. <https://doi.org/10.1016/j.conb.2019.01.013>
- Vijayan, V., Thistle, R., Liu, T., Starostina, E., & Pikielny, C. W. (2014). *Drosophila* pheromone-sensing neurons expressing the *ppk25* ion channel subunit stimulate male courtship and female receptivity. *PLOS Genetics*, *10*(3), e1004238. <https://doi.org/10.1371/journal.pgen.1004238>
- Vogt, N., & Desplan, C. (2007). The first steps in *Drosophila* motion detection. *Neuron*, *56*(1), 5–7. <https://doi.org/10.1016/j.neuron.2007.09.025>
- Wang, K., Wang, F., Forknall, N., Yang, T., Patrick, C., Parekh, R., & Dickson, B. J. (2021). Neural circuit mechanisms of sexual receptivity in *Drosophila* females. *Nature*, *589*(7843), 577–581. <https://doi.org/10.1038/s41586-020-2972-7>
- Ward, H. K. E., & Moehring, A. J. (2021). Genes underlying species differences in cuticular hydrocarbon production between *Drosophila melanogaster* and *D. simulans*. *Genome*, *64*(2), 87–95. <https://doi.org/10.1139/gen-2019-0224>
- Wheeler, D. A., Kyriacou, C. P., Greenacre, M. L., Yu, Q., Rutila, J. E., Rosbash, M., & Hall, J. C. (1991). Molecular transfer of a species-specific behavior from *Drosophila simulans* to

- Drosophila melanogaster*. *Science*, 251(4997), 1082–1086.
<https://doi.org/10.1126/science.1900131>
- Wiley, E. O. (1978). The evolutionary species concept reconsidered. *Systematic Zoology*, 27(1), 17. <https://doi.org/10.2307/2412809>
- Yang, C., Rumpf, S., Xiang, Y., Gordon, M. D., Song, W., Jan, L. Y., & Jan, Y.-N. (2009). Control of the postmating behavioral switch in *Drosophila* females by internal sensory neurons. *Neuron*, 61(4), 519–526. <https://doi.org/10.1016/j.neuron.2008.12.021>
- Yapici, N., Kim, Y.-J., Ribeiro, C., & Dickson, B. J. (2008). A receptor that mediates the post-mating switch in *Drosophila* reproductive behaviour. *Nature*, 451(7174), 33–37. <https://doi.org/10.1038/nature06483>
- Yu, J. Y., Kanai, M. I., Demir, E., Jefferis, G. S. X. E., & Dickson, B. J. (2010). Cellular organization of the neural circuit that drives *Drosophila* courtship behavior. *Current Biology*, 20(18), 1602–1614. <https://doi.org/10.1016/j.cub.2010.08.025>

Supplementary Tables

Table S1. *Drosophila* stocks obtained from Bloomington Drosophila Stock Centre

BDSC #	Genotype	Usage, Description, and/or Notes
3703	$w^{1118}/Dp(1;Y)y^+$; <i>CyO/nub¹ b¹ sna^{Sco} lt¹ stw³</i> ; <i>MKRS/TM6B, Tb¹</i>	Standard balancer stock used in this project. Has mutant eye pigmentation (white).
58492	y^1 M{ <i>Act5C-Cas9.P.RFP</i> }ZH-2A w^{1118} <i>DNAIig4¹⁶⁹</i> ; +; +	Injection stock. Ubiquitously expresses Cas9. DNAIig4 mutation reduces non-homologous end joining events.
66696	w^* ; +; TI{ <i>GAL4</i> } <i>fru^{GAL4.P1.D}/TM3, Sb¹</i>	Expresses GAL4 under control of <i>fru^{P1}</i> regulatory sequences.
4775	w^{1118} ; P{ w^{+mC} =UAS- <i>GFP.nls</i> }14	Expresses nuclear GFP under control of UAS.
5137	y^1 w^* ; +; P{ w^{+mC} =UAS- <i>mCD8::GFP.L</i> }LL5, P{UAS- <i>mCD8::GFP.L</i> }2	Expresses membrane-bound GFP under control of UAS.
26263	w^* ; P{ $y^{+7.7}$ w^{+mC} =UAS- <i>TrpA1(B).K</i> }attP16; +	Expresses temperature sensitive neuronal hyperactivator TrpA1 under control of UAS.
44222	w^* ; +; P{ w^{+mC} =UAS- <i>sh^{ts1}.K</i> }3	Expresses temperature sensitive neuronal silencer shibire ^{ts} under control of UAS.
6596	w^* ; P{ w^{+mC} =UAS- <i>Hsap\KCNJ2.EGFP</i> }1; +	Expresses constitutive neuronal silencer Kir2.1 under control of UAS.
28838	w^* ; P{ w^{+mC} =UAS- <i>TeTxLC.tnt</i> }G2; +	Expresses constitutive neuronal silencer TeTxLC under control of UAS.
5824	w^{1118} ; P{ w^{+mC} =UAS- <i>rpr.C</i> }14; +	Expresses inhibitor for anti-apoptotic proteins Reaper under control of UAS.

Table S2. *Drosophila* lines produced in this project

Name	Genotype	Usage, Description, and/or Notes
bal- w^+	+; <i>CyO/nub¹ b¹ sna^{Sco} lt¹ stw³</i> ; <i>MKRS/TM6B, Tb¹</i>	Alternate balancer line containing first chromosomes donated from CS. Has normal wildtype eye pigmentation.
bal-3	+; +; <i>MKRS/TM6B, Tb¹</i>	Alternate balancer line containing first and second chromosomes donated from CS. Has normal wildtype eye pigmentation.
<i>fru^{P2-T-GEM}</i>	+; +; TI{ <i>RFP^{3xP3.PB=T-GEM}</i> } <i>fru^{P2-TG4.2}/TM6B, Tb¹</i>	Phase 2 TI{T-GEM} DNA cassette inserted into first coding intron downstream of the P2 exon to express Trojan-GAL4 under regulatory regions of <i>fru^{P2}</i> .
N/A	+; P{ $y^{+7.7}$ w^{+mC} =UAS- <i>TrpA1(B).K</i> }attP16; TI{ <i>RFP^{3xP3.PB=T-GEM}</i> } <i>fru^{P2-TG4.2}/TM6B, Tb¹</i>	Phase 2 TI{T-GEM} DNA cassette inserted into first coding intron downstream of the P2 exon to express Trojan-GAL4 under regulatory regions of <i>fru^{P2}</i> . Expresses temperature sensitive neuronal hyperactivator TrpA1 under control of UAS.

Table S3. Primers used for PCR and related Sanger sequencing

Primer Pair		Sequence (5'->3')
tgt_seq	Fwd	CTCGAGCCAGGAGCCATTAG
	Rev	TTTTTCGCAGTGCACCGATTG
5arm	Fwd	<u>acaata</u> accggt GTTCTGAATTTTCCGTTTCGCACT
	Rev	<u>acaata</u> agcggcgcgc GAATGGAATCTGGTCTGAAATTTGCA
3arm	Fwd	<u>acaata</u> aggcgcgcgc CATGACACGGTCCGGCC
	Rev	<u>acaata</u> aactagt AACAATCGCAGCAGAAGCCC
ins_ver	Fwd	GCTGCAAAAAGAACTCAGTCCGC
	Rev	CCAATCGAAGCCGTGCAGGG

Note 1: underlined bases represent buffer bases for optimizing restriction enzyme activity at ends of linear DNA

Note 2: underlined bases represent restriction sites added for PCR cloning

Table S4. Cas9 target oligonucleotides

Strand	Sequence
Sense	5' - (P) - <u>cttcGGCCGGGCCGTGTCATGGAA</u> - 3'
Antisense	3' - <u>CCGGCCCGGCACAGTACCTTcaaa</u> - (P) - 5'

Note 1: lowercase bases represent non-annealing nucleotides for producing sticky ends

Note 2: P represents phosphoryl group

Table S5. Microinjection mix recipe

Reagent	Final Concentration	Volume (μ L)	Calculation
pU6-3-gRNA	100 μ g mL ⁻¹		$(100 * V_F) / C_{pU6-gRNA}$
pT-GEM ^{phase2}	500 μ g mL ⁻¹		$(500 * V_F) / C_{pT-GEM}$
Sterile food dye	5% V/V		$0.05 * V_F$
Water	NA		$V_F - V_{pU6} - V_{pT-GEM} - V_{dye}$

Note: C = concentration in μ g mL⁻¹, V_F = final volume

Table S6. Apple juice agar recipe

Ingredient	Final Concentration	Volume (μ L)	Calculation
Water	50% V/V		$V_F / 2$
Apple Juice	50% V/V		$V_F / 2$
White Sugar	60 μ g mL ⁻¹		$60 * V_F$
Agar-C	25 μ g mL ⁻¹		$25 * V_F$
Propionic Acid	3 μ g mL ⁻¹		$3 * V_F$

Note 1: V_F = final volume

Note 2: bring liquids to a gentle boil with stirring, add solid ingredients, reduce heat, add propionic acid

Table S7. Primers used for RT-PCR and related Sanger sequencing

Primer		Sequence (5'->3')
P2	Forward	GGTCATAAAAATCGCTCGGTT
P1	Forward	ACACAATCCCTTCGAAGGAA
S	Forward	GCACAAGCGGAACATCGAAA
COM3	Reverse	TCTGAACTACCGTCCGACT
GAL4	Reverse	CCAATCGAAGCCGTGCAGGG
RpL32	Forward	GGCATCAGATACTGTCCCTTG
RpL32	Reverse	CCAGTCGGATCGATATGCTAA

Supplementary Figures



Figure S1. Sexing flies in late-pupal stage by presence or absence of sex combs. Males (right pupa) are observed to have sex combs (highlighted by yellow circles) while females are not (left pupa). Flies are genotype *fru*^{P2-T2A-GAL4}/*TM6B*, *Tb*¹.

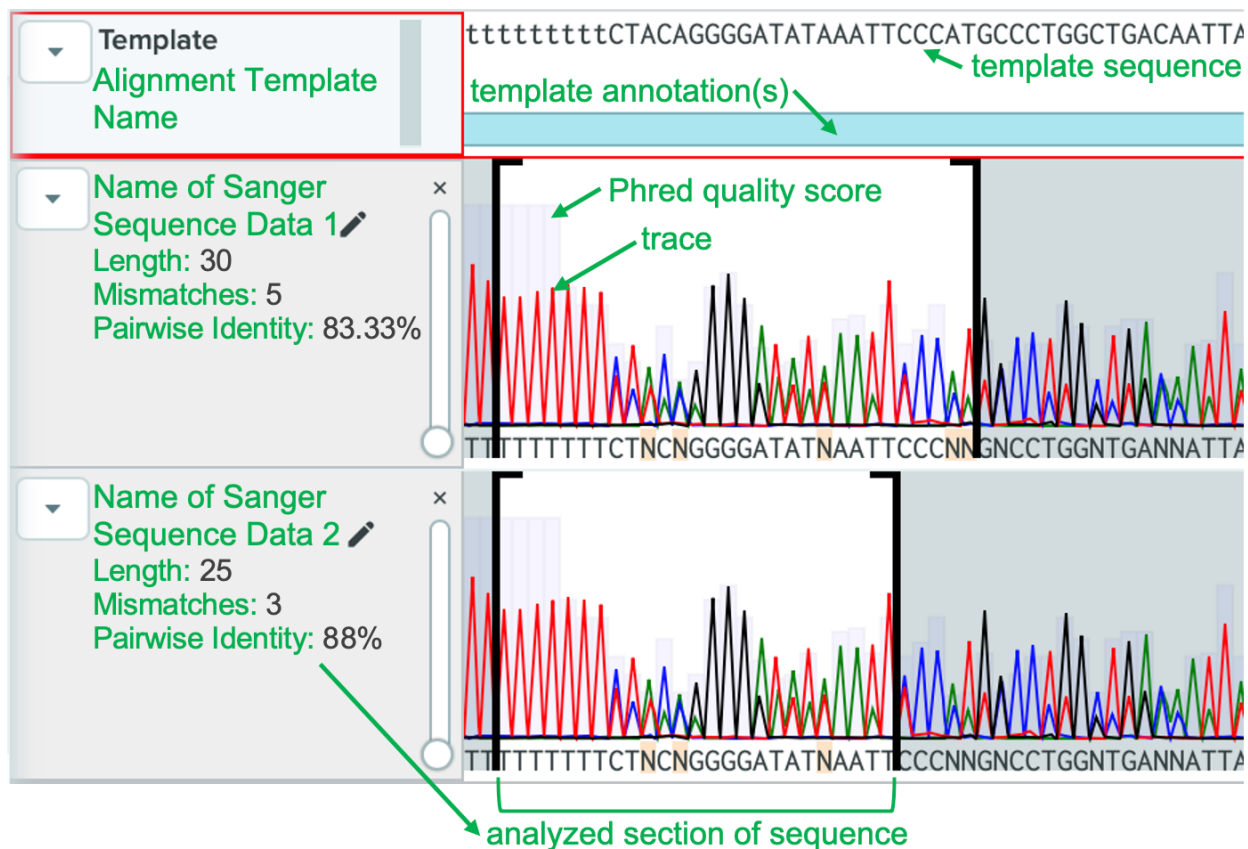


Figure S2. Sanger sequencing chromatogram sample figure with annotations. Top row represents alignment template; left column contains name and right column contains sequence and/or annotations. All rows below the alignment template row represent individual Sanger sequence data; left column contains sequence name and statistics for analyzed section of sequence (Length = size of sequence in bases, Mismatches = number of bases that deviate from the alignment template, Pairwise Identity = % of bases that match the alignment template); right column contains traces (colour represents base-call; green = adenine, red = thymine blue = cytosine, black = guanine), grey bars behind each trace represents quality score (Phred+64 encoding), and black brackets denote section of sequence analyzed for row statistics. Image adapted from Benchling (2021).

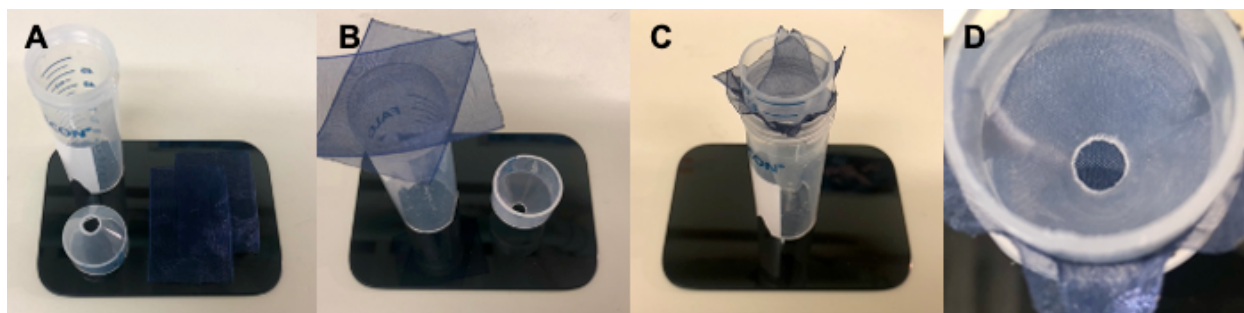


Figure S3. Embryo collection basket apparatus components and assembly. A) Components of the apparatus: one Falcon 50 mL conical tube was used to produce a funnel and holder, and two strips of synthetic sheer ribbon are used as a filter. B-C) Strips of sheer ribbon are pulled taut against bottom of the funnel by the holder. D) Exposed sheer ribbon collects embryos rinsed into the funnel.

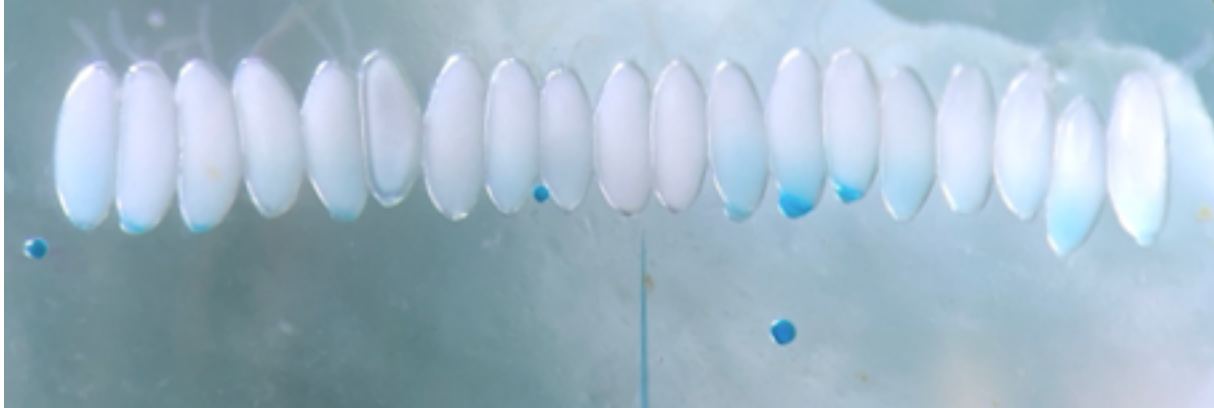


Figure S4. Embryonic microinjection. Embryos are aligned to be laterally adjacent to neighboring embryos. Embryos shown with posterior ends facing downward. Injection needle shown facing upward toward posterior ends of embryos.

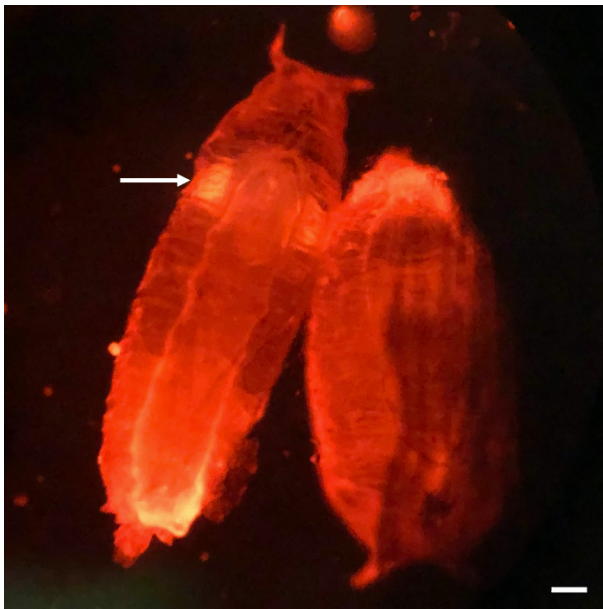


Figure S5. Epi-fluorescent imaging of late-stage pupae for screening successful transgenesis. Pupae express RFP in the eyes (white arrow), indicating successful genomic insertion of the T-GEM construct. Scale bar represents approximately 100 μm .

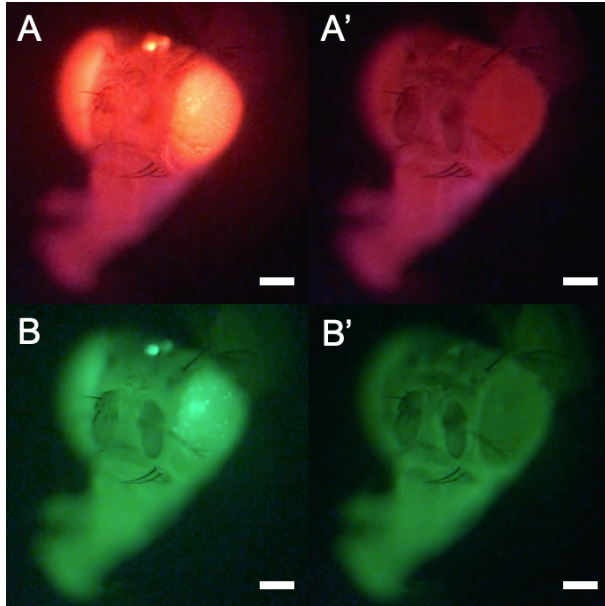


Figure S6. Epi-fluorescent imaging of whole-mounted adult female head for screening successful transgenesis of T-GEM and preliminary verification of Gal4 functionality. Flies express (A) RFP in the optic tissues, indicating presence of the T-GEM construct in the genome, and (B) nuclear GFP in tissues predicted to express *fru*^{P2} (Leader et al., 2018), indicating transcription and in-phase translation of Gal4. Scale bars represent approximately 150 μm .

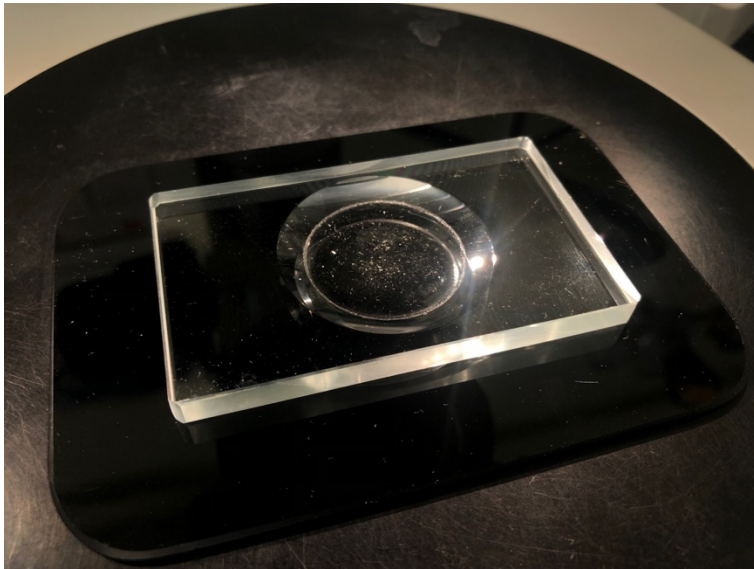


Figure S7. Dissection pad apparatus. SYLGARD™ 184 Silicone Elastomer coated round well of a 75 x 44 x 6 mm glass slide protects microdissection forceps from damage, and also allows tissue anchoring with insect pins.

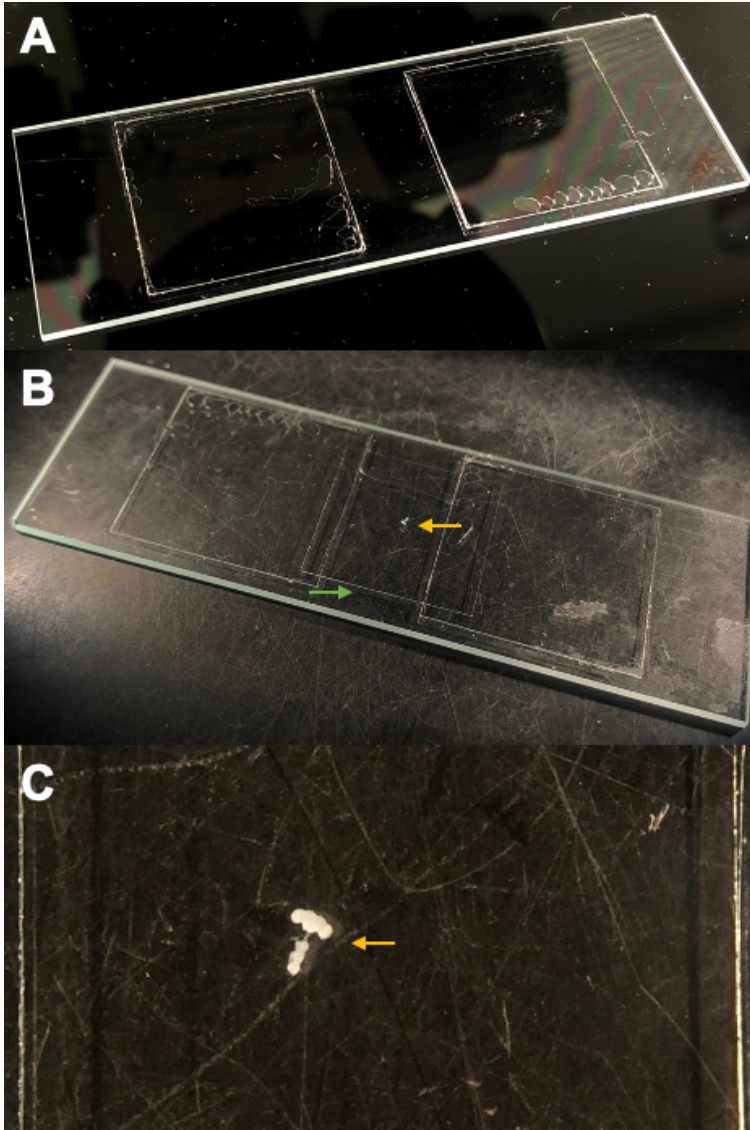


Figure S8. Mounting slide apparatus and usage. (A) Two 22 x 22 mm cover slips affixed to a 75 x 25 mm glass slide. (B) 18 x 18 mm cover slip rests on affixed 22 x 22 mm cover slips to prevent mechanical damage to tissues. Green arrow = location where DPBS is pipetted to submerge CNS. Yellow arrow = adult CNS. (C) Undamaged adult CNS submerged in 1x DPBS.

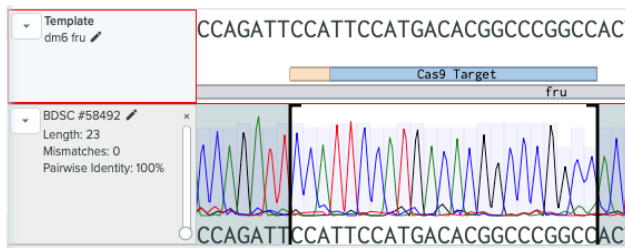


Figure S9. Sanger sequencing chromatogram of PCR amplicon generated for verifying presence and fidelity of the Cas9 target sequence in the injection line genome. PCR performed using primer set `tgt_seq`. Sequence aligned to `dm6` reference genome with annotations for Cas9 target (blue) and NGG PAM (yellow), with 100% pairwise identity for Cas9 target. Image adapted from Benchling (2021).

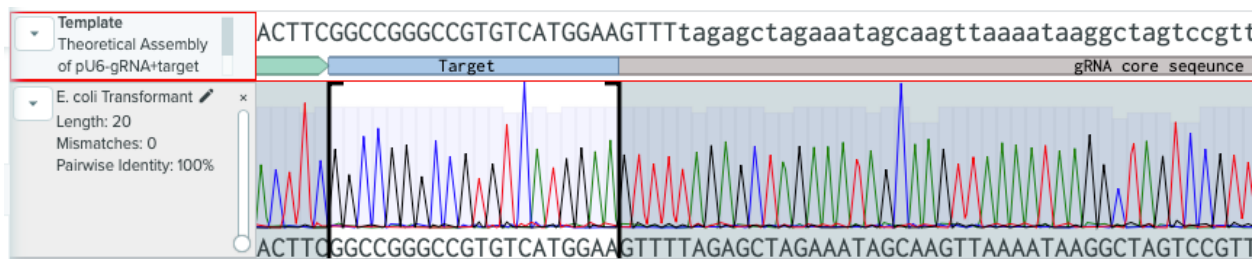


Figure S10. Sanger sequencing chromatogram of pU6-gRNA+target plasmid for verifying successful insertion of Cas9 target sequence into gRNA expression vector. Sequence alignment performed to theoretical assembly of pU6-3-gRNA+target with annotations for pU6-3 promoter (green), Cas9 target (blue), and gRNA core sequence/scaffold (grey); with 100% pairwise identity for Cas9 target. Image adapted from Benchling (2021).

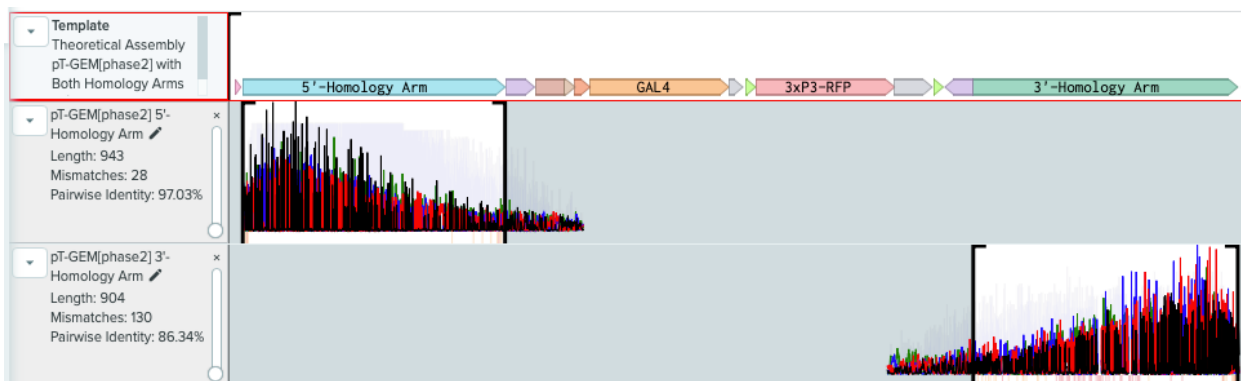


Figure S11. Sanger sequencing chromatograms of pT-GEM^{phase2} (with 5' and 3'-homology arms) plasmid for verifying successful insertion of 5'-homology arm and 3'-homology arm into T-GEM donor vector. Amplicon sequences aligned to theoretical assembly of pT-GEM^{phase2} containing both 5'- and 3'- homology arms, with annotations for 5'-homology arm (blue), GAL4 (orange), 3xP3-RFP (red), 3'-homology arm (green); with pairwise identities of 97.03% and 86.35% for 5'-homology arm and 3'-homology arm, respectively. Pairwise identities <100% were expected due to natural variation in *fru* intronic regions between the injection line and the dm6 reference genome. Note: GAL4 and 3xP3-RFP not shown to scale. Image adapted from Benchling (2021).

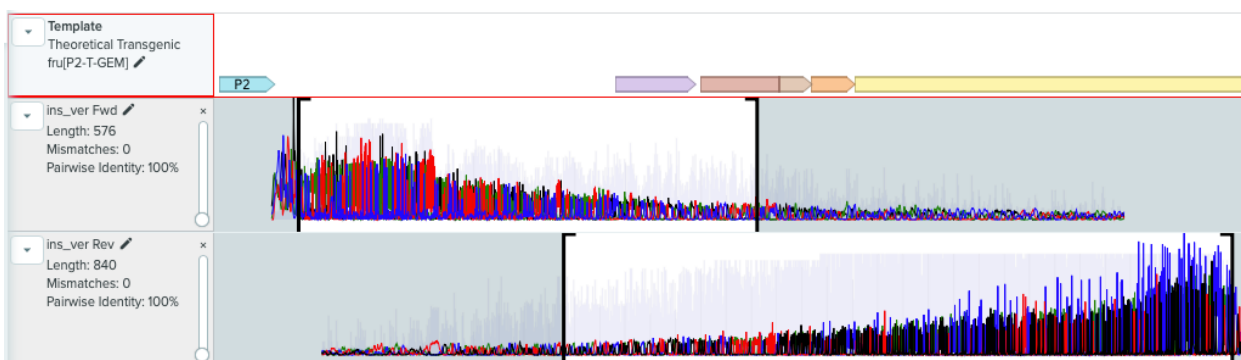


Figure S12. Sanger sequencing chromatogram of PCR amplicons for verifying successful transgenesis of T-GEM^{phase2} into the intron downstream of the P2 exon in an RFP⁺ G₁ population. Alignment performed to theoretical genomic *fru* with T-GEM^{phase2} insertion, predicted using dm6 reference genome and T-GEM^{phase2} sequence. Annotations: P2 exon (blue), T2A (orange), GAL4 (yellow). Image adapted from Benchling (2021).

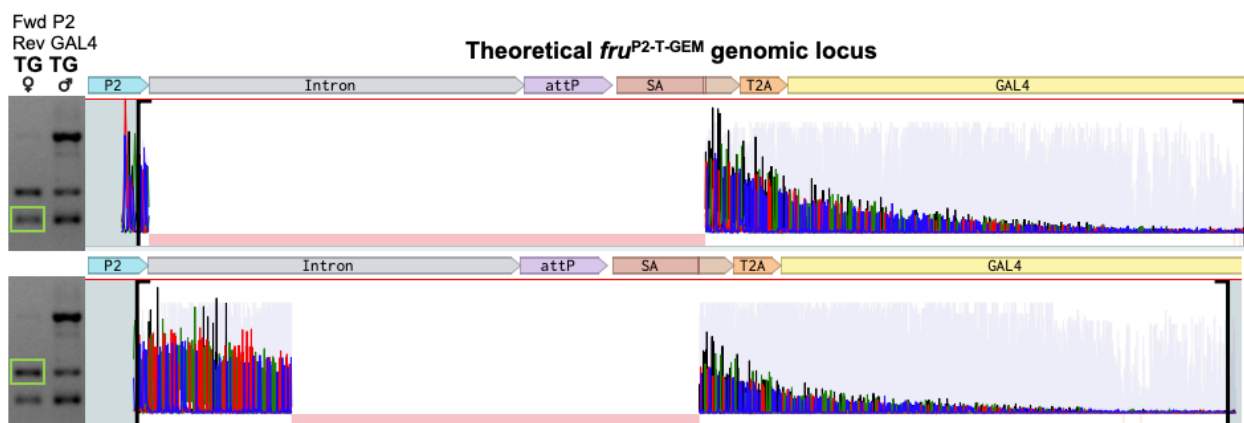


Figure S13. Sanger sequencing chromatograms of RT-PCR amplicons from *fru*^{P2-T-GEM}/*TM6B*, *Tb*¹ females produced using P2 forward and GAL4 reverse primers. Agarose gel image corresponds to box A in Figure 12, and green box denotes Sanger sequenced amplicon. Sanger sequencing was performed using P2 forward primer. Alignment was performed to theoretical *fru*^{P2-T-GEM} genomic locus, predicted using the dm6 reference genome, Cas9 target site, and T-GEM sequence. Adapted from Benchling (2021).

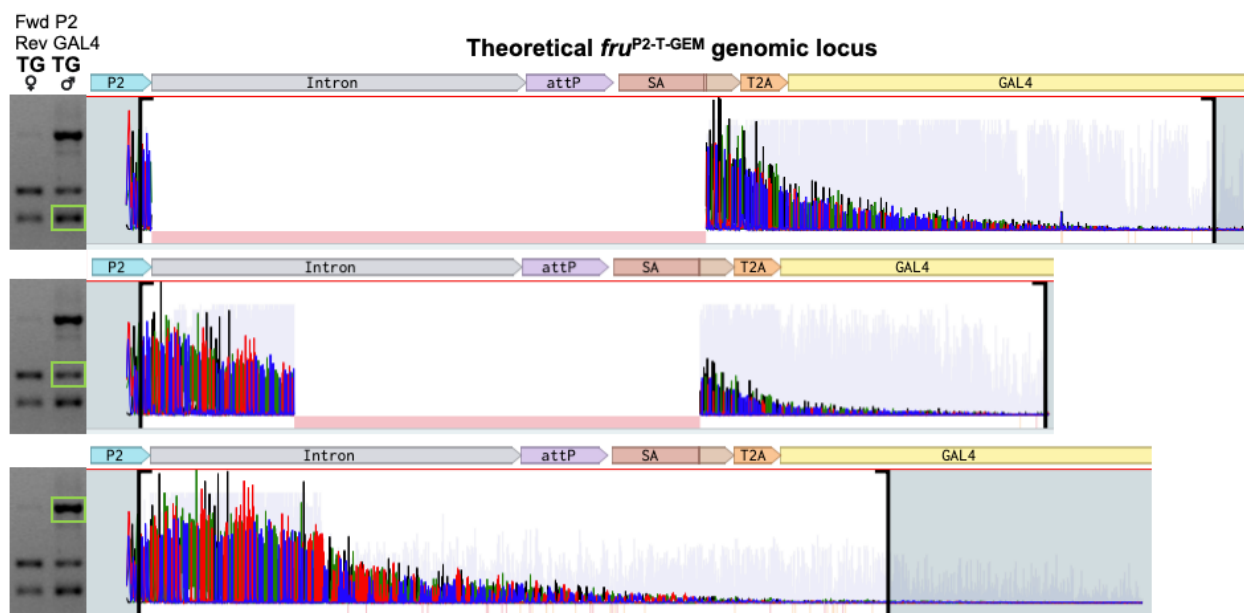


Figure S14. Sanger sequencing chromatograms of RT-PCR amplicons from *fru*^{P2-T-GEM}/*TM6B*, *Tb*¹ males produced using P2 forward and GAL4 reverse primers. Agarose gel images correspond to box A in Figure 12, and green box denotes Sanger sequenced amplicon. Sanger sequencing was performed using P2 forward primer. Alignment was performed to theoretical *fru*^{P2-T-GEM} genomic locus, predicted using the dm6 reference genome, Cas9 target site, and T-GEM sequence. Adapted from Benchling (2021).

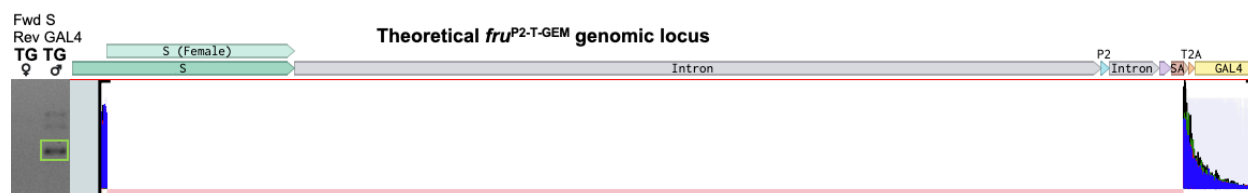


Figure S15. Sanger sequencing chromatogram of RT-PCR amplicon from *fru*^{P2-T-GEM}/*TM6B*, *Tb*¹ males produced using S forward and GAL4 reverse primers. Agarose gel image corresponds to box B in Figure 12, and green box denotes Sanger sequenced amplicon. Sanger sequencing was performed using S forward primer. Alignment was performed to theoretical *fru*^{P2-T-GEM} genomic locus, predicted using the dm6 reference genome, Cas9 target site, and T-GEM sequence. Adapted from Benchling (2021).

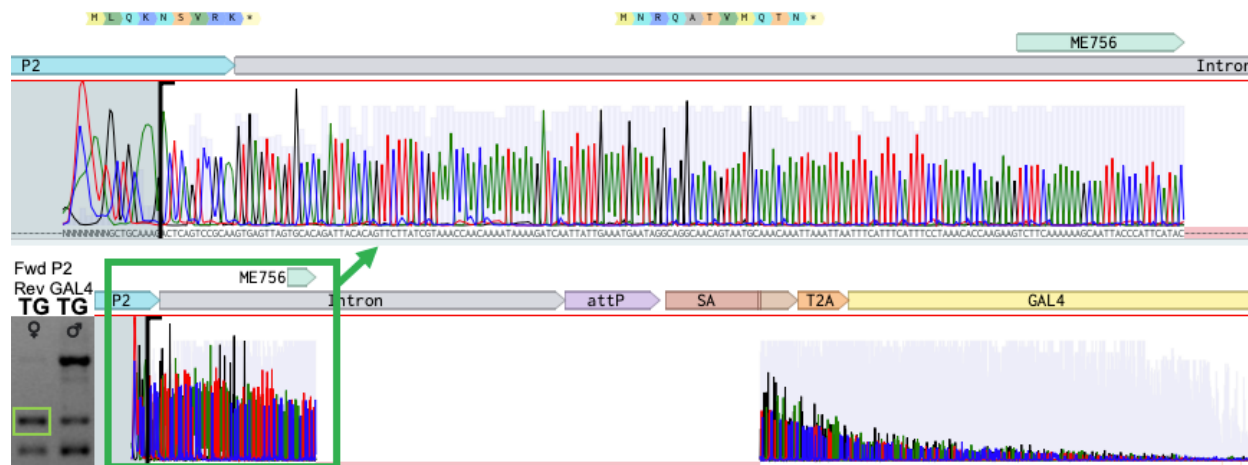


Figure S16. Sanger sequencing chromatograms and analysis of RT-PCR amplicon produced from extended *fru*^{P2} transcript in *fru*^{P2-T-GEM}/*TM6B*, *Tb*¹ females. Gel image corresponds to box A in Figure 12 with light green box denoting Sanger sequenced amplicon. Sanger sequencing was performed using P2 forward primer. Top chromatogram is an enlarged section of bottom chromatogram (dark green box with arrow). Alignment performed to theoretical *fru*^{P2-T-GEM} genomic locus, predicted using the dm6 reference genome, Cas9 target site, and T-GEM sequence. Predicted protein products from open reading frames are shown above top chromatogram, with asterisks denoting translational stop sites. The ME756 microexon is included at the 3' end of the extended P2 exon. Adapted from Benchling (2021).

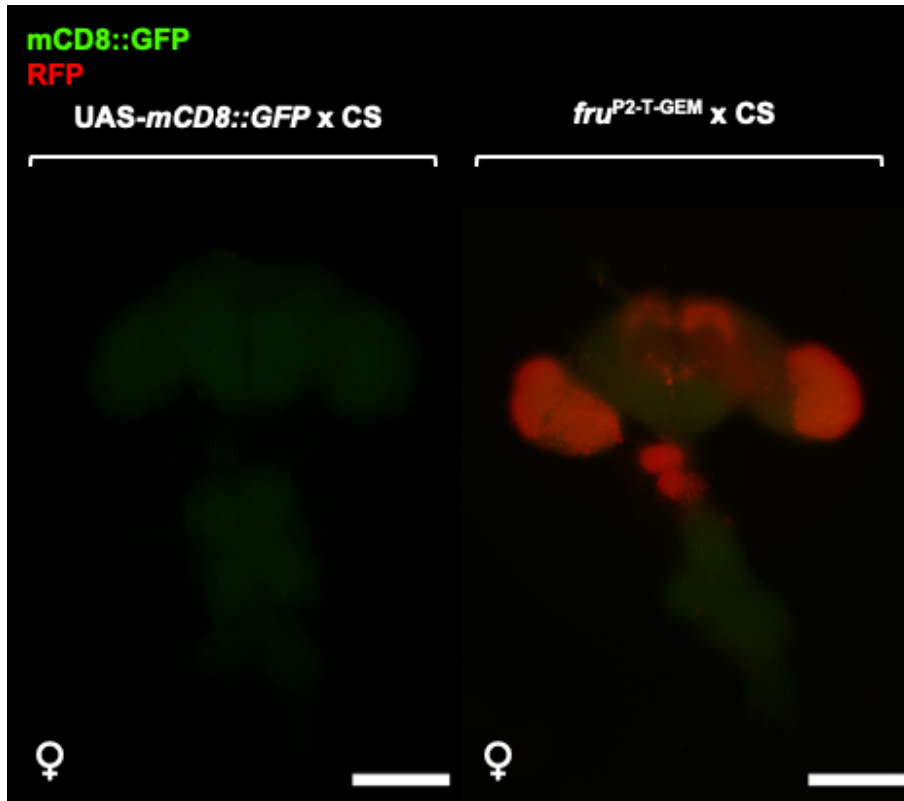


Figure S17. Epi-fluorescent imaging of whole-mounted adult CNSes for *fru*^{P2-T-GEM} and UAS-*mCD8::GFP* genetic controls. Anterior view. Red and green channels stacked. The 3xP3 artificial promoter drives *RFP* expression (red fluorescence) in *ey*-expressing tissues as a visible marker for the T-GEM construct; only observed in *fru*^{P2-T-GEM}/*TM6B*, *Tb*¹ flies as a visible marker for presence of the T-GEM construct in the genome. Green fluorescence is not observed in either genetic control. Scale bars represent 200 μm.

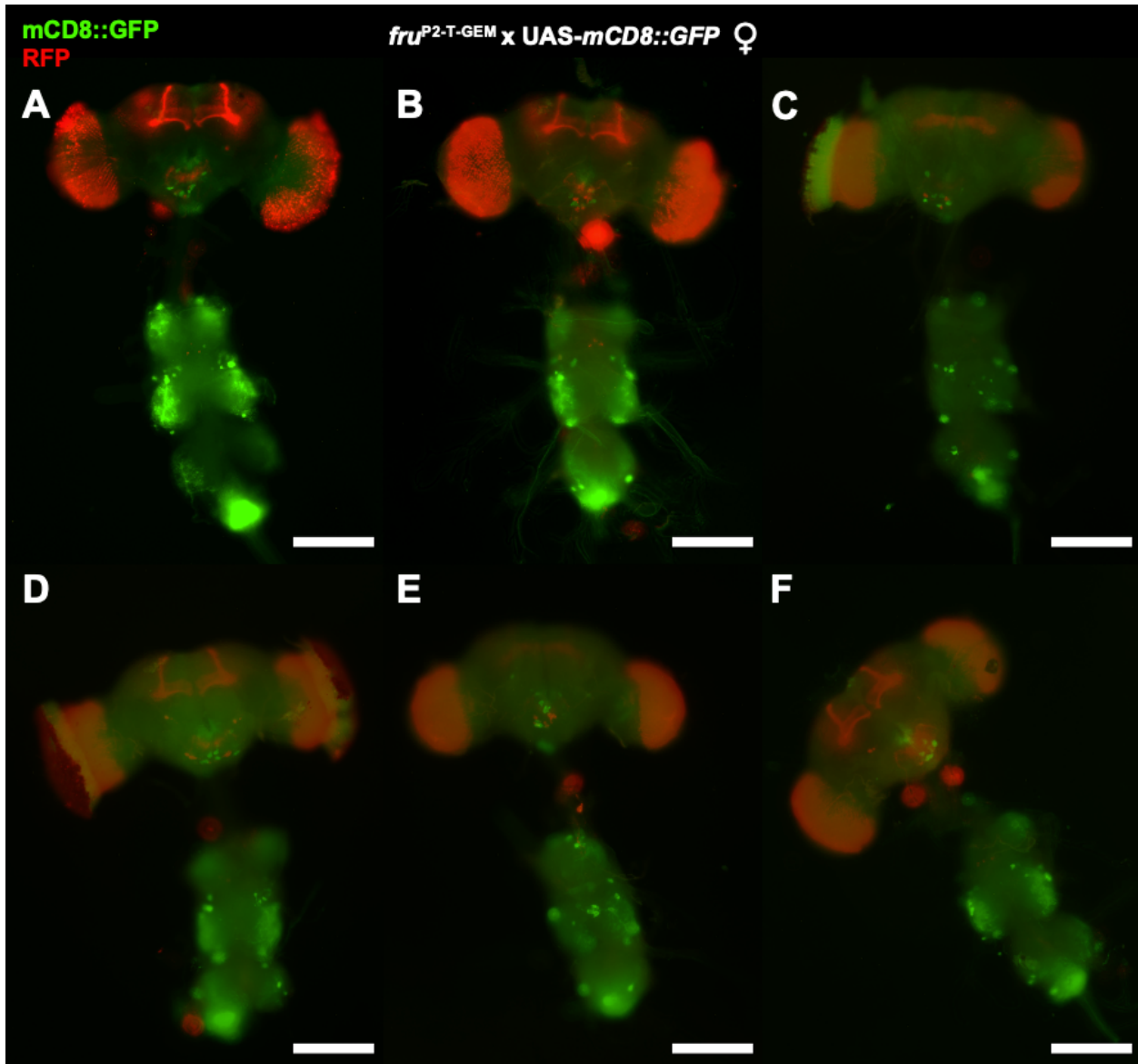


Figure S18. Epi-fluorescent imaging of whole-mounted adult female CNSes expressing mCD8::GFP under fru^{P2} regulation. The top tissue in each image for each sex is the brain, while the bottom tissue is the ventral nerve cord, shown in anterior view. Subfigures (A-F) show $fru^{T-GEM} \times UAS-mCD8::GFP$ imaging with merged RFP and GFP channels. Subfigures (C-D) show CNSes with intact laminae. $fru^{T-GEM} \times UAS-mCD8::GFP$ expresses RFP (red fluorescence) in *eyeless*-expressing tissues as a visible marker indicating presence of the T-GEM construct, and membrane bound GFP (green fluorescence) in fru^{P2} -expressing tissues. Scale bars represent 200 μm .

Curriculum Vitae

Name: William Yeung

Post-secondary education and degrees: University of Toronto Mississauga
Mississauga, Ontario, Canada
2012-2017 H.B.Sc.

Related Work Experience:

Teaching Assistant
Conestoga College
2018

Toxicology Technologist
Labstat International Inc.
2018

Graduate Teaching Assistant
Western University
2018-2021

Publications:

- Yeung, W. (2019). Digest: Sexual selection and evolution of cognition in seed beetles. *Evolution*, 73(12), 2538–2539. <https://doi.org/10.1111/evo.13858>
- Yeung, W. (2021). Digest: Female-limited X chromosome evolution in *Drosophila melanogaster*. *Evolution*, 75(1), 202–203. <https://doi.org/10.1111/evo.14125>